RICE UNIVERSITY

Developing Novel Protein-based Materials using Ultrabithorax:
Production, Characterization, and Functionalization

by

Zhao Huang

A THESIS SUBMITTED
IN PARTIAL FULFILLMENT OF THE
REQUIREMENTS FOR THE DEGREE

Doctor of Philosophy

APPROVED, THESIS COMMITTEE:

Kathleen S. Matthews, Stewart Professor,
Biochemistry and Cell Biology

Sarah E. Bondos, Assistant Professor,
Molecular and Cellular Medicine, Texas
A&M Health Science Center

John S. Olson, Ralph and Dorothy Looney
Professor, Biochemistry and Cell Biology

Michael Stern, Professor,
Biochemistry and Cell Biology

Yizhi Tao, Associate Professor,
Biochemistry and Cell Biology

K. Jane Grande-Allen, Associate Professor,
Bioengineering

HOUSTON, TEXAS
FEBRUARY 2011

ABSTRACT

Developing Novel Protein-based Materials using Ultrabithorax:
Production, Characterization, and Functionalization

By

Zhao Huang

Compared to 'conventional' materials made from metal, glass, or ceramics, protein-based materials have unique mechanical properties. Furthermore, the morphology, mechanical properties, and functionality of protein-based materials may be optimized via sequence engineering for use in a variety of applications, including textile materials, biosensors, and tissue engineering scaffolds. The development of recombinant DNA technology has enabled the production and engineering of protein-based materials *ex vivo*. However, harsh production conditions can compromise the mechanical properties of protein-based materials and diminish their ability to incorporate functional proteins. Developing a new generation of protein-based materials is crucial to (i) improve materials assembly conditions, (ii) create novel mechanical properties, and (iii) expand the capacity to carry functional protein/peptide sequences.

This thesis describes development of novel protein-based materials using Ultrabithorax, a member of the Hox family of proteins that regulate developmental pathways in *Drosophila melanogaster.* The experiments presented (i) establish the conditions required for the assembly of Ubx-based materials, (ii) generate a wide range of Ubx morphologies, (iii) examine the mechanical properties of Ubx fibers, (iv) incorporate protein functions to Ubx-based materials via gene fusion, (v) pattern protein functions within the Ubx materials, and (vi) examine the biocompatibility of Ubx materials *in vitro*.

Ubx-based materials assemble at mild conditions compatible with protein folding and activity, which enables Ubx chimeric materials to retain the function of appended proteins in spatial patterns determined by materials assembly. Ubx-based materials also display mechanical properties comparable to existing protein-based materials and demonstrate good biocompatibility with living cells *in vitro.* Taken together, this research demonstrates the unique features and future potential of novel Ubx-based materials.

ACKNOWLEGMENTS

Throughout this amazing journey of science, my thesis advisors, Dr. Kathleen Matthews and Dr. Sarah Bondos, have supported me tremendously. I would like to thank Dr. Matthews for sharing with me her critical thinking and concrete research attitude, and mentoring me in science and beyond. I am also grateful to Sarah: her energy and optimism luminesce even at the darkest hours, nurturing this research project from its infancy.

I am grateful to my committee members: Dr. John Olson, Dr. Michael Stern, Dr. Yizhi Tao, and Dr. Jane Grande-Allen for their constructive input into my thesis research. I also thank my previous advisors, Dr. Jessica Downs at University of Cambridge, and Dr. Geoffrey Baldwin at Imperial College London, for inspiring me to pursue my graduate study.

The multi-disciplinary nature of my thesis research granted me the privilege to collaborate with scientists from various backgrounds: Yang Lu and Dr. Jun Lou from Materials Science, Ravish Majithia and Dr. Keith Meissner from Biomedical Engineering, Kaiwei Liu and Dr. Lisa Biswal from Chemical Engineering, Richard Crouse from the X-ray diffraction facility of the Shared Equipment Authority, William Deery of the microscopy facility, and Patrick Spicer, Lina Mountziaris, and Dr. Antonios Mikos from Bioengineering. These collaborations were indispensable for the completion of my thesis.

I would like to thank members of the Matthews, Bondos, and Silberg laboratories, including Frances Ying Liu, Hongli Zan, Jia Xu, Alexandra Greer, Jan Patterson, Autumn Brawley, Peng Zhai, and Shirley Liu, for their support to my research. I am also grateful

to undergraduate researchers Taha Salim and Jaimin Shah, whose diligence and creativity greatly facilitated the completion of this project.

I cherish the sparks of joyful moments with fellow graduate students, especially members of the D&D and SC parties that have grown to become great friends, including Aaron Collier, Corwin Miller, Matthew Pena, Andres Benitez, John Liu, Tom Guu, Curtis Lin, and many more. I especially want to thank Jennifer Chen for her love and company.

My pursuit in science would not have been possible without my parents Qun Li and Guoqing Huang, my grandparents Shulan Yang and Yuankang Li, my aunt Ling Li, my uncle Dong Lu, my cousin Yao Lu, and all the other family members, whose constant love and encouragement propelled me towards my dream. Raised and loved in a doctors' family, I am now on route to join an even bigger family of doctors in the scientific community.

TABLE OF CONTENTS

Developing Novel Protein-based Materials using Ultrabithorax: *Production, Characterization, and Functionalization*

LIST OF FIGURES

Chapter 5

Chapter 6

Chapter 7

LIST OF TABLES

CHAPTER 1

Protein-based Materials:
Sources, Production, Properties, and Applications[1]

1.1 Protein-based materials research: Potential and focus

Animal hides and silks composed of protein polymers were used for centuries before the development of 'conventional' metallic, glass, ceramic, and polymer-based materials (Altman et al., 2003; Cigada, 2008; Eisenbarth, 2007; Fratzl and Weinkamer, 2007; Scheibel, 2004). The unique features of protein-based materials have driven increasing research efforts to develop these materials for a wide range of applications. Protein-based materials exhibit a unique combination of mechanical properties, which cannot be obtained by traditional materials science approaches (Gosline et al., 1999; Lee et al., 2009). Unlike 'conventional' materials that require high temperature/pressure to process, protein-based materials have the potential to be produced under ambient conditions, simplifying materials production and facilitating the incorporation of bioactive molecules (Sakiyama-Elbert and Hubbell, 2001). Finally, the mechanical properties and functions of protein-based materials can be altered via sequence engineering, enabling them to be engineered for a large variety of applications (Bini et al., 2006; McGrath and Kaplan, 1997; Sakiyama-Elbert and Hubbell, 2001; Teule et al., 2007).

---

[1] Parts of this chapter, including segments of the text, were reported in Greer and Huang et al., 2009; Huang and Lu et al., 2010; or Huang et al., 2011.

Recent research on protein-based materials has been focused on protein/peptide production using recombinant and synthetic approaches, processing of protein-based materials that have suitable morphologies and mechanical properties, and the functionalization and patterning of the protein-based materials for a variety of applications.

1.2 Different sources of protein-based materials

Protein-based materials are made of material-forming proteins, which can be purified from organisms in which they occur naturally, generated by recombinant methods in another organism, or synthesized chemically. For centuries, material-forming proteins could only be purified from their native organisms (e.g., silkworm silk, spider silk). However, the development of recombinant DNA technology enabled the production of these material-forming proteins in other organisms. For example, collagen has been produced in *E. coli* (Du et al., 2008), yeast (Pakkanen et al., 2003), and plants (Kyle et al., 2009; Merle et al., 2002). Additionally, self-assembling peptides that mimic natural protein-based materials or self-interacting motifs have been produced via chemical synthesis (Floss et al., 2010; Kyle et al., 2009; Papapostolou et al., 2007).

1.2.1 Naturally derived protein-based materials

A large variety of protein-based materials can be found in nature, the most studied of which are keratin, collagen, elastin, and silk. Since their remarkable properties inspired *in vitro* production of protein materials, these proteins serve as both a guide and a benchmark by which successful design and engineering are measured. Extensive studies have provided insight into their structures, mechanical properties, and formation mechanism as shown in **Table 1.1** (Altman et al., 2003; Cigada, 2008; Daamen et al.,

2007; Fratzl et al., 1998; Fuchs and Weber, 1994; Karthikeyan et al., 2007; Marshall et al., 1991).

Table 1.1 Common natural protein-based materials and their properties.

	Keratin	**Collagen**	**Elastin**	**Silk**
Morphology	Fibers/Sheets	Fibers	Fibers	Fibers
Mechanical Properties	Strong, Elastic	Inelastic, Strong	Elastic, Extensible	Sequence dependent
Natural Function	Hair, Nail, Feathers	Tendon, Ligament	Tendon, Ligament	Web, Cocoon
Structure	Coiled coil	Triple-helix	Aggregates	Stacked β-sheets, Random coils
Site of Assembly	Intracellular	Intracellular, Extracellular	Intracellular, Extracellular	Specialized Glands
Inter-molecular Forces	Hydrophobic, Disulfide bond	Disulfide bond, Complementarities, H-bonds	Hydrophobic, Cross-linking	van der Waal's, H-bonds

Keratin: Found in hair, nail, and feathers, keratin molecules contain a rod region flanked by the N-terminal head and the C-terminal tail domain (**Fig. 1.1A**). The central rod region is composed of alpha-helical segments (1A, 1B, 2A, and 2B) separated by short linker regions (L1, L12, and L2). (Coulombe and Omary, 2002). Keratins can form filaments spontaneously via a series of assembly steps: two keratin molecules first interact to form a dimer that adopts an α-helical coiled-coil structure (**Fig. 1.1B**). These dimers further oligomerize into filaments and higher order structures as shown in **Fig. 1.1C** (Marshall et al., 1991). Hydrophobic interactions are the major force driving the formation of keratin-based materials (Marshall et al., 1991). The α-helical domains (1A,

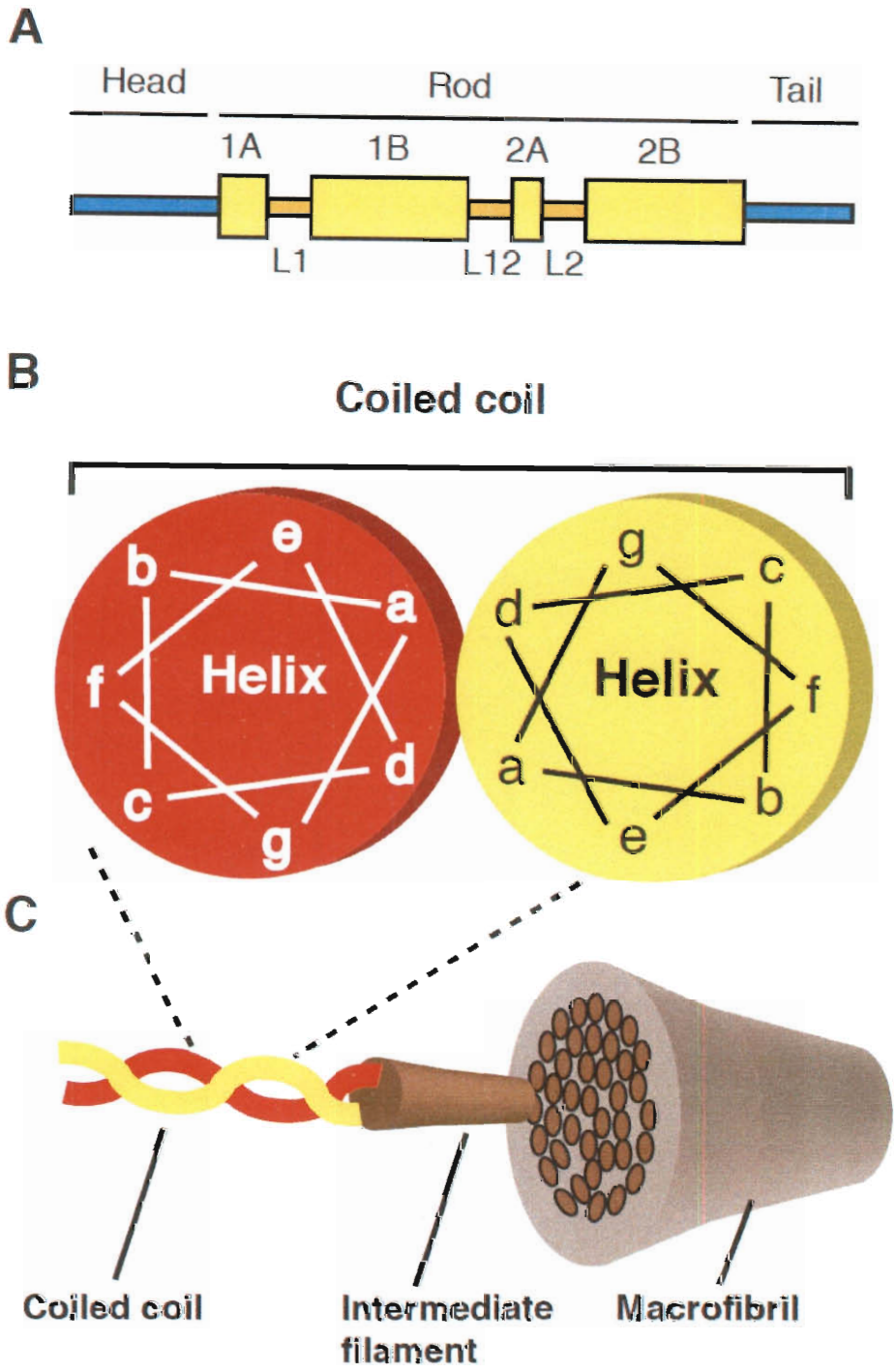

Figure 1.1 Structure and assembly of keratin molecules. (A) Domain structures of keratin molecules. Adapted from Coulombe and Omary, 2002. (B) Hydrophobic interactions between α-helices drive coiled-coil formation. (C) Schematic of the keratin helix assembly into coiled-coil structures, intermediate filament, and finally hair macrofibril. Inspired by Marshall et al., 1991.

1B, 2A, and 2B) contain heptad repeats (abcdefg) in which nonpolar amino acids in positions a and d interact via hydrophobic interactions to form the coiled-coil structure as shown in **Fig. 1.1B** (Coulombe and Omary, 2002; Fratzl et al., 1998). Disulfide bonds control cross-linking of the filaments, which affects the mechanical properties of the materials: The stronger and harder keratin materials (e.g., nail) have more disulfide bonds, whereas the more flexible and elastic materials (e.g., hair) have fewer disulfide bonds (Marshall et al., 1991).

Collagen: Collagen fibrils and networks are present in the highly organized, three-dimensional extracellular matrix in tissues such as bone, cartilage, tendon and cornea (Cen et al., 2008; Jhon and Andrade, 1973). Collagen molecules assemble in a hierarchical manner: procollagen molecules associate to form triple helices, which in turn assemble into collagen fibrils and ultimately collagen fibers (**Fig. 1.2**). Steric complementarity and disulfide bonds contribute to the formation of the collagen triple helix. Procollagen polypeptides contain characteristic tripeptide repeats (Gly-X-Y), which position glycines inside the triple helix to facilitate close packing between chains, making the formation of the triple-helix sterically feasible. (Fratzl et al., 1998; Fratzl and Weinkamer, 2007). Following close packing, disulfide bonds form between individual collagen molecules, enabling the formation of procollagen triple helices. (Khoshnoodi et al., 2006). Following the export of procollagen triple helices outside the cells, their N- and C-terminal propeptides are cleaved to form tropocollagen triple helices. Tropocollgen triple helices spontaneously aggregate to form head-to-tail fibrils, which are stabilized by hydrogen bonds and extensive crosslinking. Finally, collagen fibrils further assemble into collagen fibers (Khoshnoodi et al., 2006; Kyle et al., 2009).

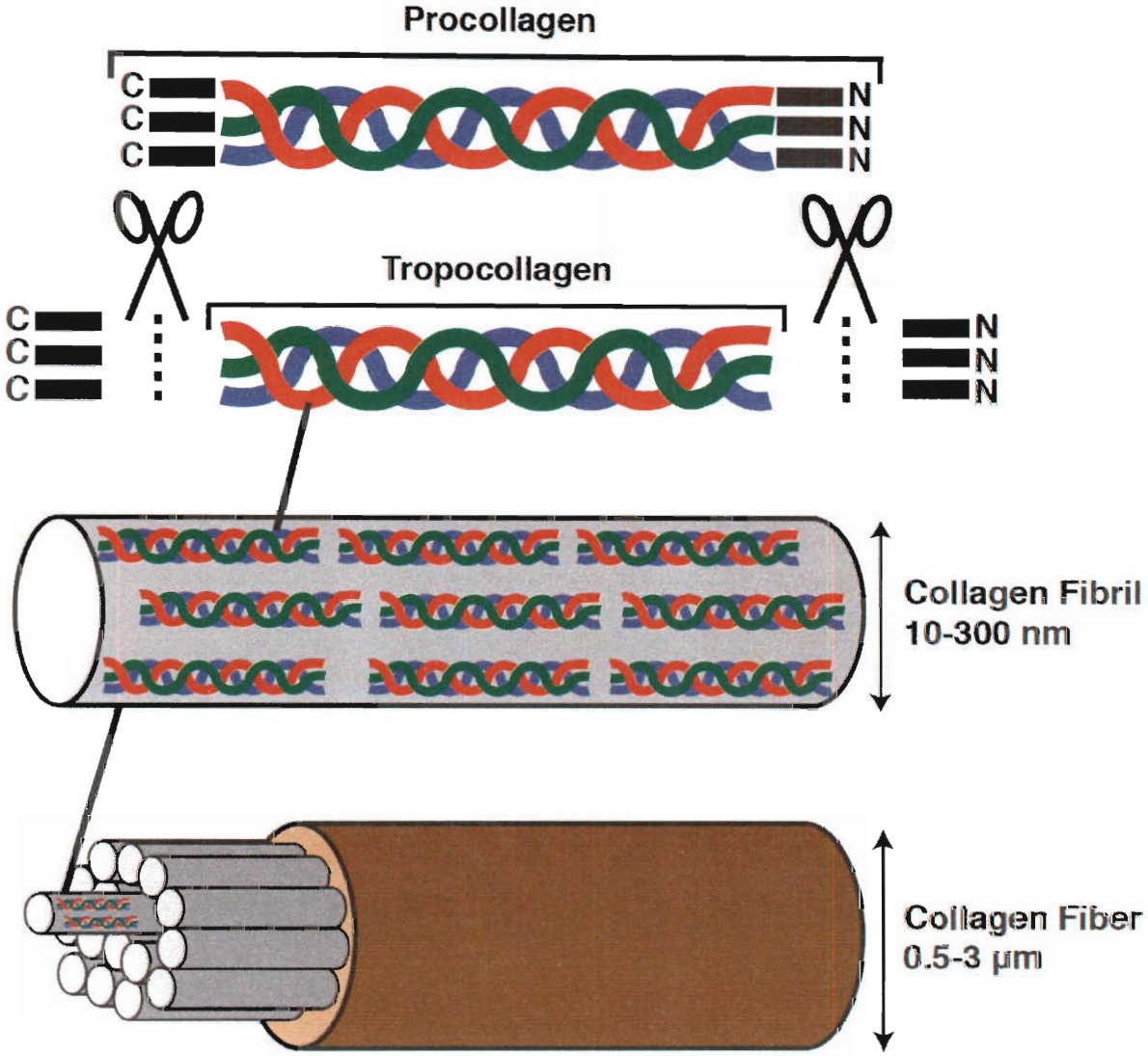

Figure 1.2 Assembly of collagen triple helices into collagen fibers. After the procollagen triple helix is exported from the cell, the N- and C-terminal propeptides are cleaved. The resulting tropocollagen triple helix undergoes extensive crosslinking and self-assembly into collagen fibrils of diameters between 10 and 300 nm. These fibrils then assemble into bundles, forming collagen fibers of diameters between 0.5-3 μm. Figure was inspired by Kyle et al., 2009.

Elastin: Elastin is an extracellular matrix protein that is found in blood vessels, tendons/ligaments, skin, and other tissues/organs that require elasticity to undergo stretch/relax cycles (Faury, 2001; Martyn and Greenwald, 2001; Pasquali-Ronchetti and Baccarani-Contri, 1997). The insoluble and hydrophobic elastin proteins form

extensively cross-linked fibers. Despite ongoing research, limited information is known about the molecular structure of elastin fibers due to insolubility. Elastin forms materials in a process called coacervation, during which tropoelastin, the precursor protein of elastin, is intermolecularly crosslinked to form aggregates and then assembled into fibers **(Fig. 1.3)** (Cox et al., 1974; Wu et al., 1999). The resultant elastin fibers are extremely stable and have a half-life of 70 years (Powell et al., 1992). Elastin-like biomaterials have been used for a wide variety of applications, including skin substitutes (Powell et al., 1992), vascular grafts (Boland et al., 2004; McClure et al., 2010), heart valves (Neuenschwander and Hoerstrup, 2004; Schmidt et al., 2006a; Schmidt et al., 2006b), and elastic cartilages (Daamen et al., 2007; Kusuhara et al., 2009; Xu et al., 2005).

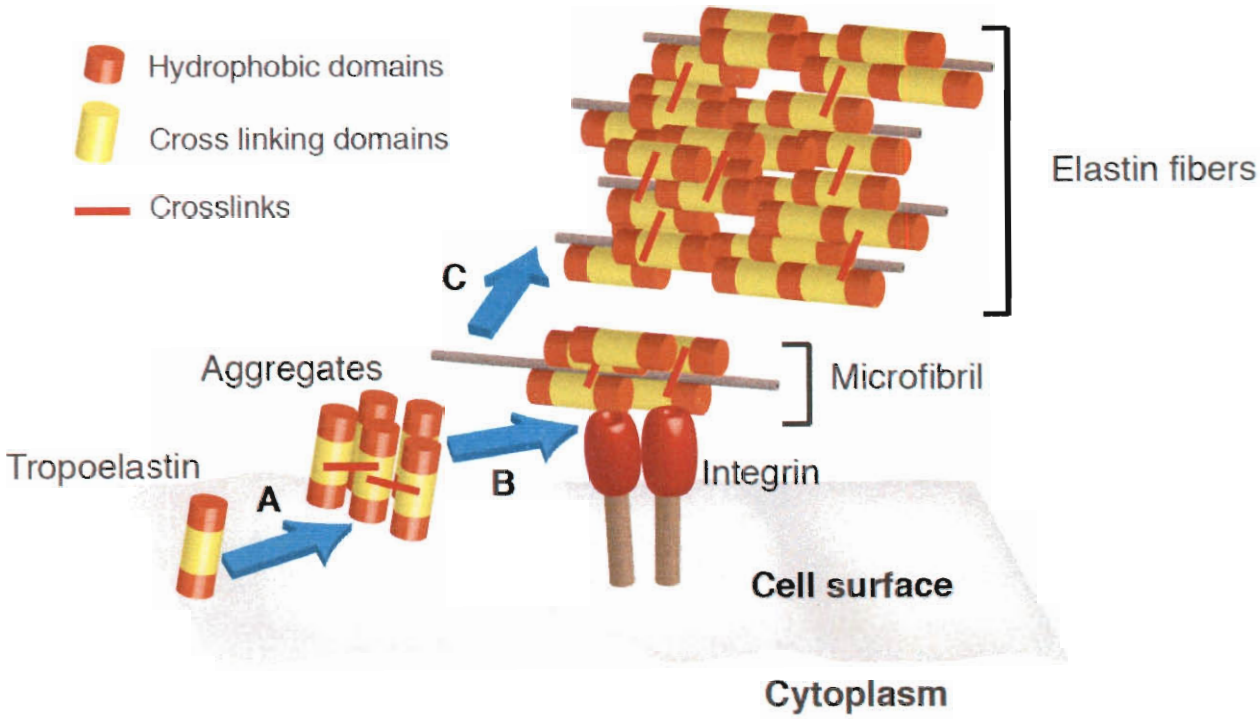

Figure 1.3 Assembly of elastin fibers. (A) Tropoelastins are transported to the cell surface and crosslinked by lysyl oxidase to form tropoelastin aggregates. (B) The resulting aggregates are transferred to extracellular microfibrils that are bound to integrins. (C) Elastin aggregates are first assembled on the microfibril and then coalesced into elastin fibers. Lysyl oxidase results in the crosslinks within the mature elastin fiber. Figure is modified from Kyle et al., 2009.

Silk: Silk protein polymers are spun into fiber by a variety of organisms, including silkworms and spiders (Altman et al., 2003; Kaplan, 1998). Different types of silks have diverse mechanical properties depending on the mixture of proteins and their amino acid composition (Saravanan, 2006; Vepari and Kaplan, 2007). Silk proteins have stacked β-sheet structures separated by glycine-rich amorphous regions (Altman et al., 2003; Kaplan et al., 1994; Kaplan, 1998; Lazaris et al., 2002; Romer and Scheibel, 2008). Because of this arrangement, silks have been considered as semicrystalline materials with amorphous regions as depicted in **Fig. 1.4** (Romer and Scheibel, 2007, 2008; van Hest and Tirrell, 2001).

The assembly process of spider silk protein has been studied extensively *in vivo*. Spider dragline silk proteins are stored in silk-producing glands. Under these conditions, the polyalanine motifs form α-helical structures, whereas glycine-rich regions form β-turns or random-coil conformations. However, during assembly of the fiber, these proteins undergo secondary structure transitions (van Beek et al., 1999). As spider silk protein passes through the spinning duct, it experiences a decrease in pH and an increase in flow rate/shear force. The decrease in pH is thought to contribute to the denaturation of these proteins, whereas the increase in flow rate has been postulated to facilitate protein unfolding, as well as to promote structural transitions of poly(A) and poly(GA) from an α-helical to a stacked β-sheet structure (Hu et al., 2006). Within the stacked β-sheet, β-strands interact with each other via backbone hydrogen bonds and β-sheets are stabilized by van der Waal's forces (Romer and Scheibel, 2008).

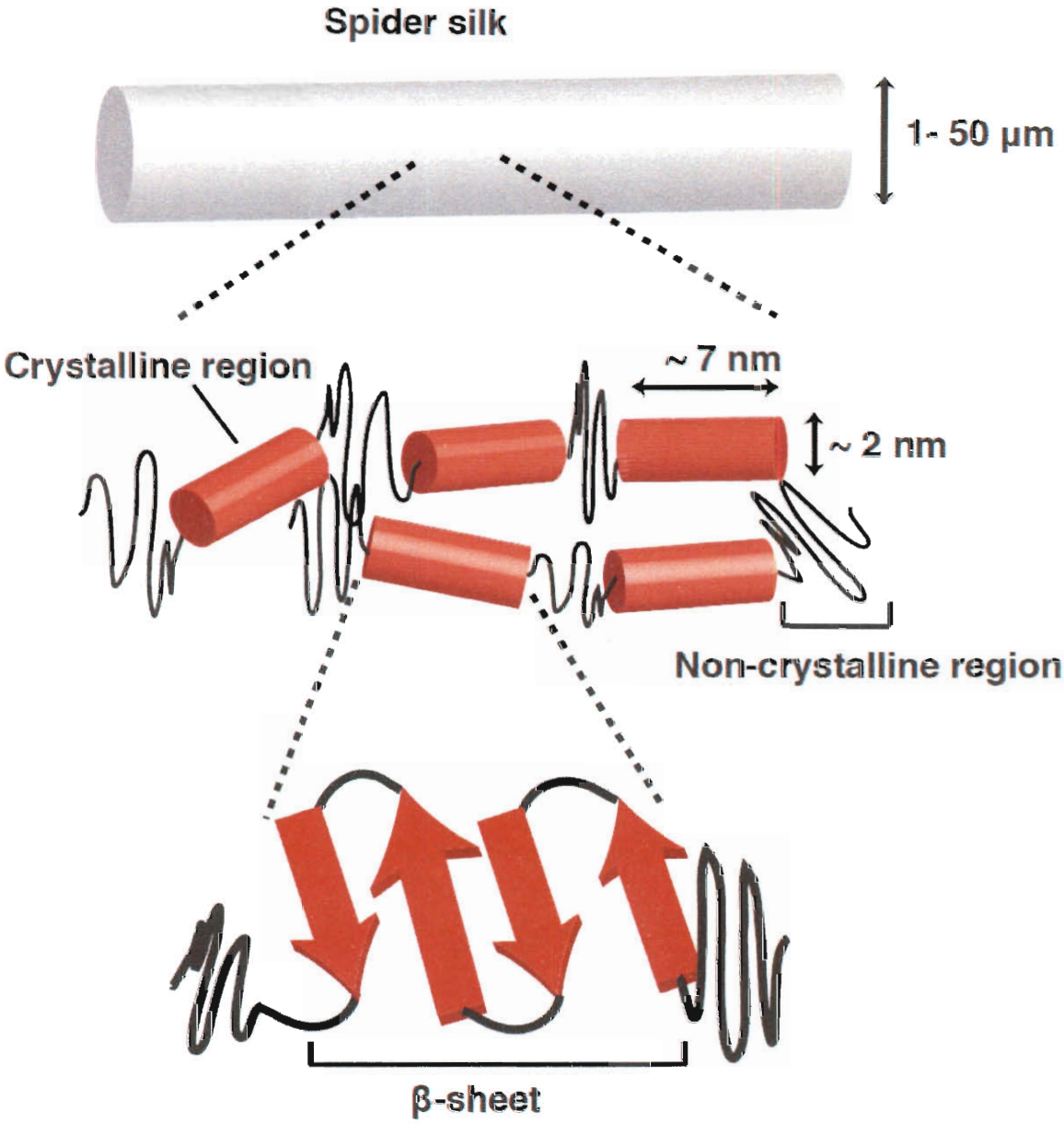

Figure 1.4 Schematic structure of spider major ampullate (MA) silk. MA silk consists of crystalline β-sheet rich subunits (small red cylinders) covalently joined by noncrystalline regions (black lines). The crystalline regions provide strength, and the noncrystalline regions provide ductility. Inspired by Romer and Scheibel, 2008.

1.2.2 Recombinant protein-based materials

Extraction of natural protein-based materials suffers from a variety of limitations. For example, spiders cannot be raised in large groups because of their predatory and solitary behaviors (Kluge et al., 2008). In these circumstances, recombinant production of the material-forming protein in another host is an alternative. A variety of natural material-forming proteins (e.g., silkworm silk, spider silk, elastin, and collagen) have been successfully produced in various recombinant systems in *E. coli*, yeast, and plants (Du et al., 2008; Kyle et al., 2009; Merle et al., 2002; Pakkanen et al., 2003).

Recombinantly produced material-forming proteins can be processed into a variety of morphologies such as fibers, films, hydrogels, capsules, and spheres (Hardy and Scheibel, 2009; Huemmerich et al., 2004; Huemmerich et al., 2006; Nazarov et al., 2004; Rammensee et al., 2006; Rammensee et al., 2008; Slotta et al., 2008). Additionally, recombinant production also enables the design of functional and mechanical properties via sequence engineering, a process that would be slow and difficult in the native organism (Hardy and Scheibel, 2009; Heim et al., 2009; Heim et al., 2010; Leal-Egana and Scheibel, 2010; Rabotyagova et al., 2009; Romer and Scheibel, 2007; Vendrely and Scheibel, 2007; Wright et al., 2005).

1.2.3 Self-assembling peptides

The material-forming capacity of proteins appears to be driven by their amino acid sequences. This observation led to the development of self-assembling peptides that produce materials and mimic the sequence of silk, elastin, or other protein-based materials (Daamen et al., 2007; Gosline et al., 2002; Herrero-Vanrell et al., 2005; Woolfson and Mahmoud, 2010). One advantage of these peptides is their ability to self-

assemble into materials, including fibrils, films and hydrogels, under the appropriate chemical and physical conditions (Cen et al., 2008; Chilkoti et al., 2006; Deming, 2007; Hartgerink et al., 2001; Herrero-Vanrell et al., 2005; Lutolf et al., 2003; Sargeant et al., 2008; Zhang and Zhao, 2004; Zhang et al., 2010). For example, recombinant elastin-like proteins (ELPs) are composed of repeats of elastin sequences, such as VPGXG (Floss et al., 2010; Urry et al., 1998). Like natural elastin, ELPs can coacervate to form more ordered structures under various physicochemical stimuli, including elevated temperature, lowered pH, and increased ionic strength (Li and Daggett, 2003; Nicol et al., 1992; Urry, 1993). ELP fibers and gels have been used as injectable scaffolds for cartilage tissue repair (Betre et al., 2002; Ong et al., 2006) and soft tissue replacement (Srokowski and Woodhouse, 2008).

Recently, a number of *de novo* designed self-assembling peptide systems were chemically synthesized. These peptides are also capable of forming fibrous materials (Hartgerink et al., 2001; Jimenez et al., 2002; Woolfson and Mahmoud, 2010) and other complex structures such as gel, film, vesicles, and nanotubes (**Fig. 1.5**) (Beniash et al., 2005; Galler et al., 2008; Gelain et al., 2006; Kyle et al., 2009; Narmoneva et al., 2005; Silva et al., 2004; Zhang et al., 2010).

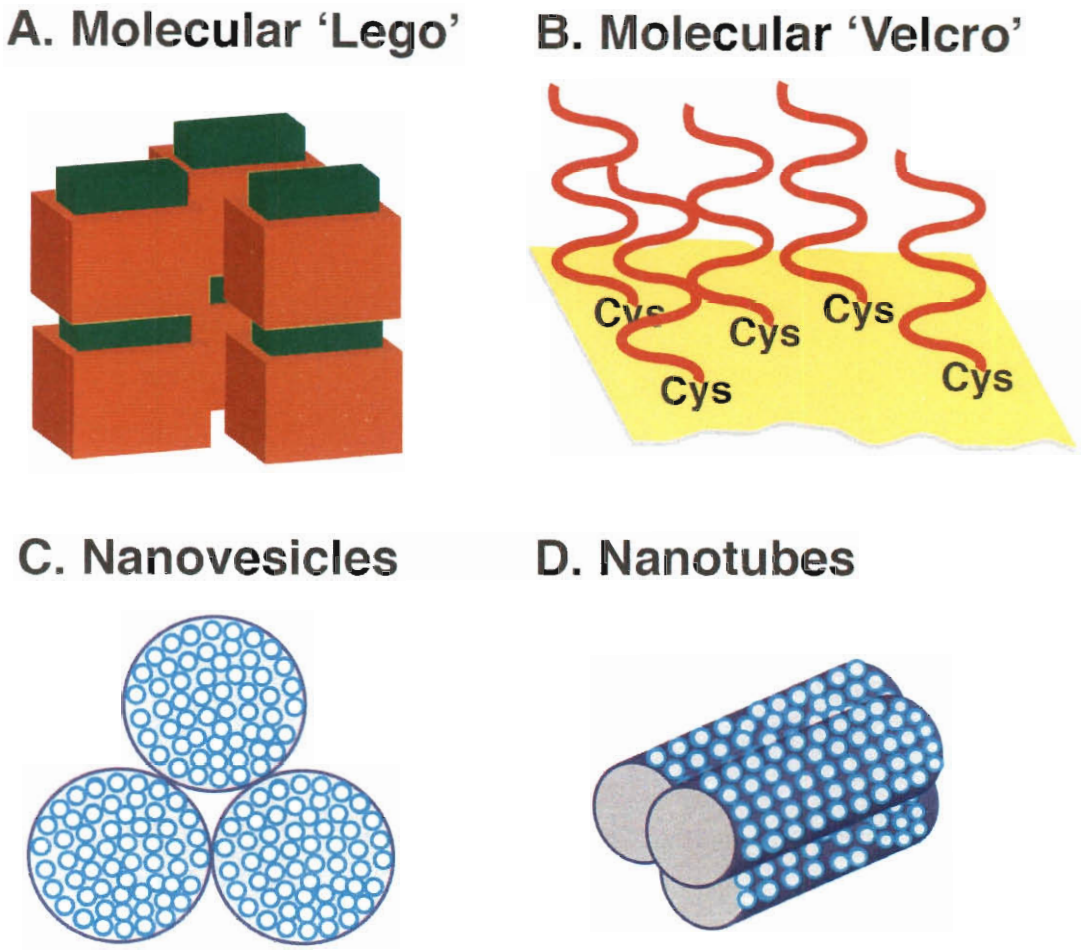

Figure 1.5 Examples of structures produced by self-assembling peptide systems. (A) Molecular 'Lego' contains β-sheet structures formed through interactions between hydrophobic and hydrophilic domains. (B) Molecular 'Velcro' forms monolayers on surfaces through covalent bonds between cysteines and gold atoms. (C) Nanovesicles or (D) nanotubes are formed by the self-assembly of peptides. Modified from Kyle et al., 2009.

1.3 Production methods of protein-based materials

For centuries, protein-based materials such as silk and spider silk fibers could only be produced by their native organisms (Altman et al., 2003). Under ideal circumstances, these proteins should self-assemble into materials *in vitro*, just as they do *in vivo*. In practice, however, most proteins require chemical or physical cues to trigger assembly, as detailed in the following sections. Together, these techniques make it possible to produce a variety of morphologies for various applications (Buttafoco et al., 2006; Kluge et al., 2008; Koh et al., 2008; Lazaris et al., 2002; Yao and Asakura, 2003). It is worth noting, however, that the chemical and physical stress introduced in these techniques may harm the mechanical properties of the resulting materials and preclude incorporation of active proteins via chimeric fusion with the self-assembling protein.

1.3.1 Natural production of protein-based materials

The natural process of producing silkworm silk and spider silk is called "spinning". During spinning, concentrated (up to 50 % w/w) silkworm silk and spider silk protein solutions produced at the secreting gland are forced through a narrow S-shaped duct that generates mechanical forces (Romer and Scheibel, 2008; Vollrath and Knight, 2001) (**Fig. 1.6**). The secretory cells surrounding the spin duct generate chemical changes such as ion exchange, water removal, and acidification (Rammensee et al., 2008; Vollrath and Knight, 1999). Together, these mechanical and chemical stimuli promote spider silk proteins to assemble into fibers that are spun out of the spinneret (Hardy and Scheibel, 2009; Romer and Scheibel, 2008; Vollrath and Knight, 2001; Vollrath et al., 2001). Properties of spider silks are influenced by a number of production conditions. For example, spinning in water produces stiffer and more resilient fibers than natural air-spun

fibers (Guess and Viney, 1998). The size of the spin duct also affects the diameter of the fibers (Xu and Lewis, 1990). Additionally, spinning speed can be controlled to produce fibers of different toughness (Saravanan, 2006; Vollrath and Porter, 2009).

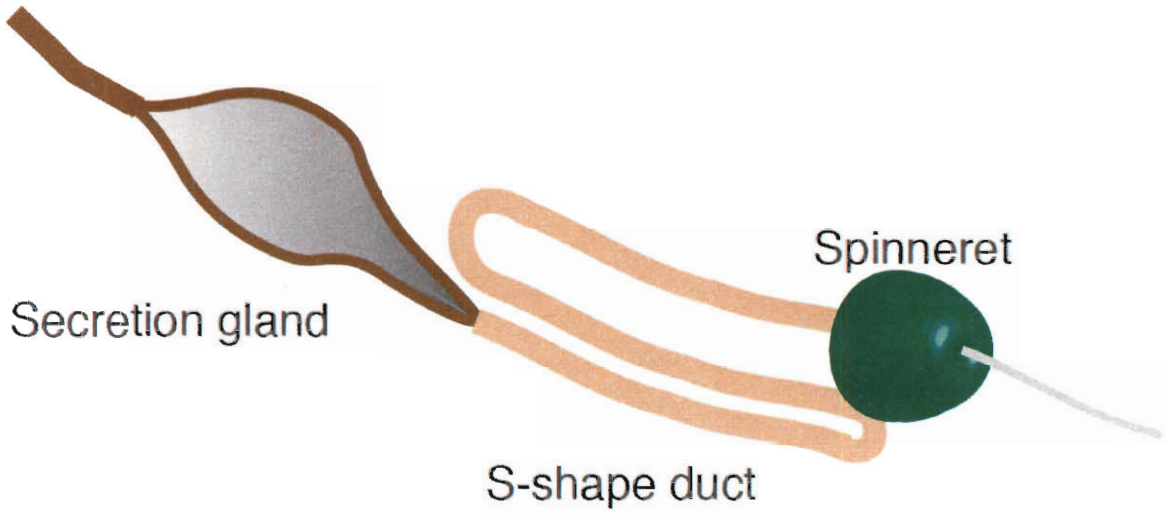

Figure 1.6 Spinning of spider silk. Spider silk proteins are produced at the secretion gland and forced through a narrow S-shaped duct, where mechanical and chemical stimuli promote spider silk proteins to assemble into fibers. Fibers are extruded from the spinneret. Inspired by Saravanan, 2006.

1.3.2 Solvent extrusion

During solvent extrusion, protein is dissolved to form a liquid "dope", which is then passed through a coagulation bath, which solidifies the dope into fibers (**Fig. 1.7A**). The quality of the fibers produced is dependent on the solvents used to dissolve material-forming proteins and the spinning conditions. Commonly used solvents include saturated ammonium sulfate solution, concentrated ortho-phosphoric acid, hexafluoro-2-propanol, hexafluoroacetone hydrate, and formic acid (Matsumoto et al., 1996; Trabbic and Yager, 1998; Um et al., 2001; Um et al., 2004; Xie et al., 2006; Yao et al., 2002). Spinning conditions such as spinning rate and postspinning draw ratio (the percentage of extension

of fibers after being spun) can also be varied (Corsini et al., 2007). Together, varying solvents and spinning conditions enable the production of fibers with different mechanical properties and diameters (Ha et al., 2005; Um et al., 2001; Um et al., 2004). However, the solvents used are harsh, hazardous, or very expensive, which together prevents large scale industrial production (Corsini et al., 2007)

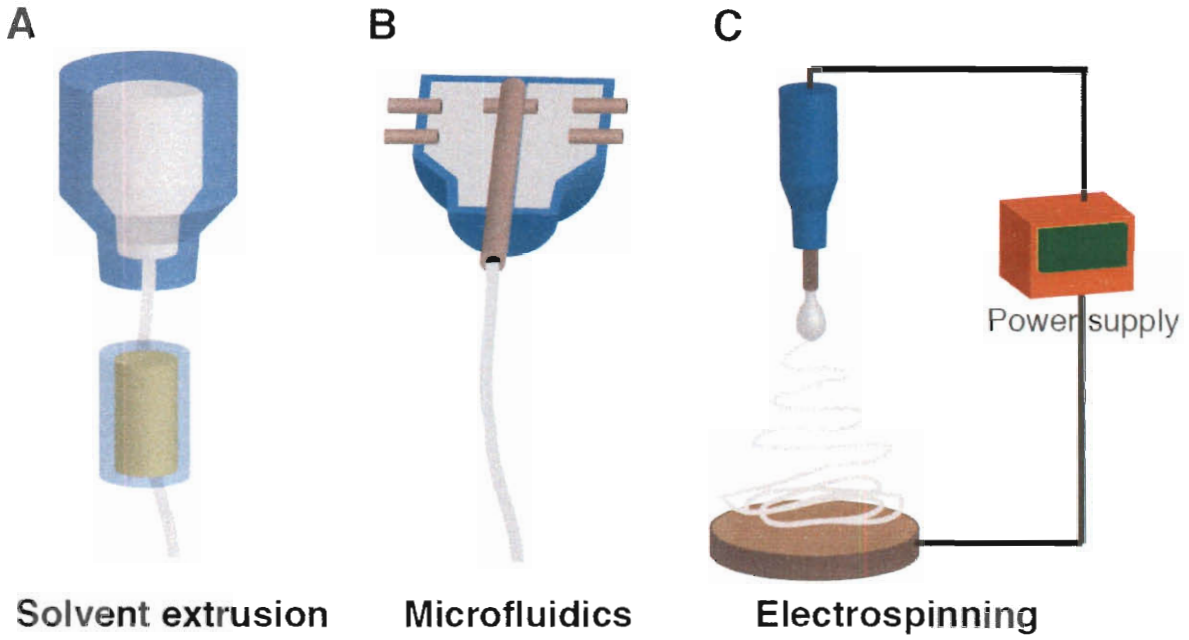

Figure 1.7 Schematics showing different methods used to generate protein-based materials. (A) In solvent extrusion, fibers are drawn though a coagulation bath. (B) Microfluidic devices use narrowing channels and multiple solvent inputs to control the dimension and composition of the fibers produced. (C) Electrospinning processes utilize high voltage and syringe extrusion to generate fibers. Figure is adapted from Kluge et al., 2008.

1.3.3 Microfluidics

Microfluidic devices are used to mimic the chemical and flow conditions found in spider glands (Bettinger et al., 2007; Domachuk et al., 2010; Rammensee et al., 2008). A typical microfluidic device has multiple solvent input channels and a single materials output channel (**Fig. 1.7B**). The presence of multiple input channels enables the fine

control of pH and ion concentrations required for protein assembly, whereas the narrowing output channel generates elongational forces in the direction of the flow, resulting in molecular alignment and fiber formation (Rammensee et al., 2008). Microfluidic devices have been used to study fiber formation under various solvent compositions and flow conditions (Bettinger et al., 2007; Domachuk et al., 2010; Kluge et al., 2008; Rammensee et al., 2008).

1.3.4 Electrospinning

Invented in the first half of the 20th century, electrospinning was developed by Reneker and coworkers to produce small-diameter (40-2000 nm) fibers for various applications (Buttafoco et al., 2006; Reneker and Chun, 1996; Reneker et al., 2000). In electrospinning (**Fig. 1.7C**), a polymer/protein solution is pressed through a thin needle opposite a grounded collecting plate. Under an electric field, the solution becomes charged and is pulled towards the collecting plate. If a sufficiently high voltage is supplied, the solution will overcome the surface tension and travel towards the grounded collecting plate. As solvent evaporates during travel, fibers form and are deposited on the collecting plate in the form of a mesh (Buttafoco et al., 2006; Reneker and Chun, 1996). The solvents used to dissolve proteins in electrospinning are usually volatile, which facilitates the evaporation process during fiber formation. For example, hexafluoro-2-propanol (HFP) has been used in the spinning of collagen and elastin fibers (Boland et al., 2004; Buttafoco et al., 2006). The diameter of the fibers can be controlled by protein concentration and spinning conditions (Li et al., 2005; Shen et al., 2010; Zhang et al., 2009), whereas fiber alignment can be achieved via the use of rotating collectors (Badrossamay et al., 2010; Xu et al., 2004; Yang et al., 2008). The morphologies of these

electrospun meshes mimic the natural extra-cellular matrices, making them applicable as tissue engineering scaffolds (Buttafoco et al., 2006; Chew et al., 2005; Huang et al., 2000; Koh et al., 2008; Li et al., 2005; Xu et al., 2004). The large surface area of these meshes is also suitable for applications such as vascular tissue engineering, which requires a large surface area for seeding the cells (Buttafoco et al., 2006; Ju et al., 2010; Vaz et al., 2005). For example, collagen and elastin have been electrospun into fiber meshes with high porosity and surface area, which have been used for tissue engineering of small diameter blood vessels (Buttafoco et al., 2006; Choi et al., 2010; Ju et al., 2010; Li et al., 2002; Marelli et al., 2010; Sell et al., 2009; Vaz et al., 2005; Xu et al., 2004; Zhu et al., 2010).

1.3.5 Solvent casting/Self-assembly

In solvent casting, protein/peptide molecules are allowed to self-assemble into various morphologies in suitable solvent and environmental conditions. Silk fibroin from silkworm *Bombyx mori* has been cast into films using a variety of solvents that include hexafluoroisopropanol (HFIP) (Zhao et al., 2003), formic acid (Um et al., 2001), and trifluoroacetic acid (Ha et al., 2005). Silk fibroin can also self-assemble into a hydrogel given suitable environmental conditions (Ayub et al., 1993; Kim et al., 2004; Nagarkar et al., 2010; Nagarkar et al., 2009; Rammensee et al., 2006). During the "Sol-Gel" transition, increases in silk fibroin concentration and temperature can accelerate cross-linking and assembly. A decrease in pH also results in shorter gelation time by reducing repulsion between silk fibroin monomers (Kim et al., 2004).

1.4 Essential features of protein-based materials

Protein-based materials have been used in a variety of applications, including drug delivery, surgical sealants and tissue engineering (Deming, 2007; Place et al., 2009). These applications require materials to be compatible with biological systems (Astbury and Woods, 1934; Grevellec et al., 2001; Rodriguez-Cabello et al., 2007; Velema and Kaplan, 2006) and to exhibit diverse morphologies, suitable mechanical properties, and appropriate functional properties (Maskarinec and Tirrell, 2005).

1.4.1 Biocompatibility

The behavior of biomaterials when interacting with the surrounding environment *in vivo* (cells, tissues, organs) is often called biocompatibility (Remes and Williams, 1992; Sierpinski et al., 2006; Williams, 2008). For any materials designed to interact with biological systems, low level toxicity, inflammation, and immunogenic responses are critical (Crawford and Hatton, 2008; Williams, 2008, 2009). In applications where biomaterials are intended to interact with cells and body fluids, biocompatibility tests need to be carried out using *in vitro* cell cultures, *in vivo* animal models, and clinical trials (Babensee et al., 1998; Ghanaati et al., 2010; Williams, 2008).

In vitro testing is commonly used as the first step of biocompatibility screening, which involves the evaluation of toxicity and cellular responses caused by materials. To examine the toxicity of the materials and the molecules leached from materials, *in vitro* cell viability tests such as contact assays and elution assays can be used. The growth and morphology of cells can also be monitored to evaluate a number of cellular responses to materials, such as adhesion, migration, and proliferation (Babensee et al., 1998; Ghanaati et al., 2010; Williams, 2008). This approach is relatively inexpensive and fast, making it

suitable as the first step of biocompatibility testing. However, since these *in vitro* systems lack the complex interactions that are present in body, additional tests *in vivo* are required (McGrath and Kaplan, 1997; Remes and Williams, 1992; Williams, 2009).

Following initial *in vitro* tests, successful materials are tested in animal models, which can be classified as either non-functional tests or functional tests (Remes and Williams, 1992; Williams, 2008). In non-functional tests, materials are inserted to soft tissues (e.g., silk fibers in connective tissue) for the examination of potential complications. In functional tests, materials are inserted to the targeted site (e.g., collagen mesh to wounds) to assess the efficacy of the materials. Although animal models enable the examination of biocompatibility in the presence of complex *in vivo* interactions, testing materials in animal models is expensive and cannot guarantee their biocompatibility in humans. However, it is a necessary step prior to clinical trials (Babensee et al., 1998; Crawford and Hatton, 2008; Ghanaati et al., 2010; McGrath, 1997), which form the final step before a material is available to the general public. During clinical trials, biomaterials are implanted into patients, and a variety of parameters, dependent on the specific use, are thoroughly monitored (Babensee et al., 1998; Place et al., 2009; Stegemann et al., 2007; Williams, 2008).

1.4.2 Diverse morphologies

Protein-based materials can adopt a variety of morphologies. For example, recombinant silk proteins can be processed into fibers (Rammensee et al., 2008), films (Huemmerich et al., 2006; Junghans et al., 2006; Metwalli et al., 2007), foams (Romer and Scheibel, 2007), hydrogels (Rammensee et al., 2006), capsules (Hermanson et al., 2007a; Hermanson et al., 2007b) or spheres (Lammel et al., 2008; Slotta et al., 2008).

These morphologies enable a variety of applications in drug delivery and tissue engineering (Agapov et al., 2009; Dutta and Dutta, 2009; Fan et al., 2009; Lee and Mooney, 2001; Liebmann et al., 2008).

Fibers/meshes: Silkworm silk and spider silk fibers have been used as surgical sutures (McGrath and Kersey, 2009; Moy et al., 1991). When woven or electronspun into meshes, these protein fibers can also be used as scaffolds for a variety of tissue engineering applications (Beachley and Wen, 2010; Neal et al., 2009; Schneider et al., 2009). The diameter of fibers and their arrangement within the mesh can affect various parameters, including cell shape, spreading, proliferation, and differentiation (Badami et al., 2006; Beachley and Wen, 2010; Xu et al., 2004).

Films: Protein films represent an interesting form of materials with a wide range of potential in fields ranging from medicines to electronics (Kim et al., 2010; Parker et al., 2009). Silk fibroin films enhance healing compared to conventional dressings (Sugihara et al., 2000) and have been used in corneal tissue engineering (Lawrence et al., 2009). Additionally, silk fibroin films have been used as scaffolds to immobilize enzymes (Demura et al., 1992) and have been employed as a platform for transistors, photonic devices, and ultrathin electronic circuits (Amsden et al., 2009; Kim et al., 2009; Parker et al., 2009).

Hydrogels: Hydrogels are networks of molecules that have high water content and porosity, thereby mimicking the extracellular matrix component of the human body (Jhon and Andrade, 1973). Hydrogels can be made from polymers, proteins, and peptides and are used in tissue engineering and drug delivery (Dutta and Dutta, 2009; Lee and Mooney, 2001). Collagen gels are used for reconstruction of various organs such as liver

(Kaufmann et al., 1997), skin (Auger et al., 1998), blood vessels (Seliktar et al., 2000), and small intestine (Lee and Mooney, 2001; Voytik-Harbin et al., 1998). Gelatin gels have been utilized for delivery of growth factors, which promote vascularization (Yamamoto et al., 1999). Hydrogels assembled from peptides that mimic natural materials have also demonstrated potential in tissue engineering (Dutta and Dutta, 2009; Lee and Mooney, 2001; Urry et al., 1998).

1.4.3 Suitable mechanical properties

Each potential application of protein-based materials requires very specific mechanical properties. For example, elastin is very extensible and is found in heart valves and blood vessels, sites where elasticity and resistance to fatigue are required. Collagen has suitable tensile stress for tissues such as bone, cartilage, and tendon (Faury, 2001; Martyn and Greenwald, 2001; Pasquali-Ronchetti and Baccarani-Contri, 1997). Many mechanical properties of materials can be described by their stress-strain curves. For example, spider dragline silk and elastin have distinctive mechanical properties as indicated by their stress-strain curves (**Fig. 1.8**).

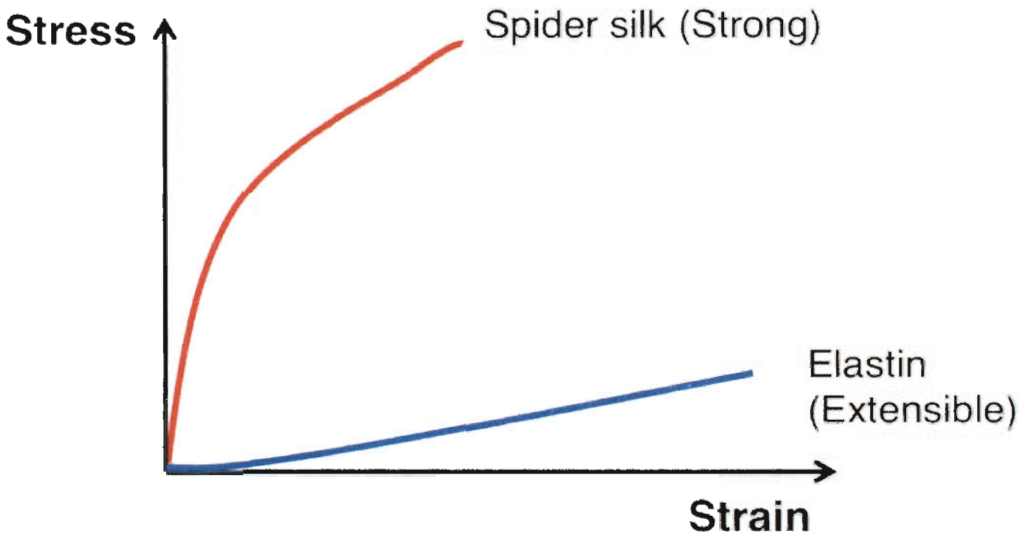

Figure 1.8 Schematic depicting differences in the stress-strain curves of spider dragline silk and elastin fibers. Stress is the force experienced per unit area of the cross-section. Strain is the extended length divided by initial length. Spider silk (dragline) is strong, able to withstand high stress before breaking. Elastin fibers are extensible, able to be stretched greatly before breaking. This diagram is not to scale.

Cells can sense the mechanical properties of their surroundings via mechanotransduction receptors. These transmembrane receptors have intracellular domains that interact with the cytoskeleton and extracellular domains that bind to the extracellular matrix (Vogel, 2006; Vogel and Sheetz, 2009). Under tension, the kinase active sites of these receptors are exposed and activated, resulting in the transduction of mechanical signals into biochemical signals that trigger cellular responses such as adhesion, proliferation, differentiation, and apoptosis (Helenius et al., 2008; Vogel, 2006; Vogel and Sheetz, 2009).

In vitro, differentiation of naive mesenchymal stem cells (MSCs) is extremely sensitive to the elasticity (also called stiffness) of the surroundings. For example, soft brain-like matrices (elasticity = 0.1-1 kPa) are neurogenic, stiffer muscle-like matrices (8-17 kPa) are myogenic, and more rigid matrices that mimic collagenous bone (25-40 kPa)

are osteogenic (Engler et al., 2006). *In vivo*, cells can also sense and respond to the mechanical properties of their surrounding tissues/organs. Georges and co-workers (2007) showed that, in carbon tetrachloride-induced liver fibrosis, the increase of liver stiffness leads to an increase in matrix production and deposition by hepatic myofibroblasts (Georges et al., 2007). Together, these results demonstrate that the mechanical properties of scaffold materials must match their target cells and organs (Leal-Egana and Scheibel, 2010).

1.4.4 Incorporation of bioactive molecules into protein-based materials

To permit specific cellular responses, protein-based materials with bioactive components must reproduce the functions of the extracellular matrix (ECM) (Hubbell, 1999; Imen et al., 2009; Sakiyama-Elbert and Hubbell, 2001). The incorporation of bioactive molecules, such as growth factors and cell-binding peptides, into protein-based matrices, either at the surface or the interior (bulk), is a strategy to enable material-cell interactions (Gobin and West, 2002; Halstenberg et al., 2002; Hynd et al., 2007; Imen et al., 2009; Lutolf and Hubbell, 2003, 2005; Rodriguez-Cabello et al., 2006; West and Hubbell, 1999).

Surface immoblization: Surface immobilization can be achieved by physical adsorption driven by a variety of interaction types or by covalent attachment (Beachley and Wen, 2010). Covalent immobilization at the surface of materials can be achieved by chemical- or radiation-induced cross-linking, both of which generate efficient coating and long-term retention of the activity of biomolecules (Kim et al., 1998; Koh et al., 2008; Kuhl and Griffith-Cima, 1996). For example, mouse EGF, covalently linked to glass via polyethylene oxide, retains its native functions (Kuhl and Griffith-Cima, 1996). Acryloyl-

PEG-RGD can be linked to PEG-diacrylate-based hydrogels via irradiation (Hahn et al., 2005). In both cases, cross-links form between a chemical moiety attached to the bioactive molecule and a target attached to the biomaterials. However, cross-linking may occlude the active site of the protein or prevent the motion required for function, thereby compromising activities (Bini et al., 2006; Cigada, 2008; Leal-Egana and Scheibel, 2010; Qiu et al., 2009).

Bulk incorporation: Compared to surface modification, bulk incorporation methods generate a higher level of incorporation and improved bioactivity (Beachley and Wen, 2010). Proteins can be incorporated into bulk materials via direct mixing, electrospinning, or direct gene fusion (Beachley and Wen, 2010; Bini et al., 2006; Huang et al., 2007; Nagaoka et al., 2010; Yanagisawa et al., 2007). During direct mixing, proteins (e.g., enzymes, myoglobin, and growth factors) can be mixed with silk fibroin during casting to generate biologically functional films (Hofmann et al., 2006; Lawrence et al., 2008; Wu et al., 2006; Zhang, 1998). In electrospinning, growth factors can be mixed with polymers and electronspun into nanofibers that favor bone marrow stem cell attachment and subsequent proliferation (Buttafoco et al., 2006; Sahoo et al., 2010). In the gene fusion approach, the DNA sequence coding for a peptide/protein of interest can be fused to a material-forming protein to enable recombinant production of a chimeric peptide/protein that can be processed into materials. For example, recombinant silk fused with collagen or fibronectin adhesion sequences (RGD) can generate materials that have cell adhesive abilities (Yanagisawa et al., 2007). Similarly, recombinant mussel adhesive protein fused with RGD sequences can be processed into materials with enhanced cell adhesion and spreading abilities (Hwang et al., 2007; Hwang et al., 2010). Recently, the

carboxyl terminal domain of dentin matrix protein 1 has been fused to recombinant spider silk protein to produce a chimeric protein, which has both the self-assembly properties of spider silk proteins and the nucleation ability of dentin (Huang et al., 2007). However, this gene fusion approach has only been successful for fusion of peptides or unfolded proteins (Bini et al., 2006; Huang et al., 2007).

1.4.5 Spatial arrangement of bioactive molecules in protein-based materials

The spatial arrangement, surface density, and distribution of biomolecules within biomaterials have been demonstrated to provide cues for cell responses (Falconnet et al., 2006; Healy et al., 1996; Maheshwari et al., 2000; Rajagopalan et al., 2004). A wide range of methods has been employed to create spatial patterns of bioactive molecules in biomaterials, including microcontact printing, microfluidic patterning, photolithography, plasma polymerization, photoimmobilization, stencil assisted patterning, jet printing, and laser-guided writing (Falconnet et al., 2006; Folch and Toner, 2000; Hahn et al., 2005; Shin, 2007; Wong et al., 2004). For example, silk film surfaces can be patterned using soft lithographic methods to produce high-resolution features such as microfluidic channels, hexagonal patterns, and nano-patterned diffraction gatings (Bettinger et al., 2007; Gupta et al., 2007; Lawrence et al., 2008). PEG-based hydrogel surfaces can be patterned by confocal-based laser scanning lithography to create patterns of peptides that promote cell adhesion (Hahn et al., 2005). However, these patterning approaches usually require chemical attachment of peptides and proteins in biomaterials, using harsh conditions such as high temperatures, high voltages, exposure to organic chemicals, and/or extreme pHs (Falconnet et al., 2006; Hahn et al., 2005). These conditions can compromise the activity of bioactive molecules.

1.5 Ubx as a novel protein-based material

1.5.1 Limitations of existing protein-based biomaterials

Existing approaches to covalently incorporate biomacromolecules usually require chemical cross-linking (Kim et al., 1998; Kuhl and Griffith-Cima, 1996) or radiation-induced cross-linking (Hahn et al., 2005), which are costly additional processing steps that may compromise the activity of the biomolecules and may generate toxic or harmful byproducts. In contrast, direct fusion of peptides or proteins to the self-assembling protein would create active, permanently functionalized materials in a single production step (Bini et al., 2006; Huang et al., 2007; Hwang et al., 2007). However, during production of biomaterials from recombinant monomers, harsh conditions such as high temperatures, exposure to organic chemicals, or extreme pH are often employed to stimulate protein assembly (Bini et al., 2006; Dror et al., 2008; Lazaris et al., 2002; Wright et al., 2005). Such conditions are expected to compromise the function of bioactive molecules and may also leave toxic residues. Therefore, for the simplicity of materials production and retention of protein functions within materials, it is highly advantageous to establish mild conditions for the assembly of protein-based materials.

1.5.2 Native function of Ubx as a transcription factor

Unlike natural material-forming proteins such as keratin, collagen or silk, Ultrabithorax (Ubx) had not been shown to form protein-based materials prior to this study. Although many studies have over-expressed Ubx *in vivo* and subsequently used immunohistochemical approaches to gauge Ubx concentration (Tour et al., 2005; Weatherbee et al., 1999), no evidence of Ubx aggregates has ever been observed *in vivo* even at elevated protein concentrations (Tour et al., 2005; Weatherbee et al., 1999).

Furthermore, no evidence of aggregation has been observed at the high concentrations generated in *E. coli* during protein production for purification. Therefore, it is unlikely that these oligomeric materials form as part of the natural function of Ubx.

Ubx is a member of the Hox protein family that is involved in development and specification of body plans (Hughes and Kaufman, 2002; Lewis, 1978). As a transcriptional factor, Ubx binds DNA via its homeodomain and subsequently activates or represses transcription through heteromeric protein interactions (Cen et al., 2008; Galant and Carroll, 2002). Ubx homomeric interactions also occur *in vivo* upon binding a subset of Ubx-regulated enhancers that contain multiple DNA-binding sites arrayed in tandem (Beachy et al., 1993).

1.5.3 The potential of Ubx as a novel protein-based material

Purified Ubx is highly prone to aggregation into amorphous flocculates (Bondos and Bicknell, 2003). While searching for conditions that inhibit amorphous aggregation, we fortuitously discovered that Ubx has the ability to assemble into materials of various morphologies under mild, aqueous conditions (Greer et al., 2009).

The easy availability and capacity of Ubx to form materials easily at much lower protein concentration and under non-denaturing, mild conditions provides new avenues for characterizing and engineering protein-based materials. First, the recombinant protein system enables rapid and large-scale production of protein materials. Second, recombinant production enables sequence engineering, which allows incorporation of peptides/proteins and modulation of mechanical properties via sequence changes. Finally, the lower protein concentration requirement and mild conditions enable facile production

of materials and also facilitate retention of solubility and function for biomolecules incorporated into the protein materials.

1.5.4 Research summary

During my thesis project I have (i) established the conditions required for the assembly of Ubx-based materials, (ii) generated a wide range of Ubx morphologies, (iii) examined the mechanical properties of Ubx fibers, (iv) added protein functions to Ubx-based materials via gene fusion, (v) patterned protein functions within the Ubx materials, and (vi) examined the biocompatibility of Ubx materials *in vitro*.

Ubx can be produced recombinantly to yield 5 mg of monomeric Ubx per gram of *E. coli* cells, enough to generate 2 m of Ubx fibers. Unlike recombinant spider silk proteins that rapidly mis-assemble (Sarvanan et al., 2006), active Ubx protein can be stored in solution at 4 ºC for days or frozen at -80 ºC for months. Ubx self-assembles in a hierarchical manner to form a variety of macroscale structures that have defined nanoscale features. Ubx fibrils interact to form fibers, films, and sheets. These structures can be manually combined to generate more complex three-dimensional architectures such as thick fibers, bundles and twists. The tensile stress and the elasticity of Ubx fibers are comparable to or exceed that of elastin fibers, making it a potential candidate for a variety of applications. Ubx chimeric materials can incorporate protein functions via gene fusions. Since neither high protein concentrations nor harsh chemical / physical processing are required for the production of Ubx materials, the activities of the appended proteins are retained. Spatial patterning of protein functions in Ubx chimeric materials can be achieved using surface arrangement and the adhesion properties of Ubx chimeric materials. Preliminary *in vitro* compatibility testing of Ubx materials indicates low

toxicity and ability for cell attachment, which suggests the potential for its use as a tissue engineering scaffold in the future.

CHAPTER 2

Materials and Methods

2.1 Plasmid constructs

Construction of Ubx truncation and point mutants

Ubx splicing isoform Ia (herein termed "Ubx") was cloned between the *Nde*I and *Bam*HI sites in the pET19b vector (Novagen), which appends a 6xHis-tag and a hydrophilic linker (SerSerGlyGlyHisAspAspAspAspLysHis) to the N-terminus of Ubx. The constructs expressing UbxIa or N-terminal truncations were the gift of Ying Liu (Rice University). To generate C-terminal truncations, two consecutive stop codons to prevent read-through were inserted into the Ubx coding region using the QuikChange site-directed mutagenesis kit (Stratagene). All the Ubx N-terminal and C-terminal deletion mutants utilized in these studies are summarized in **Table 2.1**.

Construction of plasmids encoding Ubx chimeras

To create chimeric proteins, the DNA sequence encoding the selected protein (sperm whale myoglobin, mCherry, EGFP, or firefly luciferase) was amplified using PCR from parental vectors using primers that introduce NdeI sites at both ends of the coding region. The PCR product was ligated with pGEM-T Easy linearized vector (Promega), amplified in GC5 competent cells (Gene Choice) and extracted using Qiagen miniprep kit (Qiagen). The gene of interest in the pGEM-T construct was digested with NdeI, purified using agarose gel-extraction, and the product was inserted into the NdeI site at the N-terminus of the Ubx gene in pET19b vector, followed by a DNA sequence encoding a two amino acid glycine-histidine linker without intervening stop codons. DNA

sequencing was performed to select plasmids that contain the insert with the correct sequence orientation and identity. Constructs of Ubx chimeras are summarized in **Table 2.2**.

Table 2.1 Plasmid constructs containing Ubx truncation and point mutants. The corresponding DNA sequences encoding Ubx (Ubx1a) were inserted between *NdeI* and *BamHI* sites on a pET-19b vector. Ubx 1b was inserted into a pET28a vector.

Name	Description	By
Ubx 1-380	His-tag, linker, and a.a. 1 – a.a. 380 of Ubx 1a	YFL
Ubx 19-380	His-tag, linker, and a.a. 19 – a.a. 380 of Ubx 1a	YFL
Ubx 49-380	His-tag, linker, and a.a. 49 – a.a. 380 of Ubx 1a	YFL
Ubx 88-380	His-tag, linker, and a.a. 88 – a.a. 380 of Ubx 1a	YFL
Ubx 139-380	His-tag, linker, and a.a. 139 – a.a. 380 of Ubx 1a	YFL
Ubx 174-380	His-tag, linker, and a.a. 174 – a.a. 380 of Ubx 1a	YFL
Ubx 216-380	His-tag, linker, and a.a. 216 – a.a. 380 of Ubx 1a	YFL
Ubx 235-380	His-tag, linker, and a.a. 235 – a.a. 380 of Ubx 1a	YFL
Ubx 216-356	His-tag, linker, and a.a. 216 – a.a. 356 of Ubx 1a	ZH
Ubx 216-344	His-tag, linker, and a.a. 216 – a.a. 344 of Ubx 1a	ZH
Ubx 1-356	His-tag, linker, and a.a. 1 – a.a. 356 of Ubx 1a	ZH
Ubx 1-344	His-tag, linker, and a.a. 1 – a.a. 344 of Ubx 1a	ZH
Ubx 1-243	His-tag, linker, and a.a. 1 – a.a. 243 of Ubx 1a	ZH
Ubx 1-216	His-tag, linker, and a.a. 1 – a.a. 216 of Ubx 1a	ZH
Ubx 19-243	His-tag, linker, and a.a. 19 – a.a. 243 of Ubx 1a	ZH
Ubx 49-243	His-tag, linker, and a.a. 49 – a.a. 243 of Ubx 1a	ZH
Ubx 88-243	His-tag, linker, and a.a. 88 – a.a. 243 of Ubx 1a	ZH
Ubx 139-243	His-tag, linker, and a.a. 139 – a.a. 243 of Ubx 1a	ZH
Ubx 1b 6CA	Ubx 1b, all 6 cysteines were changed to alanines	YFL

Linker: SerSerGlyGlyHisAspAspAspAspLysHis. YFL is Ying Frances Liu.

Table 2.2 Plasmid constructs containing Ubx chimeras. On pET19b, appended proteins were inserted between *NdeI* sites of pET19b; Ubx was inserted between the *NdeI* site and *BamH1* site.

Name	Description	By
EGFP-Ubx	His-tag-linker[a]-*NdeI* site-EGFP-gly-his-*NdeI* site-Ubx-stop-*BamH1* site	ZH
mCherry-Ubx	His-tag-linker-*NdeI* site-mCherry-gly-his-*NdeI*-Ubx-stop-*BamH1* site	ZH
Myo-Ubx	His-tag-linker-*NdeI* site-SW Mb[b]-gly-his-*NdeI*-site-Ubx-stop-*BamH1* site	ZH
Myo6468-Ubx	His-tag-linker-*NdeI* site-SW Mb H64Y V68F-gly-his-*NdeI* site-Ubx-stop-*BamH1* site	ZH
Luci-Ubx	His-tag-linker-*NdeI* site-Firefly luciferase-gly-his-*NdeI* site-Ubx-stop-*BamH1* site	ZH
Ubx-EGFP	His-tag-linker-*NdeI* site-Ubx-*BamH1* site-EGFP-stop-*BamH1* site	ZH
Azurin-Ubx	His-tag-linker-*NdeI* site-*Pseudomonas aeruginosa* azurin-gly-his-*NdeI*-site-Ubx-stop-*BamH1* site	ZH

[a]Linker: SerSerGlyGlyHisAspAspAspAspLysHis
[b]SW Mb: sperm whale myoglobin

2.2 Molecular biology protocols

Polymerase chain reaction (PCR)

Typical PCR reactions consisted of 10 ng of template DNA (plasmid), 1x PfuUltra buffer (Stratagene), 200 μM of dATP, dCTP, dGTP, dTTP, 0.5 μM of forward and backward primers, and 10 units of Pfu polymerase (Stratagene). Typically, each PCR reaction was 50 μl in volume. The primers were designed to a length of 20~30 nucleotides, a GC content of 40~60%, and a melting temperature of 55~65°C.

Typical PCR cycle parameters were: 95°C for 2 min, then 30 cycles of 95°C for 1 min, anneal at 5°C lower than the melting temperature of primer for 1 min, 68 °C for 1 min per Kb amplified. Reactions were given a final 5 min extension at 68°C and stored at 4°C prior to collection.

PCR-based site-directed mutagenesis

Quik Change PCRs were used to introduce stop codons within the sequence of Ubx to generate C-terminal truncation mutants. Primers were 35 to 40 bases long and contained the intended mutation in the middle, with flanking sequences matching the target gene. The melting temperature of the primer was calculated using Stratagene's Quik T_m calculator, and the primer sequence was fine-tuned to bring the melting temperature to approximately 75 °C. To avoid excessive self-annealing, M-fold was used to predict secondary structure and annealing energy. The primer is optimized so that M-fold simulations produce a folded DNA with a free 3′ end and a ΔG for self-annealing that is more positive than -1.2 kcal/mol, at a folding temperature of 50°C. Quick change PCR amplification results in the formation of circular, nicked double stranded DNA.

The products of Quik Change PCR were treated with DpnI, an endonuclease that digests the methylated parental DNA template. The circular, nicked double-stranded DNA was purified using PCR purification kit (Zymo) and transformed into GC5 competent cells (Gene Choice).

Agarose gel electrophoresis

DNA samples were diluted in loading buffer (6x stock: 50% glycerol, 50 mM Tris-HCl pH 8.0, 10 mM EDTA, 0.25% Bromophenol blue) and loaded onto 0.8% to 1.2% agarose gels made with 1X TAE buffer (50x TAE stock: 2 M Tris base, 5.7%

glacial acetic acid, 50 mM EDTA, pH 8.0). Ethidium bromide was added to the agarose gel to a final concentration of 0.5 μg/ml. DNA samples were electrophoresed in 1x TAE running buffer at 90-120 V, and ethidium-stained DNA was visualised using a UV light source.

Restriction enzyme digestion

DNA was digested in 20 μl volumes, using 1~2 μg of DNA, 2 μl of recommended 10x reaction buffer and 5 units of restriction enzyme (NEB). Reactions were incubated at 37°C for at least 3 hours. Vector digests were treated with Calf Intestinal Phosphatase (New England Biolabs) for an additional 30 min to reduce self re-ligation and heat inactivated at 65°C for 5 min.

Separation and extraction of digested DNA from agarose gel

Restriction enzyme-digested DNA, vectors and inserts, were separated by electrophoresis. The amount of DNA was estimated by comparing band intensity with molecular weight markers of known quantities. Using the molecular weight of DNA species provided by the manufacturer (New England Biolabs), the molar concentration of DNA was calculated using:

$$[\textit{DNA molar concentration}] = \textit{Mass/Molecular weight} \qquad \text{Equation 2.1}$$

Plasmid DNA was extracted and purified using a Qiagen Gel-extraction kit following manufacturer's instructions.

Ligation

DNA fragments were ligated using T4 DNA ligase (NEB) following the manufacturer's instructions. A reaction containing only the digested vectors was included for control of religation. Using established DNA concentrations, an insert to vector molar

ratio between 3:1 and 6:1 and a final DNA concentration of 10 to 50 ng/μl was used for ligation at 16°C overnight and stored at 4°C until transformation.

TA ligation into pGEM-T easy linear vectors

Direct restriction digestion of PCR products is sometimes inefficient, compromising subsequent ligation. To circumvent this problem, PCR products can be ligated to linearized vectors containing 3′ T overhangs (pGEM-T Easy Vector, Promega), which greatly improves the efficiency of ligation. If blunt-ended PCR products were used (generated by Pfu or other proof reading polymerase), an A-tailing procedure was required before the ligation reaction (for details of A-tailing, see pGEM-T Easy Systems Manual, Promega). A TA ligation reaction contains 1 μl of rapid ligation buffer, 1 μl of pGEM-T easy vector, 3-5 μl of PCR product, 1 μl of T4 ligase (NEB), and nuclease-free water (Fisher Scientific) to a final volume of 10 μl. Of the TA ligation reaction, 2 μl was transformed to GC5 cells (Gene Choice) and plated on X-Gal Amp plates. White colonies indicate potential incorporation of the PCR product, for which identity can be confirmed by restriction digest of the purified plasmid DNA and subsequent DNA sequencing.

Transformation of plasmid DNA into *E. coli*

Chemically competent cells (Sigma) were thawed on ice. Plasmid DNA (50 ng) or up to 5 μl of a ligation reaction was incubated with 50 μl of competent cells for 10 min on ice in pre-chilled 1.5 ml Eppendorf tubes. Samples were then heat-shocked at 42 °C for 45 s and returned briefly to ice. Luria Broth (LB) medium (200 μl) was added and the tubes incubated, with shaking, for 45 min at 37 °C. Between 50 and 200 μl of the reaction was plated onto LB plates containing appropriate antibiotics (200 μg/ml for ampicilin, 30 μg/ml for chloramphenicol) for plasmid selection. Plates were incubated at 37 °C

overnight.

Plasmid extraction

Single *E. coli* colonies containing the plasmid of interest were used to inoculate 5 ml cultures of sterile LB broth containing the appropriate antibiotic. Cultures were incubated, shaking at 37 °C overnight. Plasmids were extracted using Qiagen Miniprep kits. The identity of the plasmid was confirmed by restriction enzyme digest followed by DNA sequencing.

DNA sequencing

Plasmid DNA samples to be sequenced were prepared using Qiagen miniprep kits following manufacturer's instructions, eluted in nuclease-free water (Sigma) and sequenced by the sequencing facility at SeqWright (Houston). Each construct was sequenced in both the 5′ to 3′ and 3′ to 5′ directions using the T7 start and T7 termination sequencing primers (SeqWright), which recognize sequences within the pET19b vector.

2.3 Protein expression protocols

Expression of Ubx full length and deletion mutants

Plasmid constructs were transformed into BL21(DE3)pLysS *E.coli* cells. *E. coli* cultures were cultivated in LB plus 200 μg/ml carbenicillin and 30 μg/ml chloramphenicol at 37 °C. For expression, 10 ml of an overnight culture, inoculated from a single colony, was used to inoculate a 1L LB culture, which was grown to an optical density of 0.6-0.8 at 600 nm. Cell cultures were then cooled to 30°C, and Ubx expression was induced with 1 mM IPTG prior to a further 105 minutes of fermentation. Cells were harvested by centrifugation at 7000 x g for 15 minutes and stored at -20°C in aliquots

corresponding to 1 L of culture. The expression condition and yield for Ubx is listed in **Table 2.3**.

Expression of Ubx chimeras

The resulting vector containing the chimeric DNA was transformed as described previously (Greer et al., 2009), but Rosetta cells (Novagen) were sometimes used instead of BL21(DE3)pLysS cells to improve protein yield. *E. coli* cultures were cultivated in Luria broth plus 50 mg/ml carbenicillin and 30 mg/ml chloramphenicol (LB) at 37 °C unless otherwise stated. For expression, 10 ml of an overnight culture, inoculated from a single colony, was used to inoculate a 1 L LB culture, which was grown to an optical density at 600 nm of 0.6-0.8. Cell cultures were then cooled to 30 °C, and Ubx expression was induced with 1 mM IPTG for 4 hours. Cells were harvested by centrifugation at 7000 x g for 15 minutes and stored at -20°C in aliquots corresponding to 1 L of culture. The expression conditions and protein yields for Ubx chimeras are summarized in **Table 2.3**.

Table 2.3 Protein expression conditions and corresponding yields

Proteins	Expression condition	Yield (mg/L)
Ubx	2.5 h at 37 °C	4
EGFP-Ubx	3 h at 28 °C	8.3
mCherry-Ubx	16 h at 18 °C	20
Myoglobin-Ubx	16 h at 22 °C	8.2

2.4 Protein purification protocols

Affinity purification using nickel-agarose resin

His-tagged Ubx, Ubx fragments, and chimeric proteins were purified using Ni-NTA affinity purification to obtain proteins of greater than 80% purity. Cell pellets were thawed at room temperature and lysed in 20 ml of lysis buffer (50 mM sodium phosphate buffer, pH 8.0, 5% glucose w/v, 500 mM NaCl, 1 protease inhibitor tablet (Roche), 0.8 mg/L DNase I). Cell lysates were centrifuged at 18000 x g for 20 minutes. The supernatant was loaded on a nickel-nitrilotriacetic acid (Ni-NTA) agarose resin column containing 2.5 ml of original resin slurry (Qiagen), which was pre-equilibrated with 20 ml of equilibration buffer (5% glucose w/v, 500 mM NaCl, 50 mM sodium phosphate buffer, pH 8.0). The column was then washed by 10 column volumes of W1 buffer, 10 column volumes of W2 buffer, and 5 column volumes of W3 buffer (equilibration buffer containing 20 mM, 40 mM, and 80 mM imidazole, respectively). Protein was then eluted with 10 ml of elution buffer (200 mM imidazole dissolved in equilibration buffer). All fractions were analyzed using SDS-PAGE. The concentrations of the purified Ubx samples were determined using the Coomassie-blue-based Bradford protein assay from BioRad. Approximately 2 mg of DTT was added to each 1 ml elution volume to maintain the protein in the reduced state. Purified Ubx was dialyzed (twice, each time 1 hour) into 1 L freezing buffer (300 mM NaCl, 50 mM sodium phosphate buffer, 5% glucose, 1 mM DTT pH 7.5) using dialysis membrane with 10 kD cut off (Spectra/Por) hydrated in freezing buffer. Dialyzed protein solutions were concentrated using a Vivaspin 20 protein concentrator with 10 kD cut off (Sartorius Stedim) before storage at -80°C.

Cation exchange purification using phosphocellulose resin

Ubx chimeric proteins were purified using the nickel column followed by phosphocellulose chromatography to achieve greater than 75% purity. Phosphocellulose mimics the sugar-phosphate backbone of nucleic acids, which binds the DNA binding homeodomain of Ubx at low salt concentrations. Proteins were eluted from the column at high salt concentrations.

Protein purified on the Ni-NTA column was dialyzed into buffer P (containing 5% glucose, 1 mM DTT, 0.1 mM EDTA, 25 mM NaH_2PO_4, 250 mM NaCl, pH 6.8). The phosphocellulose column (~2 ml column volume) was equilibrated with 10 column volumes of buffer P before loading protein samples. The column was sequentially washed in 10 column volumes each of buffer P containing a total of 250 mM, 500 mM, 750 mM, or 1 M NaCl. Protein was eluted using 5 column volumes each of buffer P containing 1.5 M or 2 M NaCl. All fractions were analyzed using SDS-PAGE. Purified protein was dialyzed into freezing buffer (300 mM NaCl, 50 mM sodium phosphate buffer, 5% glucose, 1 mM DTT pH 7.5) and concentrated using a Vivaspin 20 protein concentrator with 10 kD cut off (Sartorius Stedim) before storage at -80°C.

Obtaining pre-purified proteins

Purified sperm whale myoglobin was kindly supplied by Dr. John S. Olson, and firefly luciferase was obtained from Promega (QuantiLum® Recombinant Luciferase).

2.5 Protein analysis methods

Staining of Ubx fibers

Izit Crystal Dye (Hampton Research, 1 ml) that detects protein presence was added to 100 mL of eluted protein on a slide and left for 1-2 hours for fibers to form.

Ropes pulled from these drops were tinted blue, indicating the presence of protein, whereas exhausted drops (*i.e.*, the remaining drop after rope formation) lacked blue color.

SDS PAGE gel-electrophoresis

Protein samples were prepared by adding SDS-PAGE SDS buffer (NuPAGE) to a final concentration of 1x and then heated at 99 °C for 10 minutes. The samples were centrifuged briefly (10 s at 13,000 rpm) and loaded onto 12% Bis-Tris pre-cast gels (NuPAGE). The samples were electrophoresed at 200 V for 50 min using the eletrophoresis apparatus (XCell SureLock) in 1x MOPS SDS running buffer (NuPAGE). Pre-stained molecular weight markers (NEB) were loaded onto each gel.

Coomassie staining

Polyacrylamide gels were incubated with gentle shaking in Coomassie stain (0.1% [w/v] Coomassie brilliant blue, 10% [v/v] glacial acetic acid, 10% MeOH) for a minimum of 45 minutes at room temperature, and then destained by incubation and gentle shaking in destaining solution (10% [v/v] glacial acetic acid, 10% MeOH) at room temperature. The destaining solution was repeatedly exchanged until excess dye was removed.

Western blot analysis

Ubx ropes were solubilized in 4X sample buffer (250 mM Tris-HCl, 40% glycerol, 4% SDS, 4% BME, 0.02 mg/ml bromophenol blue, pH 6.8) by mechanical disruption with a syringe needle followed by repeated cycles of heating (90°C for 30 minutes), vortexing, and sonication (1 minute intervals), with the entire process requiring approximately 2 hours. Ubx monomeric protein was diluted with 4X sample buffer to generate a positive control. Samples were separated using a 12% 29:1 polyacrylamide gel

prior to transfer at 150 V for 20 min to a nitrocellulose membrane (Schleicher & Schuell). Ubx was detected using FP3.38 as the primary antibody at a 1:200 dilution in phosphate buffered saline (White and Wilcox, 1984). Horseradish peroxidase-conjugated goat anti-mouse antibody (Calbiochem, 1:2000 dilution) was used as the secondary antibody.

BioRad assay

The BioRad assay is based on the original Bradford assay (Bradford, 1976). The Bradford agent, Coomassie Brilliant Blue G-250, reacts with basic amino acids and aromatic amino acids exposed at the protein surface to produce a blue color that can be monitored by absorbance at 595 nm. To create a baseline, 1 ml 1X BioRad reagent was placed in a 1 ml plastic cuvette (VWR International), and absorbance at 595 nm was measured. A standard curve of 595 nm absorbance values at different protein concentrations was produced using bovine serum albumin (BSA) (NEB) of known concentrations or by using Ubx of known concentrations (see following secton). The absorbance of protein samples added to 1 ml 1X BioRad solution at 595 nm enables the calculation of the protein concentration using the standard curve.

Magnetic circular dichroism

Magnetic circular dichroism spectra were utilized to produce a standard curve using N-acetyl-tryptophanamide in CD buffer (25 mM NaH_2PO_4, 150 mM NaCl, 5% glucose, pH 7.5) at 25 °C. By comparing the MCD signal of a targeted protein to the standard curve, the tryptophan concentration in protein can be obtained (Holmquist and Vallee, 1973; Liu et al., 2008). Since the number of tryptophan residues in a protein is known, the molarity of the protein can be obtained using the following equation:

$$[Pn] = [Tryptophan]/Number\ of\ tryptophans\ per\ molecule \qquad \text{Equation 2.2}$$

Absorbance at 280 nm was measured for protein of known molar concentration, enabling the calculation of extinction coefficient at 280 nm using equation:

$$\varepsilon_{280} = \frac{A_{280}}{cl} \qquad \text{Equation 2.3}$$

where c is the protein molar concentration and l is the path length.

2.6 Ubx material production methods

Production of Ubx materials using hanging drop

Ubx fibers can spontaneously form at the tip of the purification column. During nickel-affinity purification, a very small volume (1 ml) of elution buffer was used to elute Ubx at very high concentration (≥2 mg/ml). By controlling the flow rate using a two-way valve, fibers can form at the tip of the column overnight.

Production of Ubx materials using sessile drop

A volume of solution containing Ubx or Ubx chimera was placed on the surface of a siliconized cover slip at room temperature. After a 2 to 3 h incubation at room temperature and humidity, a film forms at the air-water interface that can be drawn into fibers using a needle or pipette tip. Details of fiber, bundle, twist and sheet production are described in Greer *et al.* (2009).

Production of Ubx materials using the buffer reservoir method

Ubx or Ubx chimera (~2-4 mg) was pipetted into a Teflon-coated tray (approx. 20 cm x 20 cm x 1 cm) (Nordicware) that was slightly over-filled with buffer (50 mM sodium phosphate buffer, 500 mM NaCl, 5% glucose w/v, pH 8.0) to yield a domed meniscus. The surface was bounded on the two short sides by Teflon bars. A film forms at the air-water interface after approximately 4 h incubation at room temperature. This

film formed by Ubx or chimeric Ubx proteins was concentrated by closing the gap between the Teflon bars (see Chapter 3). To generate fibers from the concentrated film, a motor was used to slowly turn an axle and lower a needle suspended from string to the liquid surface. Reversing the direction of the motor slowly withdrew the needle from the surface, thus drawing the fiber. To collect films, a square made from stainless steel wire (2 cm × 2 cm) was placed on the surface of the reservoir followed by lifting and rotating the square.

Production of Ubx microfibers using electrospinning

mCherry-Ubx was dissolved in equilibration buffer (50 mM sodium phosphate buffer, pH 8.0, 5% glucose w/v, 500 mM NaCl) at 12 mg/ml. Electrospinning of mCherry-Ubx microfibers was performed at a voltage of 15 kV, using a 22 gauge needle, a target distance of 13 cm, and a flow rate of 2 ml/h. Electrospun microfibers were examined by light and fluorescent microscopy.

Film formation assay

To investigate the time-scale of Ubx film assembly, sessile drops containing 0.6 mg/ml of Ubx in elution buffer and elution buffer only were incubated at room temperature. The appearance of the drops was monitored over 5 hrs.

Fiber formation assay

Fiber formation assays were performed to compare the fiber formation ability of different Ubx fragments. Ubx fragments were dissolved in elution buffer to a final concentration of 0.6 mg/ml. The average length of the fibers produced following 2 hr and 4 hr incubation periods were recorded.

2.7 Production of various morphologies

Ubx film

A Ubx concentration of 0.6 mg/ml was used to generate materials using the sessile drop. Ethylenediaminetetracetic acid (EDTA) was initially added to 10 mM to prevent amorphous aggregation, although later was found to have a negligible effect and was eliminated. Ubx or Ubx chimera solution (100 μl) was placed on the surface of a siliconized coverslip at room temperature. Ubx film spontaneously forms at the air-water interface after approximately 1 hour.

Ubx fibers

A needle or pipet tip was used to contact the surface of Ubx or Ubx chimera film and withdrawn slowly to draw fibers.

Ubx sheets

Ubx protein samples were concentrated to 1 mg/ml using Vivaspin concentrators with a 10 kD cut off (Viva Science). EDTA was added to a final concentration of 10 mM. Ubx solution (100 ml) was placed at the surface of a siliconized coverslip, and covered with a 15 ml plastic tube cap to deter evaporation. Ubx sheets formed spontaneously at the air-buffer interface at room temperature overnight.

Ubx lattices

The outer turn of a paper clip, in which the inside turn had been bent out of the way, was used as a support for lattice construction. Ubx ropes were wound around the parallel arms of an opened paper clip such that the ropes intersect between the supporting arms. Freshly made Ubx ropes adhere to both the metal supports and to each other,

forming a lattice. Lattices maintain their form after 24 hours of drying in air and subsequent removal from the supports.

Ubx bundles

A dome-shaped 20 μl drop of deionized water was placed on the surface of a siliconized cover slip. A series of Ubx fibers were placed in parallel, approximately 1 mm apart, on the paper clip support, and subsequently dipped into the drop of water. Upon slow withdrawal, interactions with the shrinking water surface pull the fibers toward the middle of the series, where the fibers adhere to each other, forming a multi-rope bundle. The degree to which the fibers fuse in the bundle appears to be dependent on the age / hydration of the fiber.

Ubx tethered encapsulates: Microbaskets

Ubx sheets were prepared as described. Objects with pointed ends (pipette tip, needle *etc.*) were used to make contact with the surface of the sheet and slowly withdrawn to produce mini-encapsulated baskets.

2.8 Mechanical testing

A Gatan Microtest™ tensile tester was used to characterize the mechanical properties of Ubx fibers. The load cell had a load capacity of 2 N, sensitivity of 0.0001 N, and displacement resolution of 0.001 mm. Unless otherwise specified, the slowest possible loading speed of 0.1 mm/min was used to minimize pulling rate effects on the measurements. The sample time for a single data point during loading was 500 ms. Samples were attached to double sided carbon tape on the clamps using Loctite 495™ adhesive. Individual fibers have very uniform diameters and were cut into two sections,

one for measurement of the initial sample diameter by SEM, and one for tensile experiments followed by measurement of the final sample diameter.

In order to accurately measure the Young's modulus of these protein fibers, multiple highly consistent unloading curves in each successful tensile test were used, since only elastic deformation is recovered during unloading. The average slope of these unloading curves provides a much more accurate estimation of the Young's modulus for the fibers by avoiding uncertainties related to the initial sample alignment and the settling process in the early part of the tensile tests. For wide fibers, Young's modulus was measured using unloading curves after the yield point.

The Gatan Microtest^{TM} tensile tester is also vacuum compatible and has been modified for use inside a FEI quanta 400^{TM} scanning electron microscope. This experimental arrangement enables *in situ* tensile tests of the selected protein fibers with sufficient hydration, allowing observation of the deformation process in real time during a quantitative tensile test and linkage of specific behaviors to corresponding stress or strain values.

2.9 Generation of patterns within Ubx chimera materials

Spatial arrangement of Ubx chimera solutions in both sessile drop and trough surface collection experiments has enabled the production of a variety of patterns within a single material (Huang et al., 2011).

Manual assembly of bundles and twists

Freshly produced fibers with different chimeras can be fused via contact into a patterned bundle, which can be rotated to form a patterned twist. Even twisting alternates

chimera exposure on the surface, whereas wrapping one fiber around the other creates a core/shell arrangement.

Manual assembly of layered lattices

Ubx chimera lattices can be made as described previously (Greer et al., 2009) and stacked to form layered lattices of different chimeras.

Manual assembly of patterned tubes

mCherry-Ubx and EGFP-Ubx fibers were wrapped around a 3% agarose tube. Dehydration resulted in shrinkage of the tube and brought fibers to close contact, where the remaining hydration allowed lateral fiber fusion with good surface coverage.

Surface assembly of striped fibers

Drops of EGFP-Ubx and mCherry-Ubx solutions (200 μl) were placed adjacent to one another on a siliconized surface and incubated at room temperature for 1.5 hr. The two drops were then allowed to merge and incubate for another 20 min. An end-to-end striped fiber can be produced by drawing fibers across the green / red boundary. A side-by-side striped fiber is produced by drawing fibers along the green / red boundary.

Surface assembly of spotted fibers

A drop of EGFP-Ubx solution was placed on a siliconized surface and incubated for 1.5 hr to initiate film formation. Drops (0.2 μl) of mCherry-Ubx solution were added onto the film and incubated for another 20 min. Fibers with a spotted pattern can then be drawn from the surface.

Surface assembly of patterned films

EGFP-Ubx and mCherry-Ubx solutions were pipetted into trays containing the buffer required for material formation (see previous section on production of Ubx

chimera materials via the buffer reservoir method). Patterned Ubx film can be harvested using a stainless steel loop (2 cm x 2 cm).

2.10 Visualization techniques

Fluorescence microscopy

Fluorescence microscopy was performed using a Zeiss upright Axioplan 2 imaging microscope (Carl Zeiss) with MetaMorph Meta Series Software 7.6.5 (MDS Analytical Technologies). EGFP or mCherry-Ubx fluorescence was visualized using narrow GFP and Texas-Red filters, respectively.

Confocal microscopy

Confocal microscopy was performed using a Zeiss LSM 510 Meta confocal inverted microscope. An argon laser was used for excitation at 488 nm, and a helium neon laser was used for excitation at 543 nm. Emission filters of 500-530 nm and >543 nm were used, respectively. A pinhole size of 52 μm was used to achieve an optical slice thickness of 2.7 μm.

SEM microscopy

SEM images of Ubx chimera fibers were obtained using a FEI Quanta 400 field emission scanning electron microscope. Samples were sputter-coated with gold for 30 s at 100 mA and examined using a beam voltage of 200 kV and a spot size of 3.

2.11 Spectroscopic measurements

Circular dichroism

Circular dichroism spectra were acquired using a JASCO-815 CD spectrometer with a temperature-controlled cell holder and a 3-mm pathlength quartz cuvette. Proteins were diluted in CD buffer (25 mM NaH_2PO_4, 150 mM NaCl, 5% glucose, pH 7.5), to a

final concentration of 1 μM. Far-UV CD spectra (200-260 nm) were monitored at 25°C using a band width of 1 nm, a data pitch of 0.5 nm, a scan rate of 100 nm/min, and averaging 12 accumulations.

Fluorescence spectroscopy

Fluorescence spectroscopy was performed using a JASCO-815 fluorometer and a 3-mm pathlength quartz cuvette. Proteins were dissolved in CD buffer to a final concentration of 0.3 μM. Excitation spectra and emission spectra were monitored at 25°C using a bandwidth of 2 nm, a scan rate of 100 nm/min, and 12 accumulations. The spectra for EGFP-Ubx and mCherry-Ubx chimeras were normalized against EGFP and mCherry at the same molar concentration, with the excitation and emission peak intensity for the standard defined as 1. For EGFP and mCherry-Ubx chimeric fibers, fluorescence excitation and emission spectra were obtained by placing fibers in the excitation path, and peak intensity was defined as 1.

UV/Visible spectroscopy

UV/Visible spectra were obtained using a Cary 50 scanning UV-Visible spectrometer using a data pitch of 1 nm and a scan rate of 100 nm/min at 25°C.

Luminescence assay

Oxidation of luciferin by firefly luciferase (QuantiLum® Recombinant Luciferase, Promega) or by the luciferase-Ubx chimera was assayed using the luciferase assay system (Promega). Protein solution (10 μl) was mixed with 20 μl of luciferase assay reagent (Promega) in a 96 well white plate (Corning) used to reflect light to the detector. The resulting luminescence was monitored using a Tegan M-1000

monochromator-based micro-plate reader by integrating the total light emitted in a 1 s period.

2.12 Biocompatibility tests

Cell culture procedures

Rat fibroblast cell line (ATCC, CRL-1764) was cultured in T-75 flasks with Dulbecco's modified Eagle medium (DMEM, Gibco Life), which was supplemented with 10% (v/v) fetal bovine serum (FBS, Cambrex BioScience) and 1% (v/v) antibiotics containing penicillin, streptomycin and amphotericin (Gibco Life). Cells of passage 5-9 were cultured in a humidified incubator at 37°C and 5% CO_2.

Preparation of tested materials

Custom-made Teflon (also known as poly(tetrafluoroethylene) (PTFE)) rings were sterilized by autoclaving prior to attachment of mCherry-Ubx lattices. mCherry-Ubx lattices on Teflon rings were sterilized by 30 min UV light treatment (15 min on each side).

Live/Dead staining and quantification

The media were removed and the cells were rinsed three times with phosphate-buffered saline (PBS, Gibco), followed by the addition of calcein AM (2 mM) and ethidium homodimer-1 (4 mM) dissolved in PBS (Live/Dead Reagents, Molecular Probes). The Live/Dead reagents were exposed to the cells for 30 min at room temperature in the dark. A fluorescence plate reader (Biotek Instrument FLx800) with filter sets of 485/528 nm (excitation/emission) for calcein AM (live cells) and 528/620 nm (excitation/emission) for EthD-1 (dead cells) was used to quantify cell viability by measuring fluorescence intensity (Temenoff et al., 2003).

Direct contact assay

Cells were seeded on 24-well plates (Falcon) at a density of 40,000 cells/cm^2 in 1 ml of DMEM media per well. After 24 h incubation, the media were aspirated and Teflon rings with mCherry-Ubx lattices attached were placed inside the wells. Fresh DMEM media were added to the wells to cover the rings. The cells were incubated for 24 h before Live/Dead staining, and quantification was carried out (n = 5 wells/condition). Untreated cells that were cultured with media only served as the positive (live) control, whereas cells exposed to 70% ethanol for 10 min served as the negative (dead) control. The live and dead fractions were calculated using the following equations:

$$Live\ Control = Fg(rings + cell) - Fg(dye) \qquad \text{Equation 2.4}$$

where *Fg(rings + cell)* is the average green fluorescence of wells where Teflon rings were placed in contact with cells. *Fg(dye)* is the average green fluorescence of wells containing dyes alone.

$$Dead\ Control = Fr(rings + cells + ethanol) - Fr(dye) \qquad \text{Equation 2.5}$$

where *Fr(rings + cells + ethanol)* is the average red fluorescence intensity of wells in which cells were placed in contact with Teflon rings and were later killed by ethanol.

$$Live\ Fraction = \frac{Fg(ring + lattice + cells) - Fg(dye)}{Live\ Control} \qquad \text{Equation 2.6}$$

$$Dead\ Fraction = \frac{Fr(ring + lattice + cells) - Fr(dye)}{Dead\ Control} \qquad \text{Equation 2.7}$$

where *(ring +lattice + cells)* are the wells in which mCherry-Ubx lattices were added to cells.

Elution assay

To prepare the tested solutions that contain molecules leached from Ubx fibers,

DMEM media were incubated with mCherry-Ubx lattices for 24 hours, which were then diluted 10-fold and 100-fold. Cells were seeded on a 96-well plate (Falcon) at a density of 40,000 cells/cm^2 in 100 μl of DMEM media per well. Following 24 h incubation, 80–90% confluence was achieved. The media were removed and the cells were rinsed three times with PBS (Gibco). A volume (100 μl) of the solutions to be tested was added to the wells (n = 5 wells/dilution). Live/dead staining and quantification were carried out 24 hour after the addition of the media. The controls and live and dead fractions were calculated using the following equations:

$$Live\ Control = Fg(cell) - Fg(dye) \qquad \text{Equation 2.8}$$

where *Fg(cell)* is the average green fluorescence of wells containing cells without treatment. *Fg(dye)* is the average green fluorescence of wells containing dyes alone.

$$Dead\ Control = Fr(cells + ethanol) - Fr(dye) \qquad \text{Equation 2.9}$$

where *Fr(cells + ethanol)* is the average red fluorescence intensity of wells in which cells without treatment were killed by ethanol. *Fg(dye)* is the average red fluorescence of wells containing dyes alone, and *(MediaLattices + Cells)* are the wells where media incubated with mCherry-Ubx lattices were added to cells.

$$Live\ Fraction = \frac{Fg(MediaLattices + cells) - Fg(dye)}{Live\ Control} \qquad \text{Equation 2.10}$$

$$Dead\ Fraction = \frac{Fr(MediaLattices + cells) - Fr(dye)}{Dead\ Control} \qquad \text{Equation 2.11}$$

Attachment assay

Confluent rat fibroblasts were trypsinized (0.05% trypsin, 0.5 mM EDTA, Gibco) and adjusted to approximately 100,000 cells/ml. Trypsinized rat fibroblasts cells were added to mCherry-Ubx lattices in 24 well ultra-low-attachment well plates (Corning) to a density of 40,000/cm^2 and a final volume of 1 ml. Following 24 hr incubation, the media

in each well were carefully aspirated and rinsed with PBS three times. Live/Dead staining was then performed as described. Cells were imaged using a Zeiss LSM 510 Meta confocal inverted microscope.

2.13 X-ray fiber diffraction

mCherry-Ubx bundles were washed by gentle pipetting of deionized water to and stored overnight at 50% humidity, 4°C, before diffracting at a Bruker SMART 1000 CCD diffractometer, using a voltage of 40 kV, a current of 40 mA, a sample distance of 15 cm, a beam size of 0.1 mm, and a collection distance of 6 cm. Diffraction pattern was collected using a general area detection diffracton system (GADDS).

2.14 Surface tension measurements

Pendant Drop experiments were performed using a KSV THETA tensiomer. Langmuir Trough experiments were performed using a KSV NIMA Langmuir deposition trough. Experiments were performed at 25°C at 50% humidity.

CHAPTER 3

Production of Ubx-based Materials: *Assembly, Morphologies, and Sequence Requirements*[2]

3.1 Introduction

Protein-based materials can be customized for a variety of applications, including drug delivery, tissue engineering scaffolds, surgical sealants, and biosensors (Baneyx and Schwartz, 2007; Deming, 2007; Place et al., 2009). These applications require effective production of the proteins employed and the development of a variety of material morphologies with suitable chemical, mechanical, and functional properties (Maskarinec and Tirrell, 2005).

Protein-based materials can be derived from their natural organisms, produced recombinantly in another organism, or synthesized chemically. With the recent development of recombinant DNA technology, material-forming proteins can be expressed in other organisms, such as *E. coli*, yeast, and plants, for improved production and engineering capacity (Du et al., 2008; Kyle et al., 2009; Merle et al., 2002). Additionally, self-assembling peptides that mimic the sequence of natural protein-based materials can be produced via chemical synthesis (Floss et al., 2010; Kyle et al., 2009).

Ideally, proteins and peptides should self-assemble into materials *in vitro*, as they do *in vivo*. In practice, however, most proteins require chemical or physical cues to trigger assembly, using methods such as electrospinning, solvent casting, and

---

[2] Parts of this chapter, including text and figures, were reported in Greer and Huang et al., 2009. A. Greer contributed to the production of Ubx morphologies and western blot analysis.

microfluidics. Together, these techniques make it possible to generate a variety of morphologies, including fibers (Rammensee et al., 2008), films (Huemmerich et al., 2006; Junghans et al., 2006; Metwalli et al., 2007), foams (Romer and Scheibel, 2007), hydrogels (Rammensee et al., 2006), capsules (Hermanson et al., 2007; Hermanson et al., 2007) and spheres (Lammel et al., 2008; Slotta et al., 2008).

A key challenge is that the chemical and physical conditions required for materials assembly and processing usually entail high temperatures, exposure to organic solvents, or extreme pH to stimulate protein assembly (Bini et al., 2006; Dror et al., 2008; Kim and Conticello, 2007; Lazaris et al., 2002; Wright et al., 2005). These procedures may harm the mechanical properties of the resulting materials and compromise the activity of any incorporated proteins. We fortuitously discovered that Ubx spontaneously assembled into ordered aggregates in aqueous buffer without such harsh treatments, an interesting feature of a novel material-forming protein. This investigation focused on identification of the assembly conditions of Ubx materials, generation of a variety of Ubx materials morphologies, and determination of sequence requirements for materials formation using Ubx truncation mutants.

3.2 Generation of various morphologies

3.2.1 Self-assembly into fibril and films

Ubx is highly prone to aggregation into amorphous flocculates (Bondos and Bicknell, 2003). While searching for conditions that inhibit amorphous aggregation, we fortuitously discovered that Ubx spontaneously assembled into ordered aggregates in aqueous buffer. When incubated at room temperature and humidity, the surface of a Ubx-containing sessile drop acquires a "matte" or opaque appearance after ~ 1 h (**Fig. 3.1**).

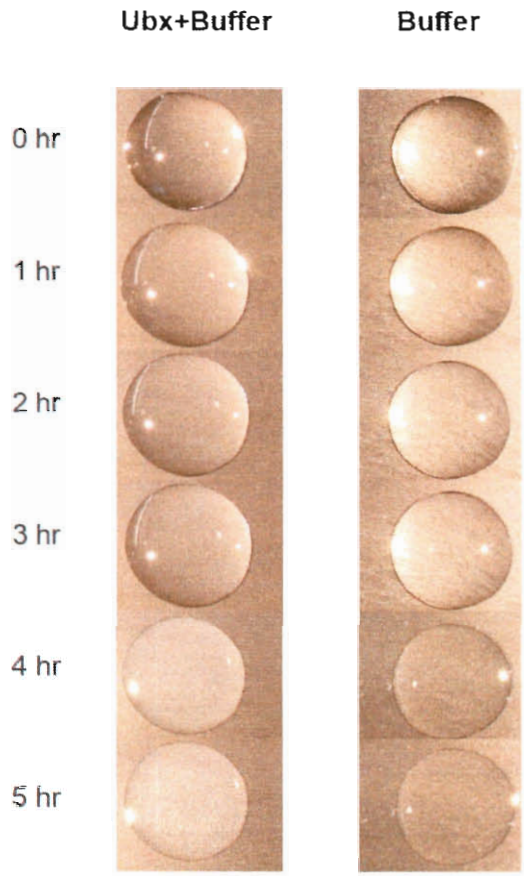

Figure 3.1 Ubx assembles at the air-water interface over time. Upon air exposure, the surface of a Ubx-containing sessile drop becomes more opaque compared to a sessile drop containing only buffer. The increase in opacity begins after a 1 hour incubation period, but becomes more visible after 2 to 3 hours, reflecting film formation. Continued incubation for a total of 4 hours allows the film to thicken into thicker, more opaque Ubx sheets. Figure taken from Greer and Huang et al., 2009.

This altered appearance is due to spontaneous Ubx aggregation into insoluble nanofibrils that are approximately 50 nm in diameter (**Fig. 3.2A**). At the air-water interface, these nanofibrils self-assemble into a film that coats the liquid surface and causes the matte appearance (**Fig. 3.2B**). Prior to this study, Ubx fibers and films had never been observed (i) during overexpression of Ubx in *Drosophila* or *E. coli* or (ii) in lysate or purified solution in the absence of air. Consequently, the assembly of Ubx into fibers and films appears to require an air-liquid interface. Similarly, self- assembly of

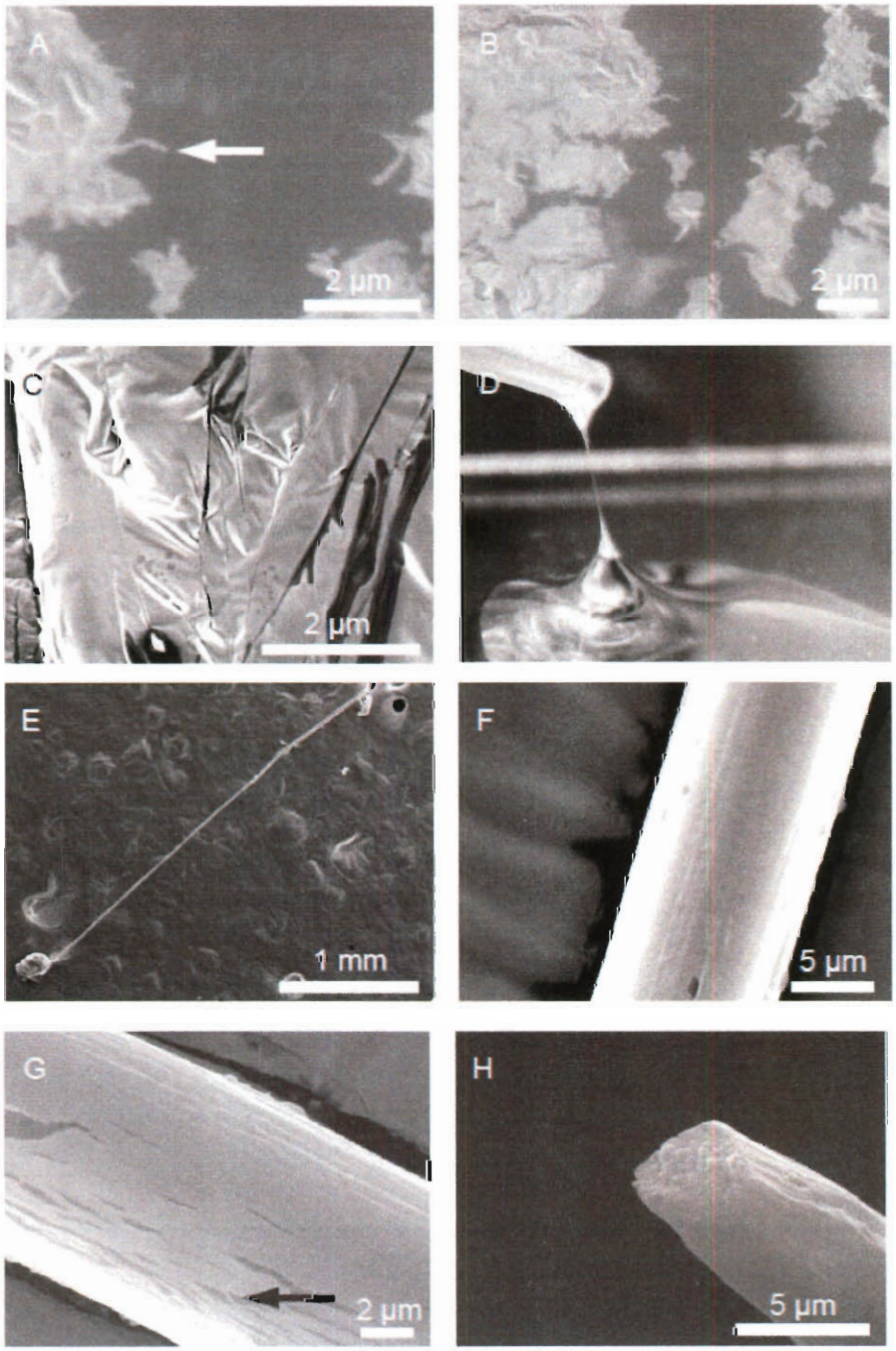

Figure 3.2 Basic materials formed in a hierarchical manner by Ubx. (A) A Ubx nanofibril, 50 nm in diameter (white arrow). (B) Ubx film, formed from self-associating nanofibrils. (C) Ubx sheet, generated by additional assembly following the formation of the Ubx film. (D) A Ubx fiber being pulled from a Ubx film at the surface of a sessile drop containing Ubx. (E,F) SEM image of a Ubx fiber at low and high magnification, respectively. (G) A Ubx fiber, fractured by the charging of the SEM beam, splinters into 50 nm nanofibrils aligned along the longitudinal axis (black arrow). (H) The free end of a severed Ubx fiber reveals a solid core. Figure is taken from Greer and Huang et al., 2009.

miniature silk lysate proteins has also been observed at the air-water interface (Stark et al., 2007). Fibril assembly and subsequent film formation are the first steps required to generate additional material architectures (Teule et al., 2007).

3.2.2 Generation of fibers

Ubx films can be drawn into fibers (**Fig. 3.2D**). The diameter of an individual fiber is uniform (**Fig. 3.2E,F**), provided that (i) the film has not begun to form a sheet (**Fig. 3.2C**), (ii) the protein concentration in the sessile drop is between 0.075 mg/ml and 0.6 mg/ml (**Table 3.1**) and (iii) the fiber was drawn at an even speed. Between fibers, diameters vary between 5 and 30 μm, apparently dependent on the degree to which the film polymerized prior to drawing the fiber. These diameters are comparable to those observed for electrospun spider silk and silkworm silk (Jin et al., 2002). Fibers are composed of longitudinally aligned fibrils (**Fig. 3.2F,G**) and have a solid core (**Fig. 3.2H**), similar to fibers assembled from a miniature version of a spider silk gene (Stark et al., 2007). The maximum possible fiber length is proportional to the area of the film at the surface of a sessile drop. For example, a 7 cm long fiber can be produced from the surface of a 200 μl sessile drop of Ubx solution. Using the sessile drop method, one liter of bacterial culture expressing Ubx is sufficient to generate more than 1 m of Ubx fiber. This procedure is similar to a study described (Teule et al., 2007), in which fibers were drawn from a spider silk-like recombinant protein. However, there are two notable exceptions: First, Ubx film adheres to the pipette tip, and thus does not have to be held by tweezers in order to be drawn into fibers. More importantly, uniform Ubx fibers can be produced at protein concentrations 2 orders of magnitude less than for the spider silk-like recombinant protein (**Table 3.2**).

Table 3.1 Dependence of fiber length on Ubx concentration. Fiber length was measured by drawing 5 fibers at each concentration of Ubx after 2 h incubation at room temperature and humidity. Average and standard deviation values of fiber length are summarized. Table is derived from Greer and Huang et al., 2009.

Ubx concentration (μg/ml)	Fiber length (mm)
500	15±7
300	10±4
150	7±3
75	3±2
50	1±1
25	0

Table 3.2 Conditions used to generate different protein-based materials. Table is reproduced from Greer and Huang et al., 2009.

Protein	Concentration (mg/ml)	Cosolvent/Method	Time
Ubx	0.075		2 hours
Proteins obtained ex vivo			
Spider silk	300 - 500	Methanol	
Silkworm silk		Methanol, HFIP	
Recombinant elastomeric proteins			
Resilin protein fragment	>100	Cross-linking agents	
Spider silk protein fragment	12.5	Organic solvent	
Spider silk protein ADF-3	100 -280	Methanol	
Spider silk nanofibers	5 - 30	Methanol	1 week
Spider silk-like protein - machine drawn	250 - 300	HFIP	
Spider silk-like protein - hand drawn	10	Aqueous	
Amyloid proteins / peptides			
Amyloid peptide fibrils	10	Low pH acetonitrile	1 week
Lactoglobulin	80 - 140	Low pH, high temperature, or alcohol / TFE	~6 hours
Human prion protein	0.03	Metal ions	Days

HFIP = hexafluoroisopropanol, TFE = Trifluoroethanol

3.2.3 Verifying material composition

The unforeseen ability of a *Drosophila* transcription factor to form materials prompted us to verify that these materials are, indeed, composed of Ubx. We demonstrated that materials cannot be produced from buffer that does not contain Ubx (**Fig. 3.1**). However, it is possible that materials are generated from a component of the purified protein solution other than Ubx. To rule out this possibility, we performed a control using *E. coli* cells that do not express Ubx. The resulting cell extract does not form materials, simultaneously demonstrating that neither buffer components nor any *E. coli* proteins that may contaminate Ubx preparations are sufficient to generate materials.

Fibers stain blue in the presence of Izit Crystal Dye, demonstrating that these structures contain protein (**Fig. 3.3A**). Denaturing gel electrophoresis followed by Western blot analysis was used to compare the protein in materials with purified Ubx. Two hours of multiple cycles of heating, vortexing, and sonication in denaturing buffer were required to depolymerize these robust materials for gel electrophoresis. Western blot analysis demonstrated that these materials are composed of a single protein, which is comparable in size to purified, monomeric Ubx (**Fig. 3.3B**). FP3.38, an antibody that interacts with the Ubx homeodomain, was used as the primary antibody for the Western blot. FP3.38 is sufficiently specific to be used for immunohistochemistry experiments and is only known to cross-react with Abdominal A, another *Drosophila* Hox transcription factor with a nearly identical homeodomain sequence (White and Wilcox, 1984). Since recombinant Ubx is purified from *E. coli* in the absence of Abdominal A, we conclude these materials are composed of Ubx.

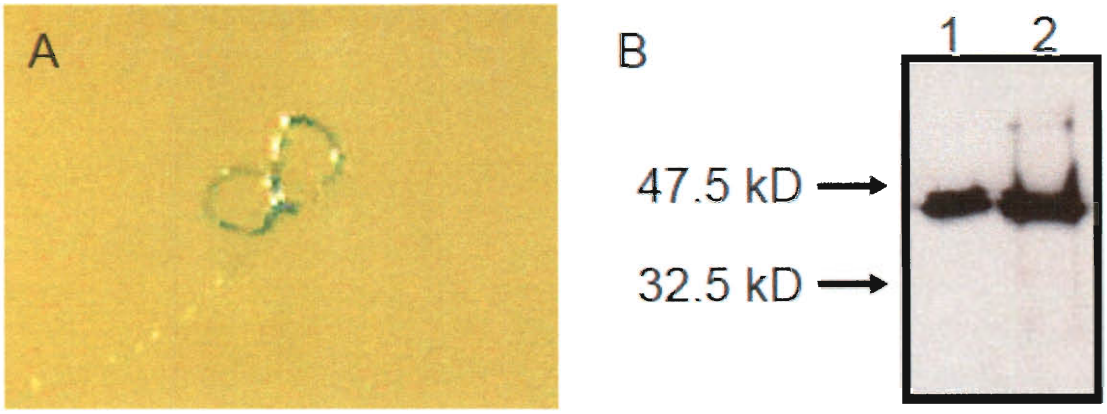

Figure 3.3 Materials are composed of Ubx protein. (A) A Ubx fiber is stained blue by Izit, a dye that selectively interacts with protein. (B) A western immunoblot demonstrates the presence of Ubx in (1) purified Ubx and (2) denatured Ubx fibers. The positions of molecular weight markers are indicated to the left. Figure is taken from Greer and Huang et al., 2009.

3.2.4 Heat stability of Ubx-based materials

The extreme measures required to depolymerize Ubx materials for gel electrophoresis suggest that these structures are resistant to heat. To test this hypothesis, a dried Ubx fiber was stained blue with Coomassie dye to aid visualization and subsequently submerged in a phosphate-buffered saline bath at 98 °C. The fiber was intact after several hours, indicating that exposure to high temperatures alone does not degrade or depolymerize the materials (**Fig. 3.4**).

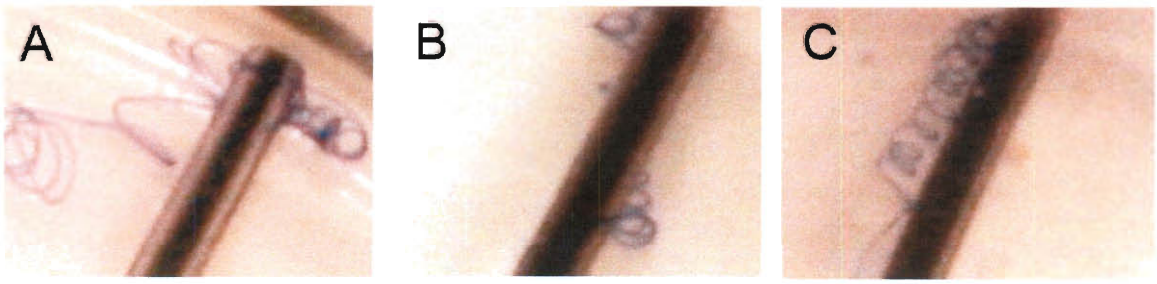

Figure 3.4 Ubx fibers have high heat stability. (A) Ubx fiber, stained with Coomassie Blue, was transferred to a phosphate-buffered saline solution attached to a syringe needle prior to heating. The same Ubx fiber was not degraded after 1 hour (B) or (C) two hours of heating at 98 °C. These data demonstrate the high level of heat resistance for these fibers. Figure is from Greer and Huang et al., 2009.

3.2.5 Ubx-based materials are adhesive

Silkworm silk fibers require additional proteins, termed "sericins", to anneal fibroin fibers (Jin and Kaplan, 2003; Vollrath and Knight, 2001). In contrast, recently generated Ubx materials adhere to glass, plastic, wood, metal, and Teflon without the help of other proteins. Fibers and sheets also adhere and meld to themselves and each other, allowing generation of more complex architectures.

3.2.6 Construction of complex Ubx materials: *bundles, twists, lattices, and tethered encapsulates.*

Because Ubx sheets and fibers are self-adhesive, they can be utilized as building blocks for either manual construction or self-assembly of materials with more complex architectures. Ubx bundles consist of aligned Ubx fibers that coalesce to form thick bundles (**Fig. 3.5A,B**). These fibers fuse to varying degrees, depending on the age of the fibers upon creation of the bundle. Aligned, but not fused, fibers can also be wound to form twists (**Fig. 3.5C**). Nonaligned Ubx fibers that intersect also fuse at their contact point, without exposure to water, to create Ubx lattices (**Fig. 3.5D**). Again, the degree of fusion is dependent on fiber age. Once the materials dry in air (overnight to one week, depending on size), these lattices stiffen and retain their original configuration when released from their support. Hanging drops of Ubx self-assemble into tethered encapsulates, or baskets, in which Ubx sheets, encapsulating liquid, are suspended from a Ubx fiber. Microencapsulates, which only encase ~1 µl or less, can be formed by attempting to pull fibers from sheets instead of film or from higher protein concentrations (**Fig. 3.5E**). Macrobaskets are formed from a hanging drop and can encapsulate 3-10 µl of liquid (**Fig. 3.5F**). Macrobaskets are sufficiently robust that they do not rupture, even

when the encapsulate is rapidly swung in circles from the distal end of its suspending fiber. Although the capsules partially collapse as the material dries, these structures are essentially stable for weeks when suspended in air.

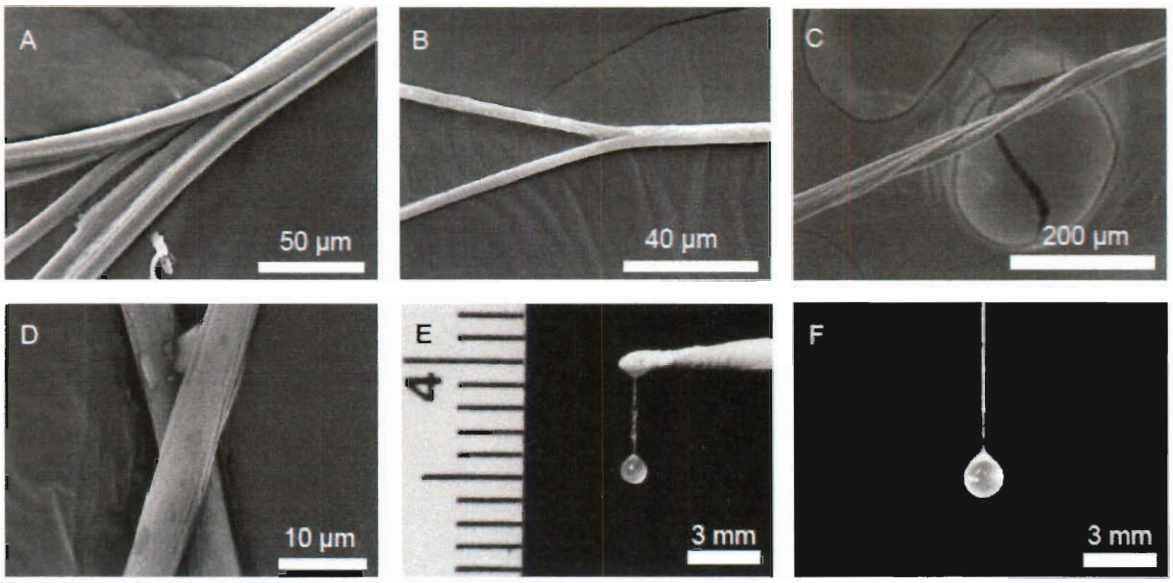

Figure 3.5 Complex architectures formed by Ubx materials. (A) A bundle composed of six partially melded ropes; (B) a bundle composed of two ropes which completely meld to one another; (C) a twist of two Ubx ropes; (D) the intersection of two ropes in a lattice, which forms a stable interaction; (E) a tethered microencapsulate, formed by drawing a Ubx sheet, contains approximately 0.5 µL of buffer; and (F) a macro-encapsulate, which contains approximately 4 µL of buffer, is formed by gradual extension of a hanging Ubx drop. Figure taken from Greer and Huang et al., 2009.

3.2.7 Hierarchical self-assembly

In both Ubx film and Ubx fibers, we were able to observe lateral interactions between Ubx fibrils (**Fig. 3.2G**). We hypothesize that further interactions between Ubx fibrils enable fiber, film, and sheet assembly and subsequent hierarchical construction of more complex structures, i.e., sheets, bundles, lattices, twists, and tethered encapsulates (**Fig. 3.6**).

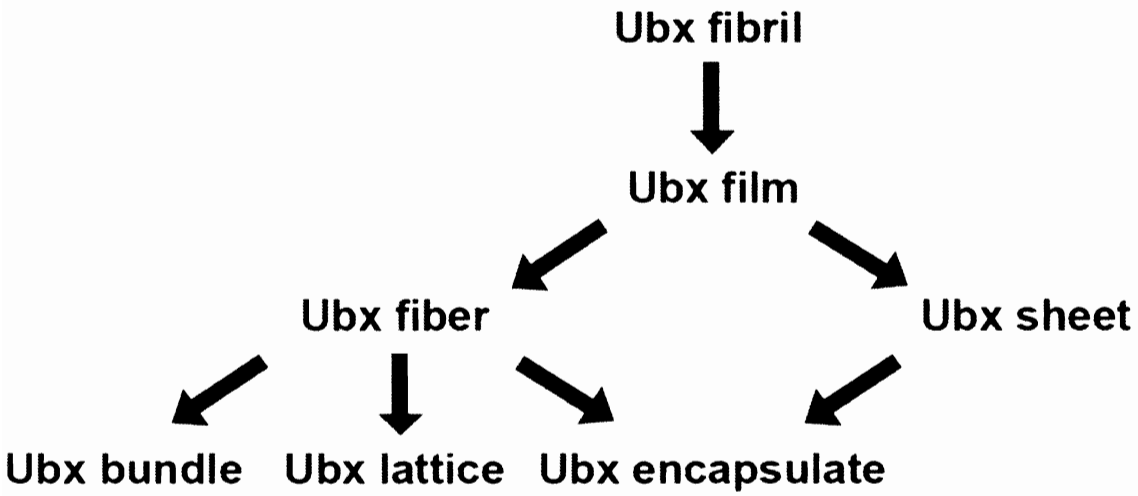

Figure 3.6 Schematic depicting the hierarchical assembly of materials architectures from Ubx fibrils. Ubx fibrils, films, and sheets form spontaneously at the air water interface. Construction of all other structures requires external forces. Ubx fibers are drawn from film. More complex architectures (bundles, lattices and encapsulates) are composed of sheets and/or fibers and are constructed by hand or by gravity. Figure is taken from Greer and Huang et al., 2009.

3.2.8 Mild material-formation conditions

Most recombinant proteins require harsh conditions to trigger materials assembly, including exposure to high temperatures, organic solvents, pH extremes, or metals (Bini et al., 2006; Bondos, 2006; Dror et al., 2008; Huang et al., 2007; Kim and Conticello, 2007; Lazaris et al., 2002; Ricchelli et al., 2006; Su and Chang, 2001; Wright et al., 2005; Zhang et al., 2006) (**Table 3.2**). Such conditions would be expected to denature and possibly aggregate many proteins (Bondos, 2006; Huang et al., 2004). In contrast, Ubx oligomerizes in nondenaturing aqueous solution near neutral pH at either room temperature or 4 °C. Furthermore, Ubx self-assembles into fibrils visible by SEM much more rapidly (2 h) than amyloidogeneic proteins form aggregates, which typically require days to weeks (**Table 3.2**). Indeed, the conditions typically utilized to trigger amyloid or elastomeric protein assembly actually inhibit generation of Ubx-based materials. Finally,

Ubx readily forms materials at concentrations as low as 0.075 mg/ml, 2 orders of magnitude lower than found for most other protein-based materials (**Table 3.2)**, thus reducing the stringent requirements on protein expression and purification for materials generation.

3.3 Sequence requirements for material assembly

3.3.1 Ubx shares sequence motifs with other protein/peptides-based materials

Given that neither physical stimuli nor exogenous chemicals are required for materials formation, the Ubx amino acid sequence is sufficient to dictate this protein's surprising ability to generate materials under mild conditions. Therefore, identification of the minimal region of Ubx required to generate these materials potentially yields insight into the molecular mechanisms underlying formation of these unique structures. An initial examination revealed similarities in the sequence of the N-terminal 216 amino acids of Ubx with other proteins that form filamentous materials (**Fig. 3.7A**). A large fraction (> 60%) of the N-terminus is composed of a disordered region greater than 100 amino acids in length (Liu et al., 2008; Romero et al., 2001) (**Fig. 3.7A**). Such regions potentially form amyloid easily, presumably because formation of amyloid precursors does not compete with folding to a stable native state (Hansen et al., 2006; Uversky and Fink, 2004). Furthermore, amyloid fibers may interact laterally with each other (Makarava et al., 2006), as we have observed in Ubx film and fibers. Thus, one possibility is that this large disordered region drives Ubx assembly into amyloid-like structures.

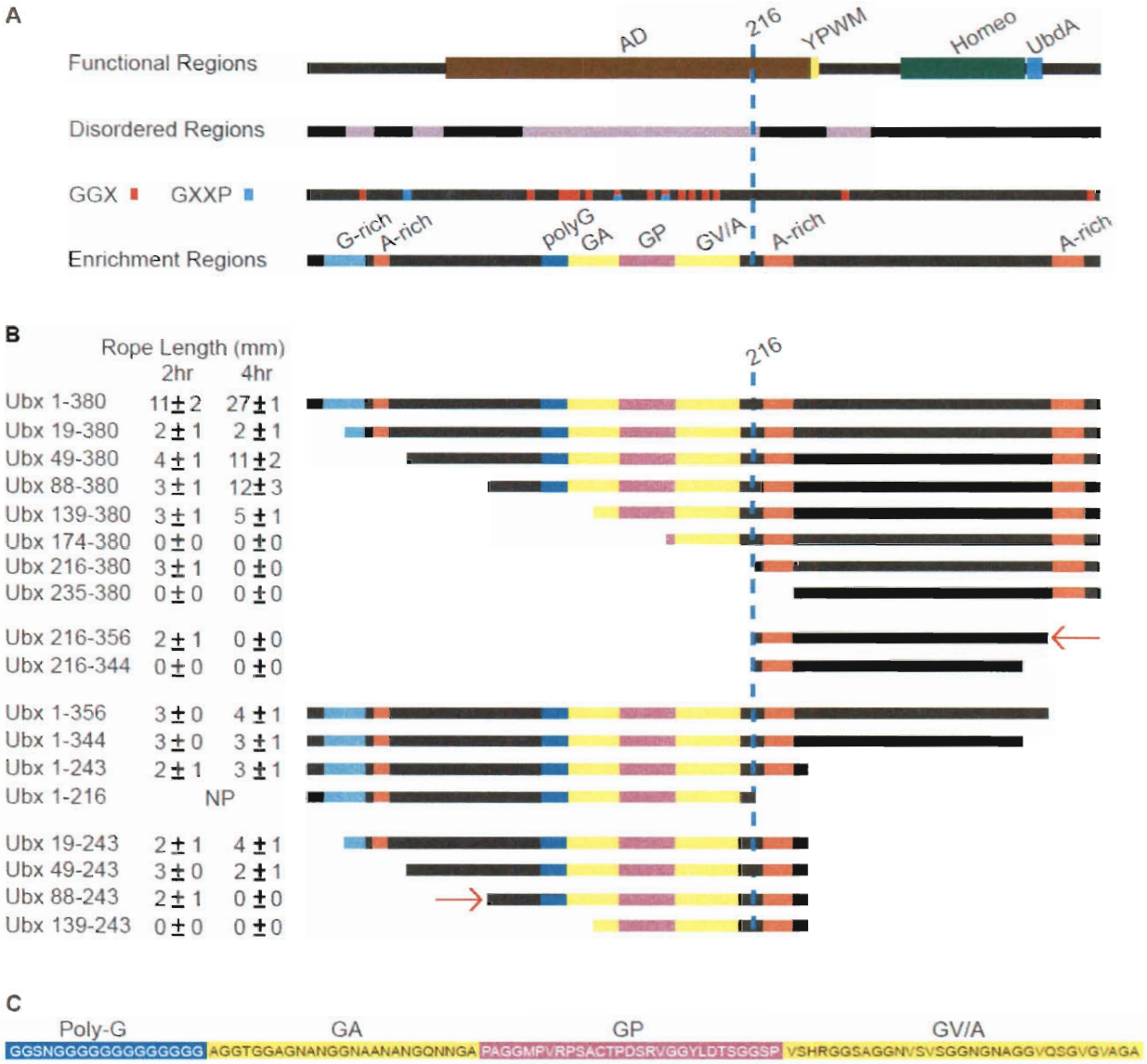

Figure 3.7 Schematic of Ubx and Ubx deletion mutants shows key sequence features. (A) Ubx sequence schematic depicts the location of functional domains, regions containing intrinsic disorder, elastomeric motifs, and regions enriched in a subset of amino acids. The transcription activation domain (AD) (Liu et al., 2008), extradenticle protein interaction motifs (YPWM and UbdA) (Merabet et al., 2007), and the homeodomain (Homeo) are labeled. (B) Ubx sequence schematics of the truncation mutants utilized to locate minimal materials-forming regions. The average length of fibers that can be produced after 2 and 4 h are listed to the left. The two minimal materials-forming domains are marked by red arrows. (C) The sequence of the glycine-rich region, subdivided into four domains based on amino acid prevalence. Figure is adapted from Greer and Huang et al., 2009.

Ubx materials also share structure and sequence similarities with elastomeric materials, such as silk, elastin, and mussel adhesive proteins. Ubx fibers and macrobaskets resemble structures created from a recombinant spider silk-like protein (Teule et al., 2007), and Ubx bundles appear similar to elastin fibers purified *ex vivo* from ligaments (Daamen et al., 2007). The Ubx sequence includes three alanine-rich or polyalanine regions, a motif common to araneoid and lepidopteran silks (Craig and Riekel, 2002; Huang et al., 2007). Ubx also contains glycine-rich regions (Liu et al., 2008), a feature common in most elastomeric proteins (Craig and Riekel, 2002; Elvin et al., 2005; Kim and Conticello, 2007; Lazaris et al., 2002) (**Fig. 3.7A**). The largest glycine-rich region, spanning amino acids 107 to 208 within the disordered domain, can be subdivided into four regions with distinct sequence features (**Fig. 3.7A,C**). The first glycine-rich region (a.a. 107-123) includes a homoglycine repeat 13 amino acids long (a.a. 111-123). The second region (a.a. 124-146) is enriched in glycine and alanine, similar to many araneoid and lepidopteran silks (Craig and Riekel, 2002). The middle region (a.a. 147-175) is weakly enriched in glycine and proline, although these residues never flank one another as found in many silks and in elastin (Craig and Riekel, 2002; Kim and Conticello, 2007). The final region (a.a. 176-209) includes a high content of glycine, valine, and alanine, a combination predicted to form amyloid rather than disorder or turns (Rauscher et al., 2006). Taken together, much of the amino acid content of the disordered region also bears some resemblance to that for natural elastomeric proteins.

Because of the high glycine content, Ubx also contains multiple copies of amino acid motifs found in elastomeric proteins. GGX and GXXP are both repeated motifs in elastin, and GGX is also found in spider silk (Huang et al., 2007; Moroy et al., 2005;

Rauscher et al., 2006). The glycine-rich region in Ubx (amino acids 107 to 209) includes 3 GXXP motifs and 13 GGX motifs (**Fig. 3.7A,C**). Although Ubx has far fewer of these motifs than a typical elastomeric protein, it has been shown that even a single elastomeric motif can undergo the structural transformations characteristic of this protein class (Reiersen et al., 1998). On the basis of these sequence similarities, we predicted that, if the molecular interactions underlying Ubx materials formation are similar to those for amyloidogenic and/or elastomeric proteins, then the region between amino acids 107 and 209 should be critical for materials formation.

3.3.2 Formation of disulfide bonds is not required to form Ubx-based materials

Disulfide bond formation is a potential mechanism for the formation of Ubx-based materials. We therefore investigated the roles of disulfide bond formation in Ubx materials formation by (i) assembling materials in strongly reducing conditions (ii) assembling materials from mutant Ubx proteins in which each of the 6 cysteine residues in Ubx was replaced with alanine, and (iii) assembling materials in an anaerobic chamber using sessile drops containing DTT (1 mM). Even though each of these conditions should inhibit disulfide bond formation, in each case Ubx assembled into fibers/materials. These results therefore indicate that disulfide bonds are not the primary contributing factor for material formation.

3.3.3 Generating Ubx fragments to identify material-forming regions

Because Ubx can be produced recombinantly in *E. coli*, we were able to generate a number of Ubx truncation fragments and then examine the ability of these fragments to form materials, in an attempt to identify regions crucial for materials assembly. All N-terminal and C-terminal Ubx deletion fragments are soluble and can be purified to

approximately 80% purity (**Fig. 3.8**). For fragments encompassing the homeodomain, the ability to bind DNA is retained (Liu et al., 2008; Tan et al., 2002). Each fragment is named for the amino acids included; for instance, the Ubx19-380 mutant includes a histidine tag, the initial methionine, and amino acids Ubx19-380. Boundaries for the truncation mutants bisect neither potential secondary structural elements nor evolutionarily conserved motifs (Liu et al., 2008) (**Fig. 3.7**).

3.3.4 Evaluating the effect of sequence on material formation

Because evaluation of fibril structure requires SEM, a much more labor-intensive process than monitoring fiber formation, the fiber formation of different Ubx fragments was used to evaluate the role of sequence on materials assembly (**Fig. 3.7B**).

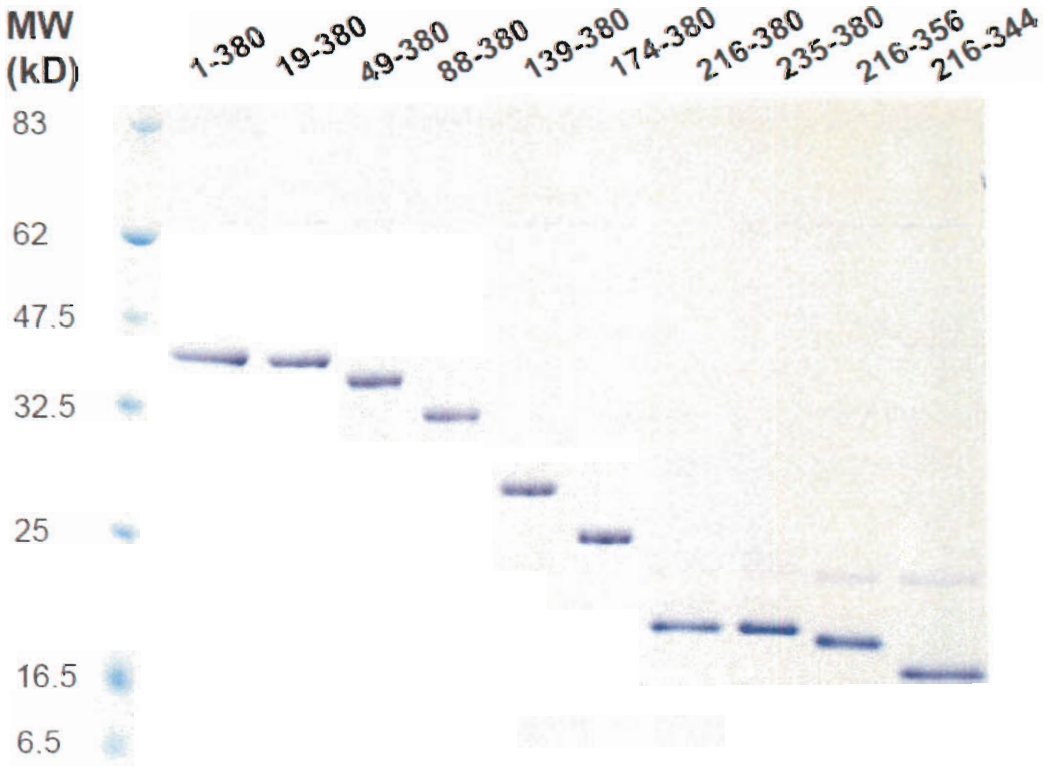

Figure 3.8 Ubx deletion fragments. Ubx deletion fragments can be purified from *E. coli*, generating soluble proteins that have ~80% purity after purification.

We noticed that various fragments required different lengths of time for assembly. Full length Ubx forms fibers within 2 h, whereas the slowest truncation mutants capable of forming fibers require 4 h at room temperature. Consequently, each protein was tested for fiber formation at two time points, after 2 and 4 h of sessile drop incubation at room temperature. In addition, the length of fiber that can be drawn correlates well with whether the rope appears robust or brittle, allowing us to parse the truncation mutants by materials quality. In general, Ubx variants either generated robust materials comparable to full-length protein (> 1 cm in length), or produced brittle and therefore short (< 5 mm) fibers.

3.3.5 Identifying the minimal material-forming region

Deleting first from the N-terminus, we found that Ubx19-380 forms short, brittle fibers (**Fig. 3.7B**). Surprisingly, this effect is ameliorated in Ubx49-380, Ubx88-380, and to some extent in Ubx139-380, which all form robust materials despite requiring a longer incubation time. Removal of amino acids 2-18 therefore exposes a region that impedes Ubx-Ubx interactions. Residues 19-48 either comprise this inhibition region or are required for its function, since removal of this segment restores the ability to form robust materials.

Surprisingly, Ubx139-380 and Ubx216-380 both form fibers, even though these truncations remove either a portion or all of the sequences resembling elastomeric proteins. However, these truncations are difficult to draw into materials, producing shorter, more brittle fibers than even Ubx49-380 and Ubx88-380. Ubx variants with further deletions from the N-terminus did not produce materials, marking amino acid 216 as the N-terminal boundary of the minimal materials-forming unit.

Even though Ubx139-380 and Ubx216-380 both generate brittle fibers, Ubx174-380, the intermediate truncation, does not form materials. Thus, removal of residues 139-173 exposes a second region of Ubx that inhibits materials assembly. Removal of this inhibitory region in the Ubx216-380 variant restores potential materials formation. Since much of the region between amino acids 173 and 215 is intrinsically disordered (**Fig. 3.7A**), the motion of this highly flexible region may physically block Ubx-Ubx interactions. Indeed, monomeric Ubx174-380 also binds DNA with an affinity more than 20 times poorer than the full-length protein, an inhibition largely absent in Ubx216-380 (Liu et al., 2008). Therefore, amino acids 173-215 debilitate multiple Ubx macromolecular interactions.

The C-terminus of the minimal unit was identified by making progressive deletions from the C-terminal end of the Ubx216-380 variant, the smallest N-terminal truncation mutant that still forms materials (**Fig. 3.7B**). Ubx216-356 does form fibers, even though a polyalanine region, a key motif in spider silks, was removed. By contrast, Ubx216-344, which additionally removes a portion of the DNA-binding homeodomain (**Fig. 3.7B**), does not generate fibers. Neither materials nor amorphous aggregates were formed by further C-terminal truncation mutants. Therefore, Ubx216-344 likely did not fail due to exposure of a second aggregation-prone region. We consequently conclude, within the resolution of our assays, that Ubx216-356 is a minimal materials-forming unit. As such, this region must include sequences permitting both fiber formation and fiber-fiber association. Curiously, none of the Ubx sequence features that resemble amyloidogenic or elastomeric proteins in the N-terminal 216 amino acids of the protein were required for materials formation, suggesting alternate mechanisms guide the

assembly of materials from this portion of the Ubx sequence.

3.3.6 Minimal material-forming region produces similar materials to full-length Ubx

The decreased robustness of fibers produced from Ubx216-356 relative to full-length Ubx indicates that sequences outside this region impact materials assembly, even though these sequences are not absolutely required. This alteration in the quality of fibers produced could be due to an alteration in the structure of the materials. However, SEM reveals that the surface of fibers composed of Ubx216-356 exhibits the aligned striations characteristic of Ubx fibers (**Fig. 3.9A,B**). Occasionally, the surface of fibers produced from severe truncations appears less smooth and uniform **(Fig. 3.9C,D)**, a trait never observed for fibers created with full-length Ubx. Thus, the appearance of Ubx216-356 fibers is generally consistent with those composed of full-length Ubx.

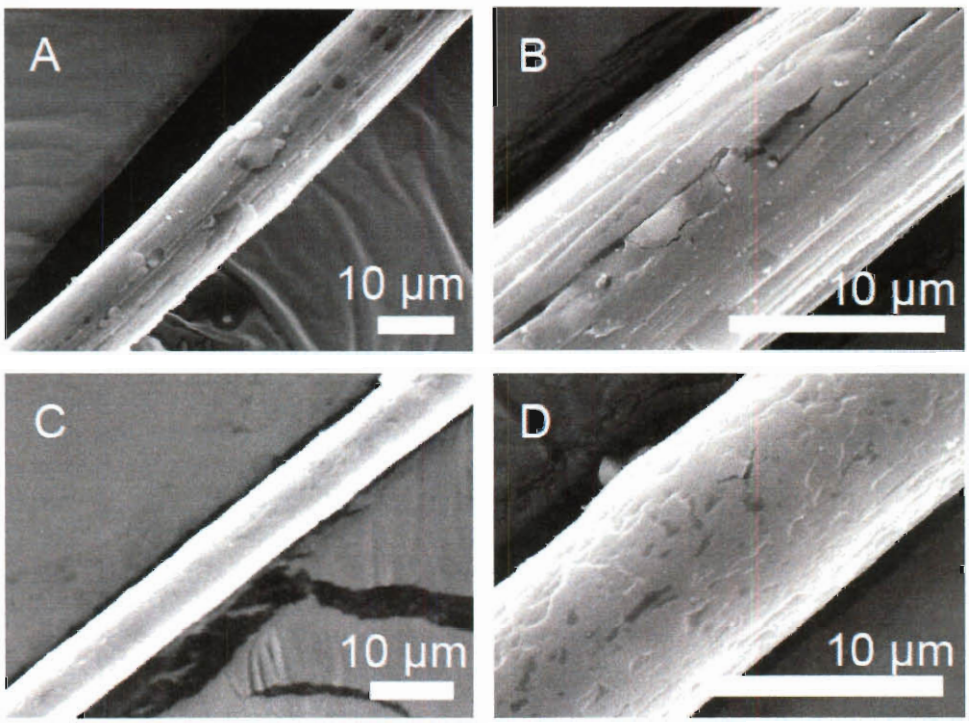

Figure 3.9 SEM of fibers generated from severely truncated Ubx fragments. (A,B) Fibers composed of Ubx216-356 have uniform diameter and a striated surface, comparable to ropes composed of full-length Ubx. (C,D) On rare occasions, fibers generated from severely truncated Ubx variants have a rougher-appearing surface lacking striations, as shown here for a Ubx216-380 fiber.

3.3.7 Additional regions contributing to fiber formation

Given that the morphology of the Ubx216-356 fibers generally appears intact, it is likely that sequences outside this minimal domain form additional interactions to enhance the robustness of the fibers. One potential mechanism would be for the Ubx sequence to contain a second region capable of forming materials and thus contribute additional stabilizing Ubx-Ubx interactions. To test this hypothesis, we generated C-terminal truncations of full length Ubx (**Fig. 3.7B**). Consistent with the existence of a second materials-forming domain, we could draw fibers using constructs with longer C-terminal truncations (past amino acid 356) when the N-terminal 215 amino acids were present. Indeed, Ubx1-243 generated fibers, although they were small and brittle.

Using the Ubx1-243 C-terminal truncation mutant as a template, we then began deleting from the N-terminus to locate the N-terminal boundary of this second materials-forming region (**Fig. 3.7B**). Ubx19-243, Ubx49-243, and Ubx88-243 generated fibers, but not Ubx139-243. Consequently, the N-terminal minimal materials-forming region in Ubx extends from amino acids 88 to 243, overlapping the C-terminal minimal materials-forming region by 28 amino acids, including the central alanine-rich region (a.a. 221-234). This alanine-rich sequence is predicted to form an α-helix whose normal function in transcription activation relies on the potential to form secondary structure (Tan et al., 2002). Intriguingly, the N-terminal minimal materials-forming region (88-243) contains the disordered region, most of the GGX and GXXP motifs, and one alanine-rich region, and thus its sequence more closely resembles the sequences of known elastomeric, materials-forming proteins. Unfortunately, fibers generated from the N-terminal minimal materials-forming region appear even weaker than those produced by the C-terminal

minimal materials-forming region. Consequently, we could not generate fibers from Ubx88-243 sufficiently long to transfer to a scanning electron microscope stub for morphology examination.

3.3.8 Sequence features of the minimal materials-forming regions

The minimal materials-forming sequences have many necessary features. These sequences must be capable of forming fibers, the fibers must be capable of self-association, and regions inhibiting either type of assembly must be excluded or inhibited. Despite these multiple requirements, large sections of the Ubx sequence can be removed without preventing materials formation: 63% of Ubx was removed to generate Ubx216-356, the C-terminal minimal materials-forming region, whereas 59% of the Ubx sequence was removed to generate Ubx88-243, the N-terminal minimal materials-forming region.

However, these minimal regions only produce very short, brittle fibers. The entire Ubx sequence, including both minimal materials-forming domains as well as regions outside these domains, is required to generate the longer, more robust fibers analogous to fibers assembled from the full-length protein (**Fig. 3.7B**). Indeed, even small truncations from either the N-terminus or the C-terminus reduce the ability of Ubx to form fibers. Given that the normal functions of Ubx (DNA binding, transcription activation and repression) can be localized to discrete domains within Ubx (Beachy et al., 1993; Galant and Carroll, 2002; Hughes and Kaufman, 2002; Lewis, 1978; Liu et al., 2008; Ronshaugen et al., 2002; Tan et al., 2002), it is interesting that robust materials assembly involves the entire sequence.

3.3.9 Ubx materials-formation *in vivo*

Given Ubx self-assembles into materials readily *in vitro*, it is tempting to

speculate that Ubx may also generate materials as part of its *in vivo* function. However, extensive immunohistochemical analysis of the distribution and concentration of Ubx proteins *in vivo* has not revealed extended Ubx oligomers within a *Drosophila* cell, even when the concentration of Ubx has been artificially elevated (Tour et al., 2005; Weatherbee et al., 1999). Furthermore, aggregates have not been observed when Ubx is over-expressed in *E. coli*. Since our data suggest Ubx requires exposure to an air-water interface to assemble *in vitro*, it is unlikely that these microscale or macroscale materials form as part of the natural function of Ubx.

Limited Ubx homomeric interactions do occur *in vivo* upon binding a subset of Ubx-regulated enhancers that contain multiple (4 to 15) DNA-binding sites arrayed in tandem (Beachy et al., 1993; Liu et al., 2008). Adjacent Ubx proteins appear to interact with one another to stabilize binding (Beachy et al., 1993). Furthermore, Ubx proteins bound to multisite DNAs can interact with Ubx proteins bound to other DNA sites to create looped DNA structures (Beachy et al., 1993). At the molecular level, the protein interfaces used to form Ubx-Ubx interactions *in vivo* may be similar to those that drive nanoscale Ubx fibril assembly *in vitro*. Therefore, while Ubx materials are likely not produced *in vivo*, the protein-protein interactions that lead to the assembly of Ubx materials may be biologically relevant.

3.4 Conclusions

Using the *Drosophila* transcription factor Ubx, we were able to mimic the material architectures previously produced with elastomeric proteins as well as generate novel structures using gentle conditions. Within the Ubx sequence, we identified two regions capable of forming film and rope with an appearance comparable to those formed

by full-length Ubx. We also demonstrated that generation of robust materials requires inclusion of both minimal regions, and consequently the majority of the Ubx sequence. These materials are exceptionally interesting because (i) Ubx does not appear to generate these materials as part of its *in vivo* function, (ii) the C-terminal minimal region lacks sequence features characteristic of other materials-forming proteins, (iii) the N-terminal materials-forming domain contains far fewer elastomeric motifs than proteins that form materials as part of their natural function, (iv) assembly of materials occurs using unusually gentle conditions, and (v) Ubx fibers are surprisingly heat stable. These Ubx materials therefore provide a novel vantage point for exploring the structure–function relationships underlying organized protein self-assembly and materials production.

The unusual properties of Ubx materials also offer several advantages for materials engineering relative to the elastomeric or amyloidogenic proteins frequently used to construct materials. The stability of Ubx in *E. coli*, combined with the ease of Ubx assembly, potentiates both facile material production and functionalization. Full-length Ubx self-assembles at 1–2 orders of magnitude lower protein concentration than required for structural protein-derived materials. The assembly also takes place under far less stringent conditions (within 2 h under ambient conditions), greatly facilitating the incorporation of chemically fragile ligands or functional proteins via gene fusions, since many ligands and proteins would be inactivated by the harsh processing methods required to trigger assembly of most other recombinant protein-based materials (Bondos et al., 2002; Huang et al., 2004). Finally, the self-adhesive properties of Ubx fibers permit hierarchical construction of complicated three-dimensional architectures.

CHAPTER 4

Mechanical Properties of Ubx-based Materials[3]

4.1 Introduction

Specific mechanical properties of protein-based materials are required for their effective application. For example, heart valves and blood vessels require elastic materials; bone, cartilage, and tendon require strong materials (Faury, 2001; Martyn and Greenwald, 2001; Pasquali-Ronchetti and Baccarani-Contri, 1997). The development of protein-based materials with diverse mechanical properties has facilitated the realization of a broad range of applications, such as body armor, surgical sutures, and tissue engineering scaffolds (Han et al., 2010; Lagziel-Simis et al., 2006; McGrath and Kaplan, 1997; Moy et al., 1991; Wen et al., 2010).

Mechanical properties also affect the behavior of cells/tissues interacting with these materials. Cells can sense the mechanical properties of the surrounding environment via their mechanotransduction receptors (Vogel, 2006; Vogel and Sheetz, 2009). These receptors enable the transduction of mechanical signals into biochemical signals that regulate cellular responses such as adhesion, proliferation, differentiation, and apoptosis (Helenius et al., 2008; Vogel, 2006; Vogel and Sheetz, 2009).

The methods used to generate and process protein-based materials can have a substantial impact on the mechanical properties of the products (Huang et al., 2000; Liivak et al., 1998; Qiu et al., 2009; Zeugolis et al., 2008). Recombinantly produced

---

[3] Parts of chapter 4, including text and figures, were reported in Huang and Lu et al., 2009. Y. Lu and J. Shah contributed to mechanical testing. R. Majithia contributed to SEM and TEM imaging of fiber cross-sections.

protein-based materials have been generated with extensibilities matching or exceeding elastin (Qiu et al., 2009; Teng et al., 2009) or with breaking strength approaching that of spider silk (Wen et al., 2010; Xia et al., 2010).

Because mechanical properties determine the utility of a protein-based material and may also affect the behavior of cells/tissues interacting with these materials (Engler et al., 2006; Georges et al., 2007; Huang et al., 2007; Leal-Egana and Scheibel, 2010), multiple approaches to engineer or control the mechanical properties of protein-based materials have been explored. These methods have included chemical cross-linking, oxidation, and incorporation of nanoparticles and metal films (Brooks et al., 2008; Grip et al., 2009; Kharlampieva et al., 2010; Lazaris et al., 2002; Lee et al., 2009; Qiu et al., 2009; Teng et al., 2009). However, these techniques may limit or preclude engineering the functional properties of the materials by incorporation of active protein chimeras.

In Chapter 3, we reported that Ultrabithorax (Ubx), a *Drosophila melanogaster* Hox transcription factor purified from *E. coli*, spontaneously self-assembles into nanoscale, microscale, and macroscale materials from an aqueous solution near neutral pH and without harsh additives (Greer et al., 2009). In this chapter, we investigate the mechanical properties of fibers composed of Ubx that are 2−40 μm in diameter and centimeters in length. The diameter of fibers drawn from film can be varied by adjusting protein concentration and assembly time, an approach that permits the production of materials with a range of properties and different mechanisms of extension using the same starting materials and basic protocol. Narrow Ubx fibers (diameter <10 μm) extend elastically, with the breaking strength and Young's modulus decreasing with increasing diameter. In contrast, the predominantly plastic deformation of wide fibers (diameter >15

μm) reflects the increase in breaking strain with increasing diameter, apparently due to a change in structure. Intermediate fibers display mixed properties. Bundles of narrow fibers retain the mechanical properties of individual fibers but can withstand much larger forces. By controlling diameter, we can generate materials with breaking stress and breaking strain matching natural bovine ligament elastin. Consequently, we anticipate that this approach to controlling diameter may be useful in fine-tuning mechanical properties to match a specific application and in the design of materials for novel applications.

4.2 Results

4.2.1 Stress-strain plots reveal that diameter affects mechanical properties

In preliminary testing of the mechanical properties of Ubx materials, we found that Ubx fibers were extensible, though the breaking strain (0.53±0.19) and the shape of the stress-strain curves varied significantly between samples (Greer et al., 2009). We have pursued this interesting dissimilarity and found that the shapes of the stress-strain curves parse into three groups based on the diameter of the Ubx fiber (**Fig. 4.1**). Whereas the diameter of an individual fiber along its length is quite uniform, diameter varies significantly between fibers. The engineering stress on narrow fibers (<10 μm) increases nearly linearly with increasing strain, suggesting elastic deformation. In contrast, the stress-strain curves of wide fibers (>15 μm) have a "yield point" indicative of an elastic-to-plastic transition. Stress-strain curves for the third group, fibers with a diameter between 10 and 15 μm, are intermediate between these two extremes. Importantly, wide fibers rupture at much higher strains than narrow fibers, explaining the wide variation in breaking strain that we reported previously (Greer et al., 2009).

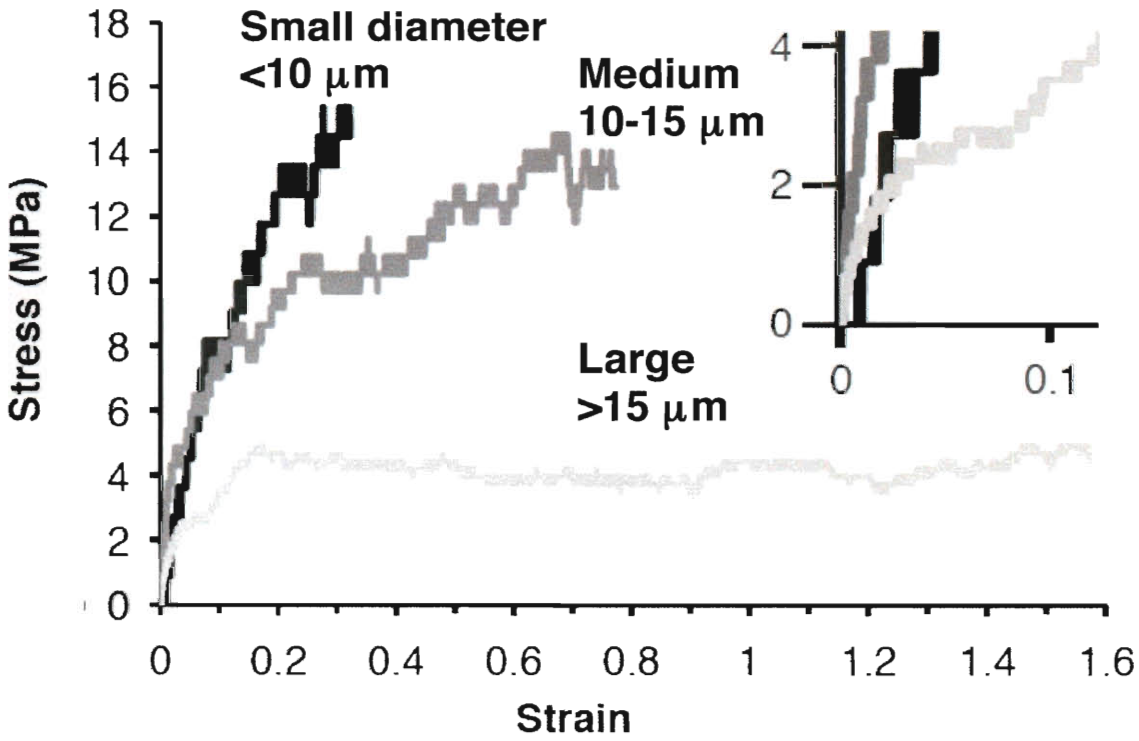

Figure 4.1 Stress-strain curves of different diameter Ubx fibers have different shapes. The shape of a representative curve for narrow fibers <10 μm in diameter (black) suggests a largely elastic deformation; a representative curve for wide fibers with a diameter >15 μm (light gray) stretches elastically before yielding to plastic deformation at a strain near 0.2. In contrast, intermediate fibers with a diameter between 10 and 15 μm (dark gray) exhibit a greater mixture of elastic and plastic deformation. Inset: the initial slope of all three stress-strain curves is similar, indicating that all fibers initially deform elastically.

4.2.2 Controlling diameters by varying production conditions

We further explored whether fiber diameter can be controlled by altering either the amount of time allowed for film assembly or by changing the concentration of Ubx monomers used for film self-assembly (**Fig. 4.2**). Either longer incubation time or increased protein concentration increases fiber diameter, presumably by increasing the density of fibrils in the film from which the fiber is drawn. The ability to control fiber diameter enabled a systematic study to determine the impact of fiber diameter on the mechanical properties and mechanism of deformation.

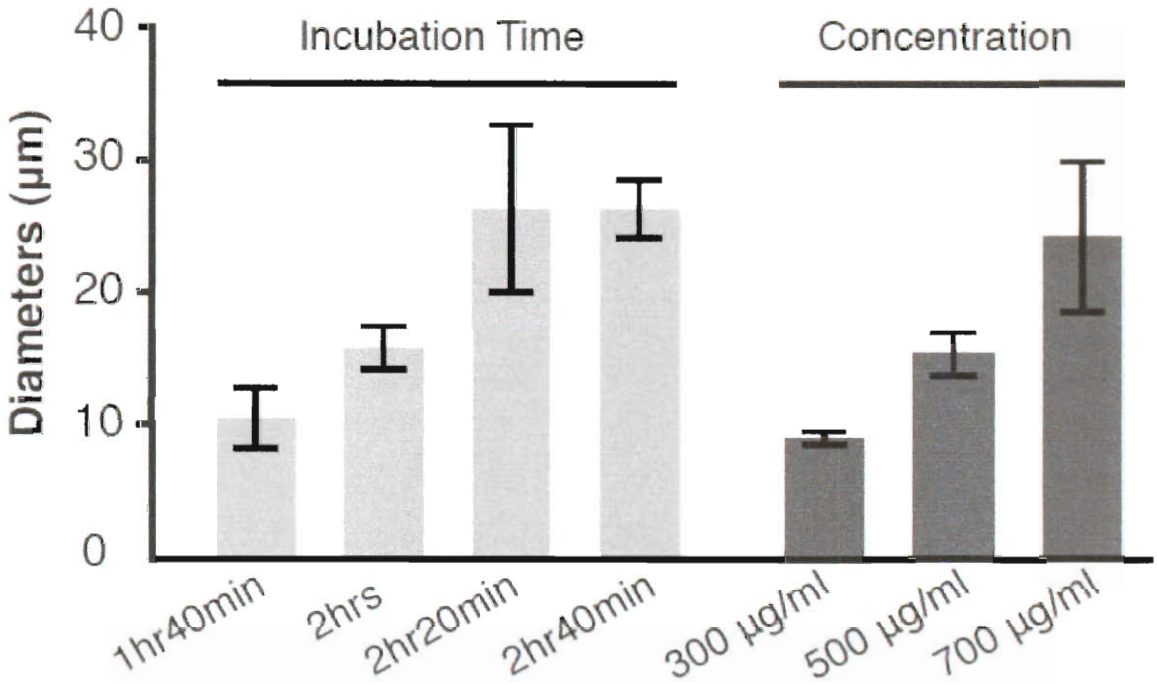

Figure 4.2 Assembly time and protein concentration affect diameter of fibers produced. (Grey bars) The diameters of Ubx fibers generated from sessile drops depend on the time allotted for self-assembly when a protein concentration of 500 μg/ml was used. (Black bars) The diameters of Ubx fibers generated from sessile drops with 2 hr incubation depend on protein concentration.

4.2.3 Ubx fibers have diameter-dependent mechanical properties

By examining fibers with a range of diameters, we found that the differences in the shape of the stress-strain curves originate from changes in the diameter-dependence of key mechanical properties (**Fig. 4.3**). For narrow fibers (0-10 μm), the breaking strength is strongly dependent on diameter: a two-fold increase in diameter is sufficient to decrease the breaking strength several fold (**Fig. 4.3A**). Consequently, the Young's modulus of narrow fibers also decreases sharply with increasing diameter (**Fig. 4.3B**). This trend is similar to that observed for elastin-like peptides (Qiu et al., 2009), for which deformation is primarily elastic. Indeed, typical stress-strain curves for narrow fibers

show little sign of nonrecoverable change (**Fig. 4.1**), a fact further confirmed by the consistency of a series of loading/unloading curves on a single narrow fiber used to determine Young's modulus. Furthermore, the initial diameter of narrow fibers is nearly identical to the fiber diameter after rupture (**Fig. 4.3C**), despite the fact that narrow fibers could be extended an additional 40% of their initial length before breaking (**Fig. 4.3D**). Finally, we observed no evidence of necking at the rupture point. Together, these data suggest that elastic deformation is the predominant deformation mode for narrow fibers.

In contrast, for wide fibers (>15 μm), both the breaking strength and Young's modulus are largely independent of diameter (**Fig. 4.3A,B**). However, the breaking strain increases rapidly with increasing diameter for wide fibers (**Fig. 4.3D**); this observation contrasts with breaking strain being independent of diameter for narrow fibers. As noted above, typical stress-strain curves for wide fibers show a distinctive "yielding" behavior after the initial elastic deformation (**Fig. 4.1**), suggesting the occurrence of large scale, nonrecoverable plastic deformation or rearrangement of fibrils within fibers. Such rearrangement could account for the surprising extensibility of wide fibers, up to 150% (**Fig. 4.3D**). The extent of plastic deformation increases with increasing fiber diameter, with the widest fibers able to sustain the most strain (**Fig. 4.3D**). Wide fibers do not return to their initial diameter after rupture (**Fig. 4.3C**), a further indication of plastic deformation. The magnitude of this deviation increases with increasing diameter. Finally, lower breaking strain and breaking strength is observed at faster pulling rates for wide fibers, suggesting that fibrils within the fibers lack sufficient time to rearrange at faster pulling rates (**Fig. 4.4**).

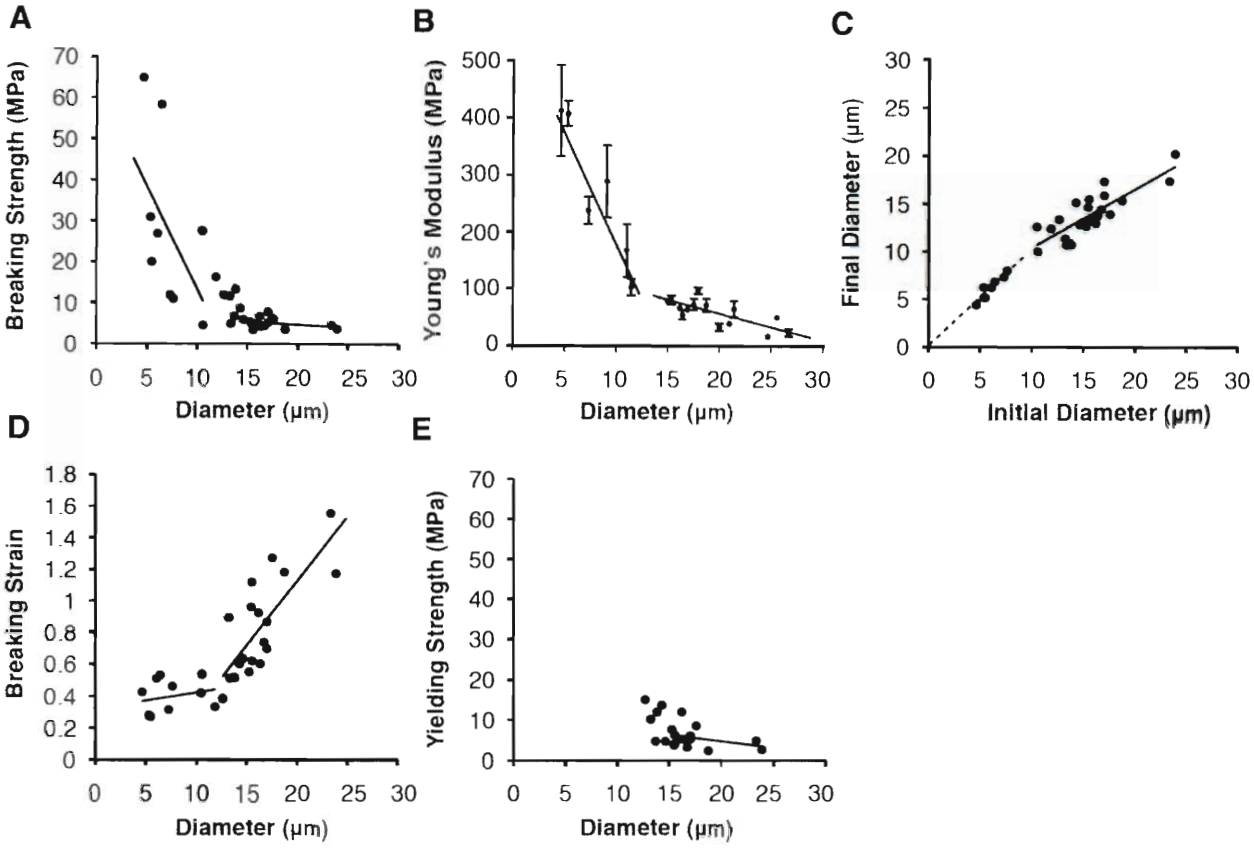

Figure 4.3 Diameters affect the mechanical properties of Ubx fibers. (A) The breaking strength depends on the initial diameter of the fibers. The diameter dependence is markedly different for narrow and wide fibers, with the intermediate fibers behaving as a mixture of the two extremes. The dependence of breaking strength on diameter for narrow and wide fibers is significantly different ($n_{narrow} = 11$, $n_{wide} = 13$, $p = 0.04$). (B) Young's modulus was measured during the unloading phase of loading / unloading cycles for both narrow and wide fibers. Again, the diameter dependence was significantly different for these two groups ($n_{narrow} = 10$, $n_{wide} = 47$, $p < 0.001$). (C) Narrow fibers return to their original diameter upon unloading (the dashed line is graphed at $x = y$), whereas wider fibers increasingly fail to recover their original shape, a mark of plastic deformation ($n_{narrow} = 11$, $n_{wide} = 13$, $p = 0.001$). (D) The breaking strain of wide fibers depends strongly on diameter, an effect greatly reduced and significantly different for narrow fibers ($n_{narrow} = 11$, $n_{wide} = 13$, $p = 0.04$). (E) The yielding strength, at which wide fibers transition from elastic deformation to plastic deformation, is only weakly dependent on diameter (Fibers with diameters of 10 μm or less do not undergo plastic deformation).

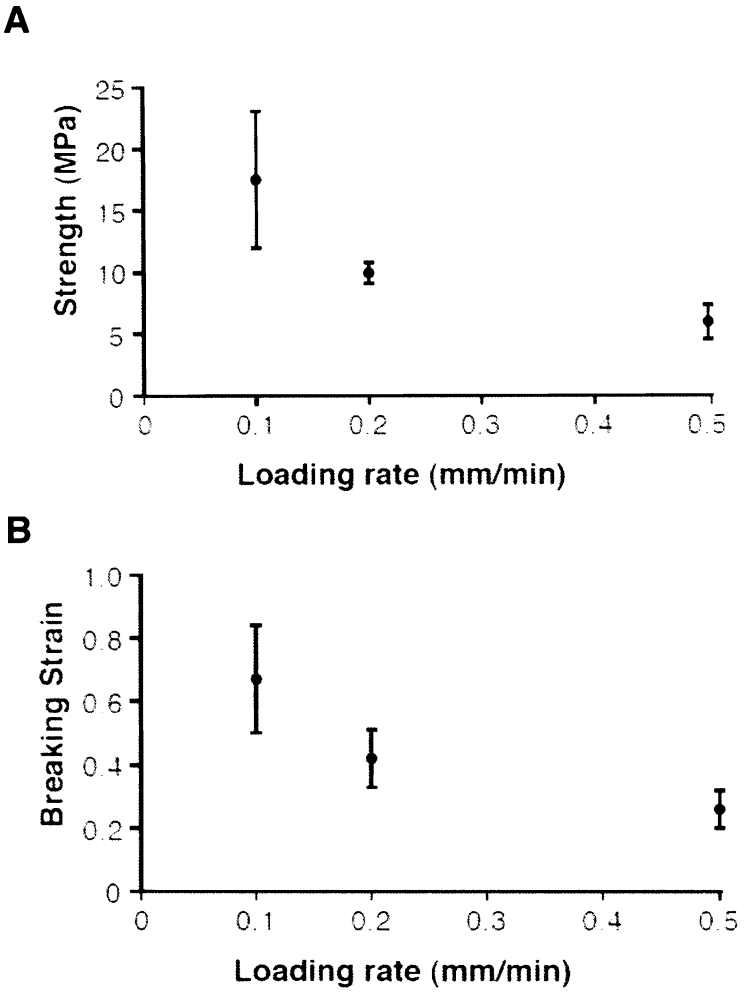

Figure 4.4 Pulling rate affects the mechanical properties of Ubx fibers. (A) Breaking strength of Ubx fibers depends on the loading rate. (B) Breaking strain of Ubx fibers is also dependent on the loading rate. The diameters of these fibers ranged from 15 to 20 μm. Fibers stretched at high rates may be less able to accommodate extension and thus rupture at lower strains. Consequently, the minimum possible pulling rate of 0.1 mm/min was used for the remainder of experiments in this work.

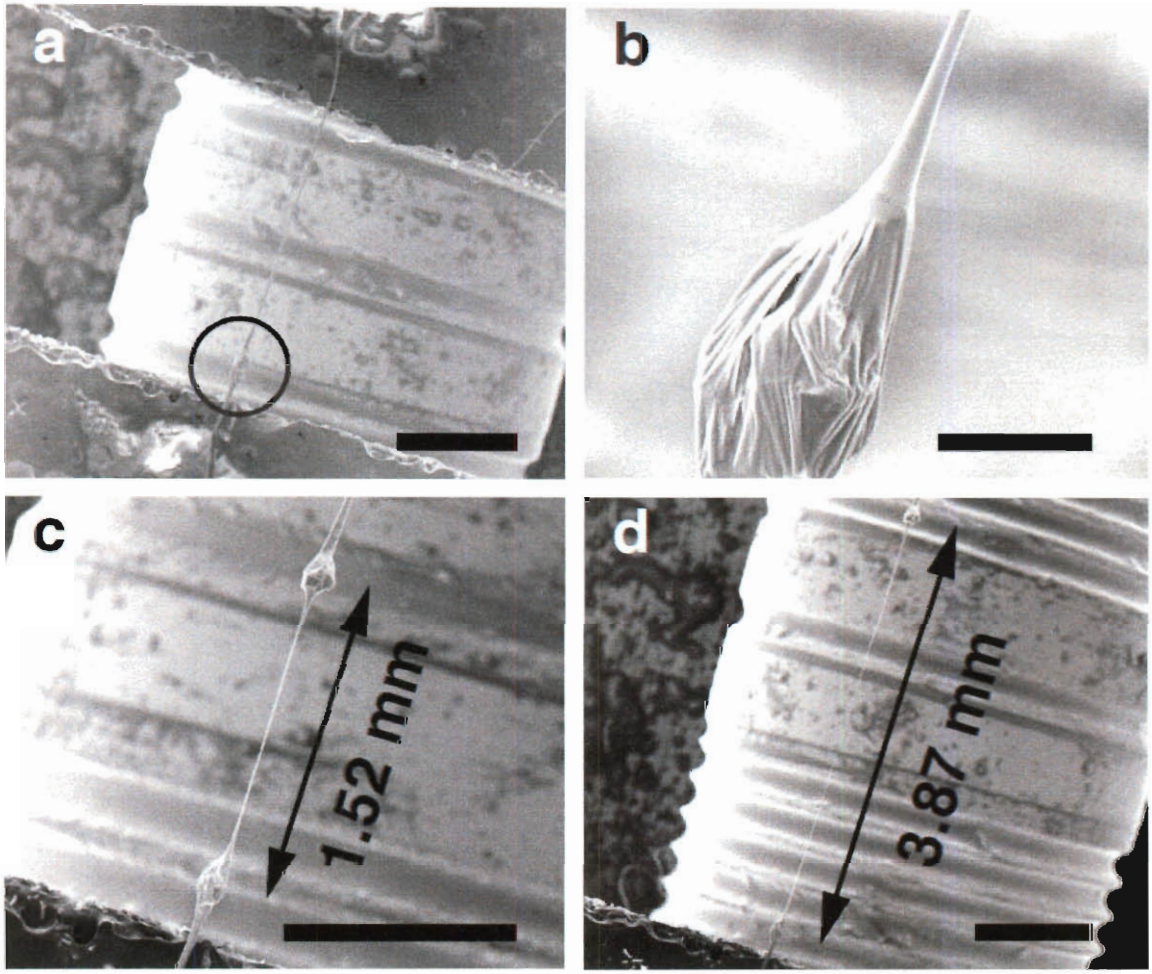

Figure 4.5 Representative frames from a scanning electron microscopy movie of a microencapsulate being drawn into a fiber. (A) Entire fiber with a 200 μm long encapsulate (circled) before stretching. Scale bar, 1 mm. (B) Magnification of the encapsulate before stretching. Scale bar, 100 μm. (C) During extension, the encapsulate stretches from its center to form a fiber 2 μm in diameter, whereas the original fiber and edges of the microencapsulate are unchanged, likely because of dehydration in the vacuum. Scale bar, 1 mm. (D) The extended fiber and encapsulate just prior to rupture. Scale bar, 1 mm.

4.2.5 Fibril-packing model explains diameter effect on mechanical properties

Fibers with intermediate diameters (10-15 μm) have mechanical properties between the extremes of those for narrow and wide fibers. The fact that both elastic and plastic traits are observed in these intermediate fibers, combined with the observation that even the highly extensible wide fibers initially deform in an elastic manner (**Fig. 4.1**),

4.2.4 Plastic deformation of Ubx microencapsulates

In confirmation of results of these mechanical tests, we were able to observe plastic deformation of Ubx materials by performing *in situ* tensile tests inside a scanning electron microscope (**Fig. 4.5**). Although Ubx fibers dehydrate and consequently become brittle in a vacuum, a subset of wide fibers incorporates buffer-filled microencapsulates (Greer et al., 2009). Ubx microencapsulates, like fibers, are constructed from fibrils but retain an aqueous buffer-filled core. Fibers containing these structures were not used for quantitative mechanical measurements; however, unlike fibers, microencapsulates remain sufficiently hydrated to allow observation of tensile load-induced structural rearrangement by scanning electron microscopy (**Fig. 4.5**). The microencapsulate extended to >1000% of its initial length, forming a fiber that had a uniform diameter of ~2 μm and a length of ~4 mm. This rearrangement of the microencapsulate structure directly demonstrates the plasticity of Ubx materials in response to tensile stress.

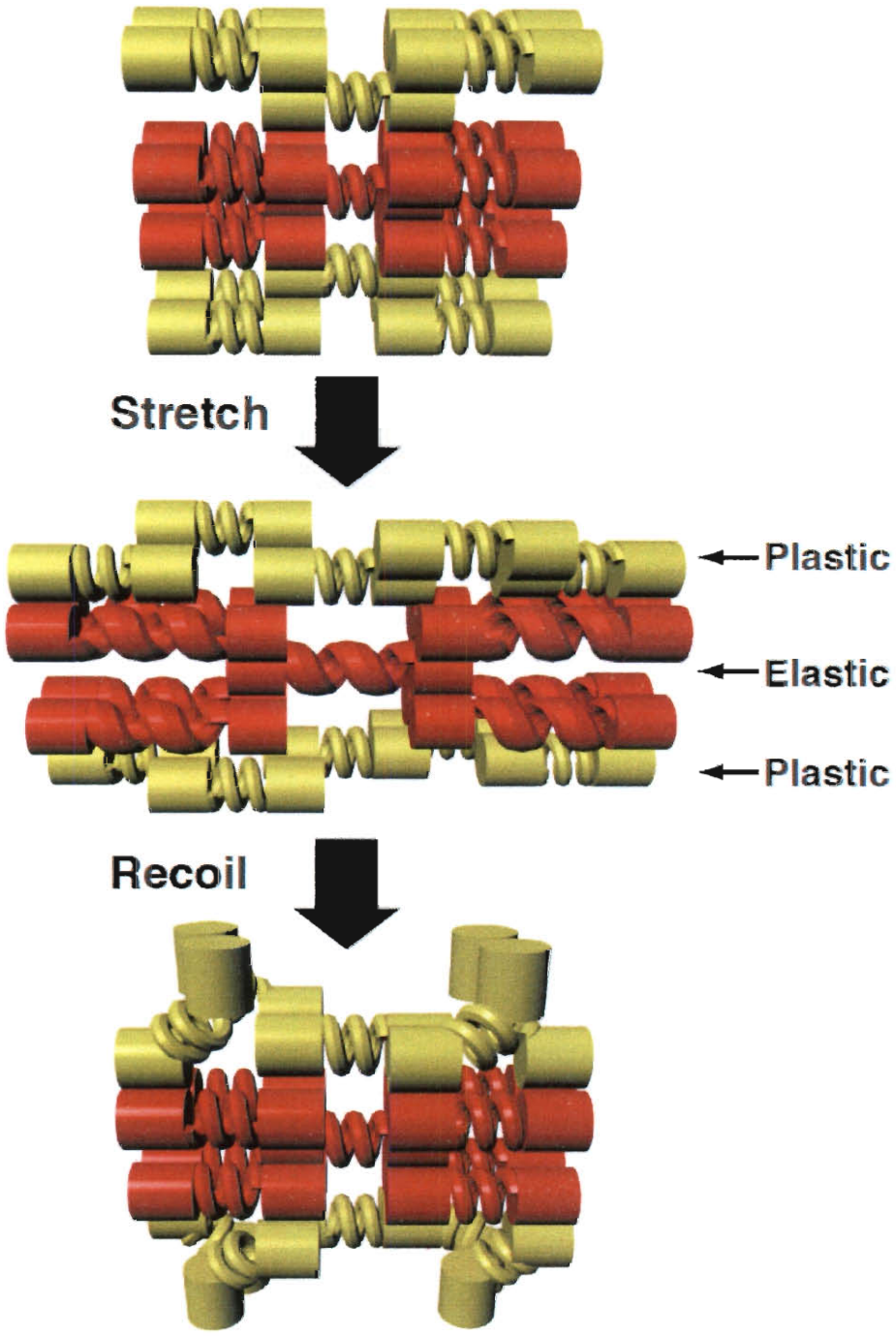

Figure 4.6 Model for extension and relaxation of wide fibers. Fibrils in the elastic core (red) of a wide fiber extend without changing fibril arrangement, whereas fibrils in the plastically deforming outer layer (yellow) repack, decreasing fiber diameter and increasing the length of outer layer while forming new fibril-fibril associations. Upon rapid unloading, these new associations are maintained, preserving the stretched length of the outer layer as the core elastically recoils to its original length. Consequently, the outer layers are expected to either wrinkle or separate entirely from the fiber core.

demonstrates that a single fiber may exhibit both properties. One can imagine two arrangements that would permit both elastic and plastic deformation: (i) wide fibers might contain different types of nanoscale fibrils, some of which inherently deform elastically whereas other fibrils deform plastically, or (ii) the fibrils themselves may be uniform but packed differently or less tightly in wide fibers, allowing fibrils to rearrange under strain locally. Regional differences in fibril packing would then produce the observed combination of elastic and plastic extension. Given that each fiber is drawn from a single film constructed of fibrils, it seems extremely unlikely that the uniform conditions used to produce fibers and film would result in a mixture of fibrils with different mechanical properties and, moreover, that plastically deforming fibrils would be incorporated into wide fibers yet excluded from narrow fibers.

Therefore, these data best fit a model in which fibers are composed of regions of fibrils that are packed differently (**Fig. 4.6**). Wide fibers consist of both tightly packed fibrils (red) and loosely packed fibrils (yellow). Closely packed fibrils undergo elastic deformation and provide most of the tensile strength of the fiber. The less densely packed fibrils rearrange plastically in response to tensile loading.

4.2.6 Electron microscopy of fiber cross sections supports the fibril-packing model

To test this model, electron microscopy of fiber cross sections was used to search for differences in fiber structure between narrow and wide fibers. Cross sections of narrow fibers reveal a closely packed interior when viewed by transmission electron microscopy (**Fig. 4.7**) and an even, smooth surface in scanning electron miscroscopy (**Fig. 4.8A,C**). In contrast, cross-sectional SEM images of wide fibers reveal smooth islands, similar in diameter to narrow fibers (~7-10 μm), surrounded by disordered regions containing fissures (**Fig. 4.8B,D**). Such structures indicate a difference in fibril packing that enables fissures to form because the narrow fibers and the cores of wide fibers both lack these structures. Therefore, the plastic nature of the large fibers appears to correlate with the presence of poorly packed regions surrounding elastic, tightly

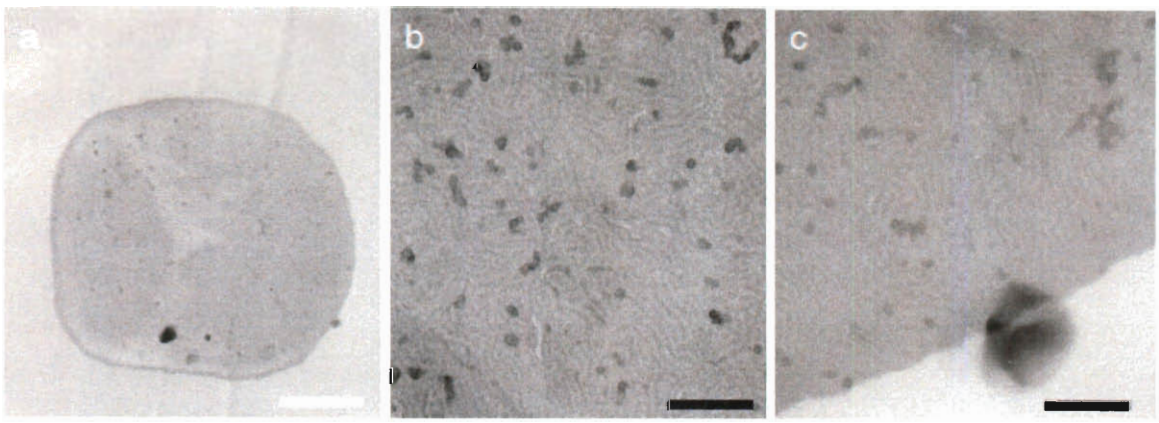

Figure 4.7 Transmission electron microscopy micrograph of a cross-section of narrow fibers. (A) TEM of a cross-section of a narrow Ubx fiber. (B) The fiber structure is organized in the interior, and (C) around much of the fiber edge. TEM sections were post-stained with 2% (wt/vol) uranyl acetate in a microwave (Biowave microwave - Ted Pella, Inc., Redding, CA) for a period of 10 seconds at 200 W, followed by four washes with warm distilled water. Grids were examined using a JEOL 1200EX transmission electron microscope at an accelerating voltage of 100 kV. The uranyl acetate stain appears to react with the Coomassie stain used to locate the fibers in the grid, leading to precipitation and blotches on the image. White scale bar, 2 μm. Black scale bars, 200 nm. In collaboration with Ravish Majithia from Keith Meissner Lab, Texas A&M University.

4.2.7 Deformation of wide Ubx fibers after unloading supports the fibril-packing model

This fibril-packing model predicts that wide fibers should wrinkle upon unloading, as the elastic cores return to their original length and the plastically deformed outer layers retain the longest length acquired under tensile stress (**Fig. 4.6**). Indeed, wrinkles are reproducibly observed in wide fibers at different strain levels after unloading. Greater wrinkling is observed for wide fibers subjected to higher strain, whereas such wrinkling is absent in narrow fibers at any strain levels (**Fig. 4.9A-J**). Furthermore, the size of the creases is also dependent on the diameter of the fiber. In wide fibers, these wrinkles can become so pronounced that the outer wrinkled layers occasionally peel from the central core upon fracture (**Fig. 4.10**). On the inside surface of these flayed sections, fibrils occasionally dislodge as if they were in the process of rearranging when the fiber ruptured. Consequently, this model correctly predicts multiple aspects of the behavior of wide fibers under tensile stress.

4.2.8 Mechanical properties of bundles depend on the diameter of individual fibers

One potential deficit of using diameter to control fiber mechanical properties is that the breaking strength and the extensibility of the fibers are coupled rather than independently designable. For instance, less overall force can be applied to the narrow, elastic fibers. Because the mechanical properties of fibers appear to be related to fiber structure, we tested whether fusing multiple narrow fibers into bundles (Greer et al., 2009) could create wide elastic fibers that would rupture at larger strains yet still behave like a single wide fiber with a diameter matching that of the bundle or whether bundles would behave like one of the individual fibers from which they are composed. We found

packed cores (**Fig. 4.6**). The surrounding regions consist of layers of fibrils that are presumably capable of plastic rearrangement. The widest fibers have the largest proportion of disordered plastic regions, potentially explaining their capacity to undergo substantial strain without rupturing (**Fig. 4.3D**).

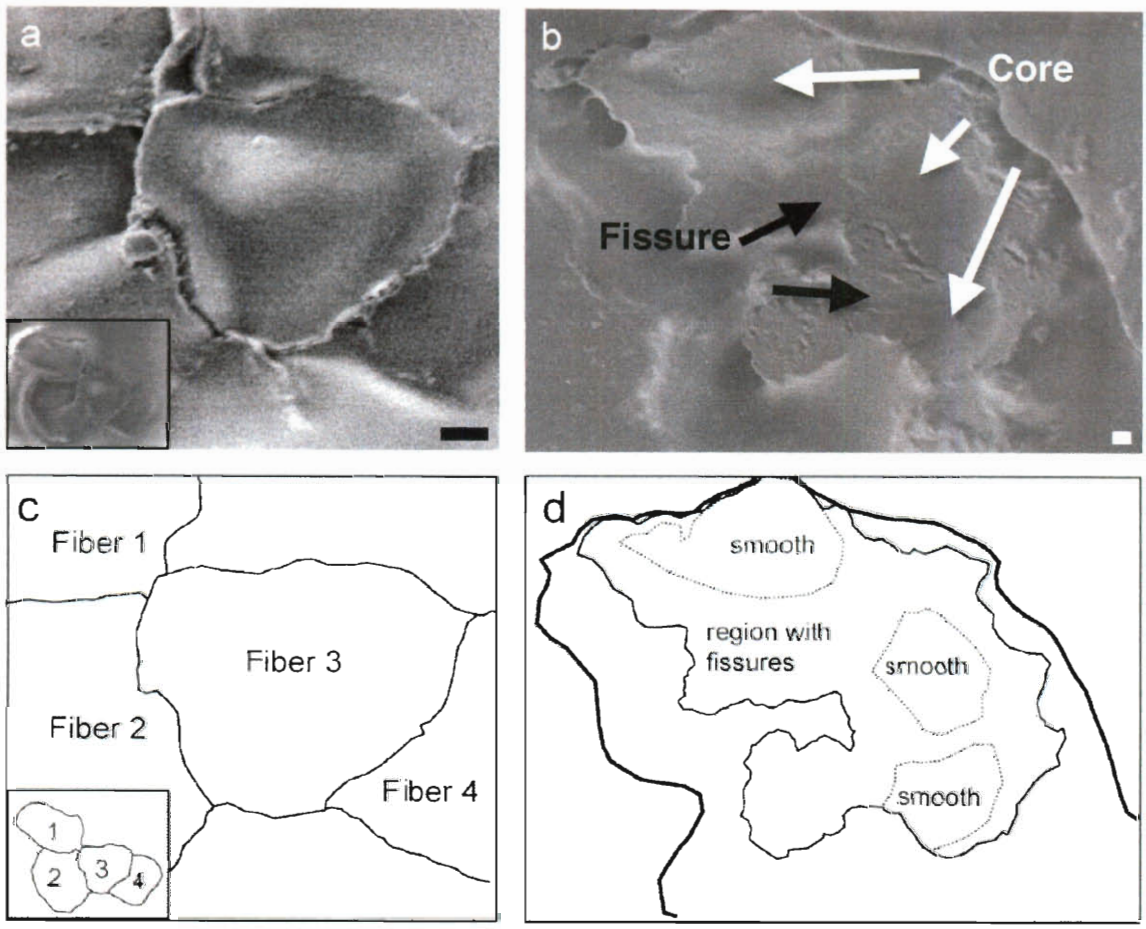

Figure 4.8 SEM images and schematics of fiber cross-sections reveal fissures only in wide fibers. (A) Cross-section of narrow fibers in a four-fiber bundle (inset) is smooth and tightly packed. (B) In contrast, a cross-section of a wide fiber reveals three tightly packed cores (white arrows) surrounded by regions with gaps or fissures (black arrow). Scale bars are 1 μm. (C) Cartoon of panel a depicting the boundaries of the four fibers in the bundle. (D) Cartoon of panel b showing the original outline of the wide fiber (thick solid line), the boundary of the wide fiber after slicing (narrow solid line), and the boundaries of the tightly packed cores (dotted lines). In collaboration with Ravish Majithia from Keith Meissner Lab, Texas A&M University.

Figure 4.11 Mechanical properties of Ubx bundles are determined by the properties of the constituent fibers. (A) SEM of a junction in a three-fiber bundle. (B) Ubx bundles (black circles) rupture under tensile stress at higher forces than individual Ubx fibers (gray diamonds). (C-H) Each panel represents measured and predicted data for a single bundle. If a bundle behaved as a single fiber with the same diameter as the bundle, then the breaking stress and strain should lie within the box with left slanting diagonal lines. The box with right slanting diagonal lines represents the entire range of predicted data for each fiber in that bundle, and hence bundles with a wide range of fibers diameters have larger boxes. The black diamond, representing data actually measured for the bundle, generally lands within the individual fibers zone. (C) Data for a 10 μm bundle (shown in panel A) composed of three fibers (4.5, 5.5, and 7 μm in diameter). (D) Data for a 24 μm bundle composed of three fibers (9, 10, and 20 μm in diameter). (E) Data for a 22 μm bundle composed of three fibers (11, 12.5, and 14.5 μm in diameter). (F) Data for a 36 μm bundle composed of three fibers (12, 16, and 30 μm in diameter). (G) Data for a 60 μm bundle composed of five fibers (15, 16, 25, 30, and 40 μm in diameter). (H) Data for a 38.4 μm bundle composed of three fibers (17, 17, and 30 μm in diameter). Note that the tendency for bundle behavior to mimic the behavior of its component fibers is consistent despite the wide range of fiber and bundle sizes assayed.

4.2.9 Ubx vs other protein-based materials

Fibers constructed from recombinant or regenerated elastin, silk, or collagen have all been reported to have mechanical properties that are dependent on fiber diameter. However, this diameter-dependence has been attributed to shear stress on the wall of the polymerizing fibers upon extrusion or electrospinning through an aperture (Liivak et al., 1998). In contrast, Ubx fibers are drawn from a film and thus never experience wall shear stress, and yet the mechanical properties of Ubx fibers are also diameter-dependent. Therefore, multiple fiber-producing processes result in materials whose mechanical properties are dependent on diameter, suggesting that this is an inherent property of many protein-based materials. Indeed, collagen fibers also flay open upon unloading (Zeugolis et al., 2008), indicating they could also have a layered architecture. For Ubx fibers, altering diameter not only changes the magnitude of the breaking strength and strain but also impacts the mechanism by which the protein fibers deform under tensile stress.

that fiber bundles do not behave like a single wide fiber of the same diameter (**Fig. 4.11**).

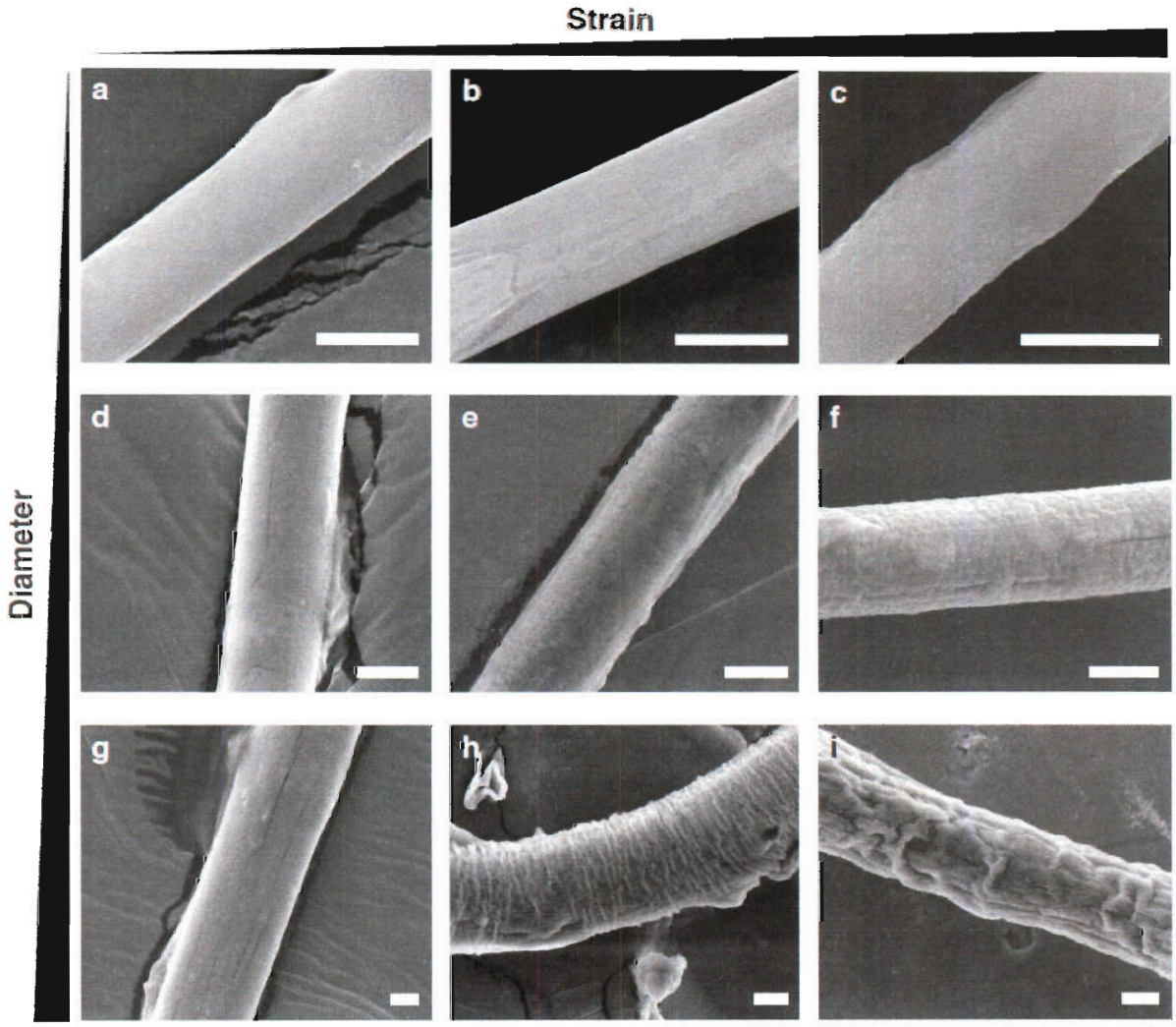

Figure 4.9 Deformation of wide fibers upon unloading or rupture indicates that they are composed of an elastic core surrounded by layers of plastically deforming fibrils. Fibers wrinkle upon unloading as the elastic core recoils to its original shape, whereas the plastic surface remains at or near its extended length. The degree of wrinkling is dependent on both the diameter of the fiber and the extension under load. (A) A 5 μm fiber is shown before extension, (B) after extension to a strain of 0.2 and unloading, and (C) after extension to a strain of 0.4 and unloading. Scale bars in panels A-C are 5 μm. A 15 μm fiber is shown (D) before extension, (E) after extension to a strain of 0.2 and after unloading, and (F) after extension to a strain of 0.4 and unloading. A 30 μm fiber is shown (G) before extension, (H) after extension to a strain of 0.2 and after unloading, (I) after extension to a strain of 0.4 and unloading. Scale bars in panels D-I are 10 μm.

Similar changes in the mechanism of extension may also explain the diameter dependence for the mechanical properties of other protein-based materials.

Table 4.1 Mechancial properties of Ubx comparing to other common materials. Table is modified from (Omenetto and Kaplan, 2010).

Material	Stiffness (Gpa)	Strength (GPa)	Extensiblity	Toughness (MJm-3)
Araneus MA silk	10	1.1	0.27	160
Bombyx mori silk	7	0.6	0.18	70
Tendon collagen	1.5	0.15	0.12	7.5
Wool	0.5	0.2	0.5	60
Elastin	0.001	0.002	1.5	2
Synthetic rubber	0.001	0.05	8.5	100
Nylon	5	0.95	0.18	80
Kevlar 49 fiber	130	3.6	0.027	50
Ubx	0.02 - 0.4	0.01 - 0.06	0.4 - 1.5	5 - 15

Protein-based materials have different sequences, leading to differences in mechanical properties (**Table 4.1**). The mechanical properties of Ubx fibers may be partially ascribed to sequence similarities among Ubx, elastin, and spider silk. Ubx has 14 GGX motifs (Greer et al., 2009), which have been proposed in elastin to interchange between folded or partially folded turn structures and less flexible extended conformations (Rauscher et al., 2006). GGX motifs are also thought to be important sequences in spider silk (Hayashi et al., 2004; Hinman et al., 2000; Huang et al., 2007; Leal-Egana and Scheibel, 2010). In addition, Ubx has three GXXP motifs, one of many glycine- and proline-rich motifs frequently present in elastomeric fibrils (Rauscher et al., 2006). These sequences are all required to generate robust, extensible materials from Ubx (Greer et al., 2009). Although Ubx has not been observed to form fibers as part of its *in*

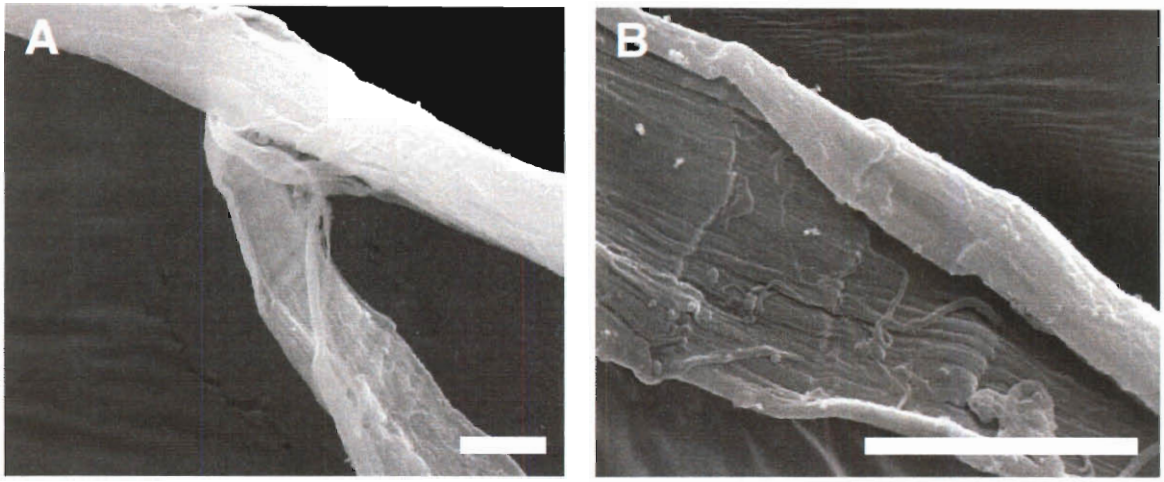

Figure 4.10 Wide fibers have outer layers surrounding their cores. (A) A 17 μm fiber in which the outer layers separated from the core upon rupture. (B) A higher magnification of the same fiber, revealing the separation of fibrils or groups of fibrils in the flayed-open surface. Scale bars for panels A and B are 5 μm.

Instead, the breaking stress and breaking strain of the bundles typically mimic the properties of its component fibers. This trend is independent of both bundle diameter and individual fiber diameters. These results demonstrate that the properties of individual fibers, such as the extent of fibril packing, determine the mechanical properties of a bundle. Because bundles have breaking stresses similar to their component fibers but have a larger cross-sectional area, they are able to withstand significantly larger forces before rupture (**Fig. 4.11B**). Consequently, creating bundles allows manipulation of the load-carrying properties of the materials.

vivo function, the breaking stress (~5 MPa) and strain (~150%) of the widest Ubx fibers (**Fig. 4.3 A,D**) are similar to the corresponding parameters for elastin (Huang et al., 2000; Qiu et al., 2009; Teng et al., 2009). Furthermore, the Young's modulus of elastin is sharply dependent on size for small diameter materials but is less dependent on diameter for larger fibers, traits Ubx fibers share with materials generated from an artificial peptide based on silk and elastin sequences (Qiu et al., 2009).

4.3 Conclusions

The range of mechanical properties reported for protein-based materials can vary significantly, even for the same materials measured in the same study (Brooks et al., 2008; Madsen et al., 1999; Qiu et al., 2009; Welsh and Tirrell, 2000). Devising mechanisms to control these variable properties is crucial, both to maintain materials quality and to engineer materials with novel properties. Other laboratories have demonstrated the ability to influence the mechanical properties of protein-based materials though sequence engineering, chemical modification of materials, or by altering fiber diameter (Brooks et al., 2008; Qiu et al., 2009; Teng et al., 2009; Xia et al., 2010). We have demonstrated that the mechanical properties of Ubx materials are also influenced by diameter and have provided a detailed analysis of the structural and mechanical changes in Ubx fibers as a function of fiber diameter.

In other protein-based materials, diameter has been controlled by the altering the concentration of protein monomers or the rate of the spinning process (Buttafoco et al., 2006; Cao et al., 2009; Corsini et al., 2007; Li and Xia, 2004; Welsh and Tirrell, 2000). By drawing fibers from a film instead, we were able to alter the diameter by changing assembly time or protein concentration. Furthermore, fibers can be fused to produce

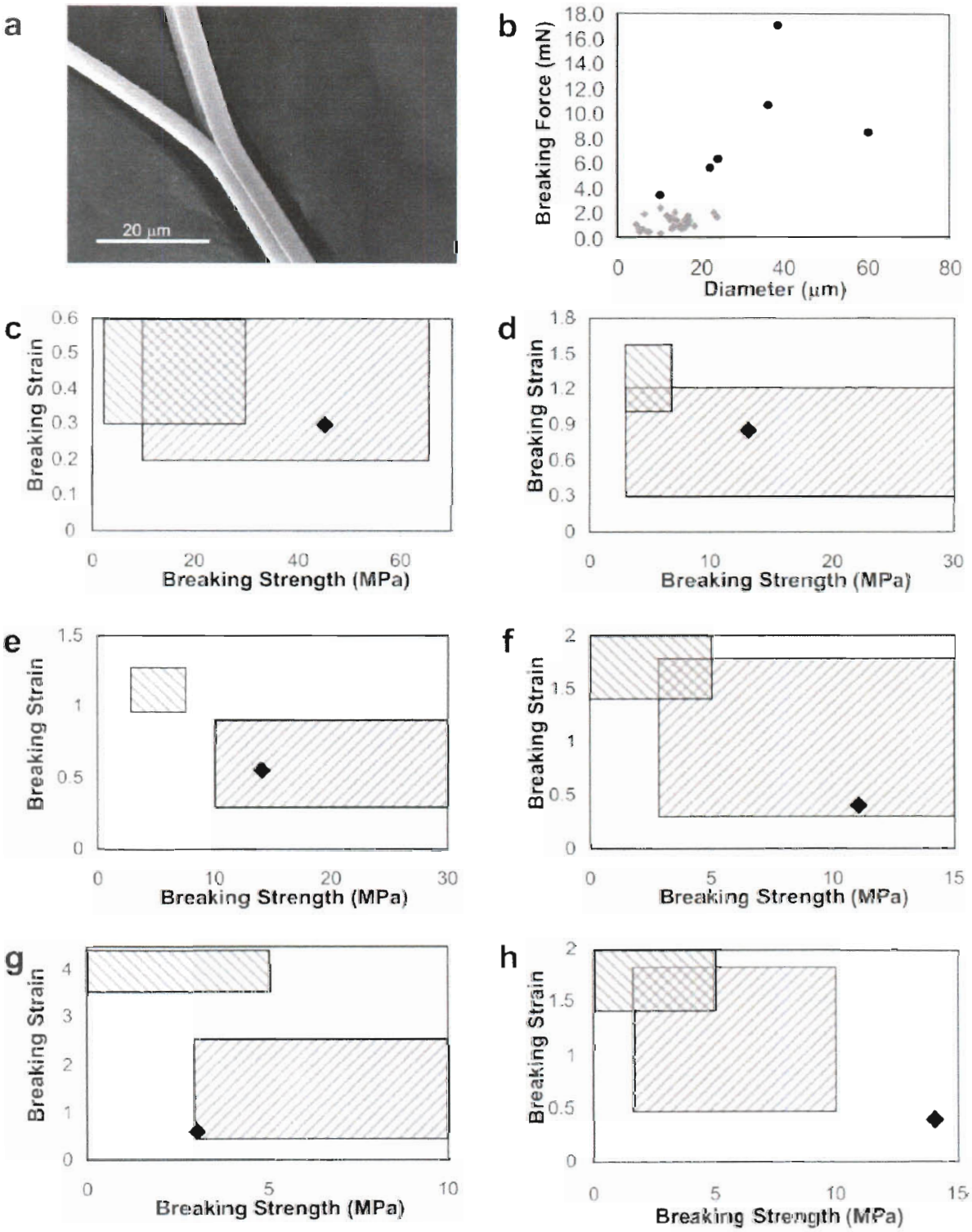
a
20 µm
b
Breaking Force (mN)
18.0
16.0
14.0
12.0
10.0
8.0
6.0
4.0
2.0
0.0
0
20
40
60
80
Diameter (µm)
c
Breaking Strain
0.6
0.5
0.4
0.3
0.2
0.1
0
0
20
40
60
Breaking Strength (MPa)
d
Breaking Strain
1.8
1.5
1.2
0.9
0.6
0.3
0
0
10
20
30
Breaking Strength (MPa)
e
Breaking Strain
1.5
1
0.5
0
0
10
20
30
Breaking Strength (MPa)
f
Breaking Strain
2
1.5
1
0.5
0
0
5
10
15
Breaking Strength (MPa)
g
Breaking Strain
4
3
2
1
0
0
5
10
Breaking Strength (MPa)
h
Breaking Strain
2
1.5
1
0.5
0
0
5
10
15
Breaking Strength (MPa)

larger diameter bundles that withstand larger force.

By characterizing in detail the dependence of the mechanical properties of Ubx fibers on diameter, we have established that the extension of narrow fibers is predominantly elastic, whereas the extension of thicker fibers combines the elastic extension of one or more cores with the plastic deformation of the surrounding layers. The outer layers of thick Ubx fibers may behave differently than the core because of (i) lamina created when drawing the fibers from film, (ii) differences in hydration between the core and exterior, or (iii) layer-specific differences in the structured versus disordered character of the protein, which may cause regional distortions upon stretching. Changing the fiber diameter alters the breaking strength, breaking strain, and Young's modulus of the Ubx materials by roughly an order of magnitude. By exploiting this diameter effect, we can generate materials from a *Drosophila melanogaster* transcription factor with initial breaking stress and strain similar to natural elastin. This ability to produce such extensible materials from a genetic regulatory protein suggests that the search for self-assembling proteins that yield practical materials need not be limited to proteins that generate materials as part of their native function.

Ubx monomers self-assemble under aqueous conditions near neutral pH (Greer et al., 2009). Although other stronger and more extensible protein-based materials have been reported (Qiu et al., 2009; Wen et al., 2010; Xia et al., 2010; Zeugolis et al., 2008), the mechanical properties of Ubx materials mimic natural materials, a rarity for materials in which the monomers are produced in *E. coli* (Bini et al., 2006; Teule et al., 2007). Ubx materials therefore combine useful mechanical properties with the potential to engineer mechanical and functional properties through molecular biology techniques.

CHAPTER 5

Functionalization and Patterning of Ubx-based Materials via Fusion Chimeras[4]

5.1 Introduction

Proteins have very diverse yet highly specific chemical functionalities. For instance, ligand-binding proteins can reliably distinguish enantiomers, enzymes substantially accelerate chemical reactions, and signaling or binding proteins accurately elicit unique cellular responses. The ability to incorporate these functions into materials creates powerful functionalized tools that can be engineered for many applications, such as chemical catalysts, biosensors, and tissue engineering scaffolds (Dutta and Dutta, 2009; Falconnet et al., 2006; Kyle et al., 2009; Lutolf and Hubbell, 2005; Williams, 2009; Wong et al., 2004; Wu et al., 2006). Enzymes, antibodies, growth factors, and peptide recognition sequences can be incorporated into biomaterials via various physical and chemical methods, including physical adsorption (Beachley and Wen, 2009), cross-linking (Kim et al., 1998; Koh et al., 2008; Kuhl and Griffith-Cima, 1996; Murphy and Kaplan, 2009), direct mixing with polymer solutions (Beachley and Wen, 2009; Wu et al., 2006), and co-axial electrospinning (Koh et al., 2008; Murphy and Kaplan, 2009; Neal et al., 2009; Schneider et al., 2009). Although chemical attachments of peptides and proteins in biomaterials offer longer term immobilization than physical adsorption, this approach often requires harsh conditions such as high temperatures, high voltages,

[4] Parts of this chapter, including text and figures, were reported in Huang et al., 2011. T. Salim, A. Brawley, and J. Patterson contributed to the patterning of chimeric materials.

exposure to organic chemicals, and/or extreme pHs (Falconnet et al., 2006), which can compromise the activity of bioactive molecules.

Patterning can further enhance the functionality and potential applications of protein-based materials. For instance, patterned enzymes could catalyze sequential chemical reactions, patterned sensors could detect multiple analytes, and patterned tissue-engineering scaffolds could elicit different cell behaviors (Jang and Koh, 2010; Kjeang et al., 2006; Mohammed et al., 2004; Vepari and Kaplan, 2006). A subset of chemical immobilization approaches such as microcontact printing, photolithography, and plasma polymerization also permit patterning of peptides and proteins (Falconnet et al., 2006; Folch and Toner, 2000; Shin, 2007; Wong et al., 2004), which have been demonstrated to be important cues for cell responses (Guler et al., 2006; Maheshwari et al., 2000; Rajagopalan et al., 2004; Silva et al., 2004).

Theoretically, functional peptides and proteins can be directly incorporated into peptide/protein-based materials without additional physical or chemical processing steps. In the gene fusion approach, the DNA encoding the functional peptide or protein is placed in tandem with DNA encoding the self-assembling protein, without intervening sequences coding for termination of transcription or translation. When these fused genes are placed in a living cell, the cell produces a protein chimera – a single polypeptide composed of the amino acid sequence of the functional protein linked to the amino acid sequence of the self-assembling protein. If the chimera generated is capable of forming materials, the functional protein would be embedded throughout the material in a single production step.

While conceptually easy, implementation of the gene fusion / protein chimera

approach is technically quite challenging. Instigation of the polymerization process typically requires chemical and physical stresses capable of unfolding or inactivating most functional proteins (Dror et al., 2008; Gupta et al., 2007; Lazaris et al., 2002). Since short peptides do not require an intricately folded structure to mediate their function, the gene fusion approach can work well for this type of chimera. For instance, cell-binding peptides such as RGD have been incorporated into protein chimeras, and the resulting materials display markedly enhanced cell attachment (Bini et al., 2006; Yanagisawa et al., 2007).

We have extended the gene fusion approach to incorporate several full-length, folded proteins into materials to add new functions. We previously demonstrated that Ubx, a *Drosophila* transcription factor, has the ability to assemble into materials with various morphologies under mild, aqueous conditions near neutral pH (Greer et al., 2009). Here, we report generation of Ubx protein chimeras with enhanced green fluroescent protein (EGFP), mCherry, sperm whale myoglobin (Mb), and luciferase. Although these proteins have different sizes (18 kD to 61 kD), different charges at pH 8.0 (+2 to -9), and distinct secondary structure content (α, β, and $\alpha + \beta$), each of these chimeras can self-assemble under mild, aqueous conditions, and the materials produced exhibit the functional features of the parental components over an extended period of time. Control over the spatial arrangement of these functional proteins within the fibers and films can be achieved during assembly via solution surface arrangement and self-adhesion. Further, the self-adhesive properties of Ubx materials permit manual construction of larger scale patterns. Thus, Ubx materials can be functionalized and patterned to produce complex 3D structures in 1-2 steps without requiring specialized

equipment or harsh chemical or physical processing, enabling a wide variety of applications.

5.2 Results

5.2.1 Generation of protein-Ubx fusions

To create Ubx chimeras with various functional proteins, DNA constructs were created that encode a single polypeptide, including a 6 histidine tag at the N-terminus, followed by a hydrophilic spacer, the selected functional protein, a Gly-His flexible hydrophilic linker, and the Ubx sequence at the C-terminus (**Fig. 5.1A**). The proteins chosen for fusion to Ubx have easily assessed properties: EGFP and mCherry are fluorescent; myoglobin absorbs visible light; luciferase catalyzes an enzymatic reaction that yields luminescence. Proteins were purified to generate free Mb, EGFP, mCherry, luciferase (> 85% purity), and the corresponding N-terminal Ubx fusion chimeras (Mb-Ubx, EGFP-Ubx, mCherry-Ubx, luciferase-Ubx, > 70% purity) (**Fig. 5.1B**).

5.2.2 Development of a buffer reservoir method for producing Ubx materials

At the air-water interface, Ubx self-assembles into nanoscale fibrils, which in turn associate into macroscale structures such as fibers that can be processed into more complex structures such as bundles and lattices. We previously described the production of various Ubx-based materials from sessile drops (**Fig. 5.2A**) (Greer et al., 2009). To increase the surface area available for assembly and extend the polymerization time, which competes with dehydration in the sessile drop approach, we devised a "buffer reservoir" method for pulling fibers. Our custom-made device, based on the design of the Langmuir trough, consists of a shallow reservoir for material assembly, two Teflon sweepers for concentrating surface material (**Fig. 5.2B**), and a needle for material

collection (**Fig. 5.2C**). This buffer reservoir approach has a number of advantages over our previous sessile drop method. First, the trough has a much larger surface area than a sessile drop (~400 cm^2 vs 1 cm^2), enabling a larger quantity of film to be produced. Second, the film assembled at the surface can be concentrated using a pair of Teflon sweepers to facilitate lifting the film or drawing fibers. Third, the trough can hold a large volume of buffer (~500 ml), which eliminates the problem of dehydration encountered

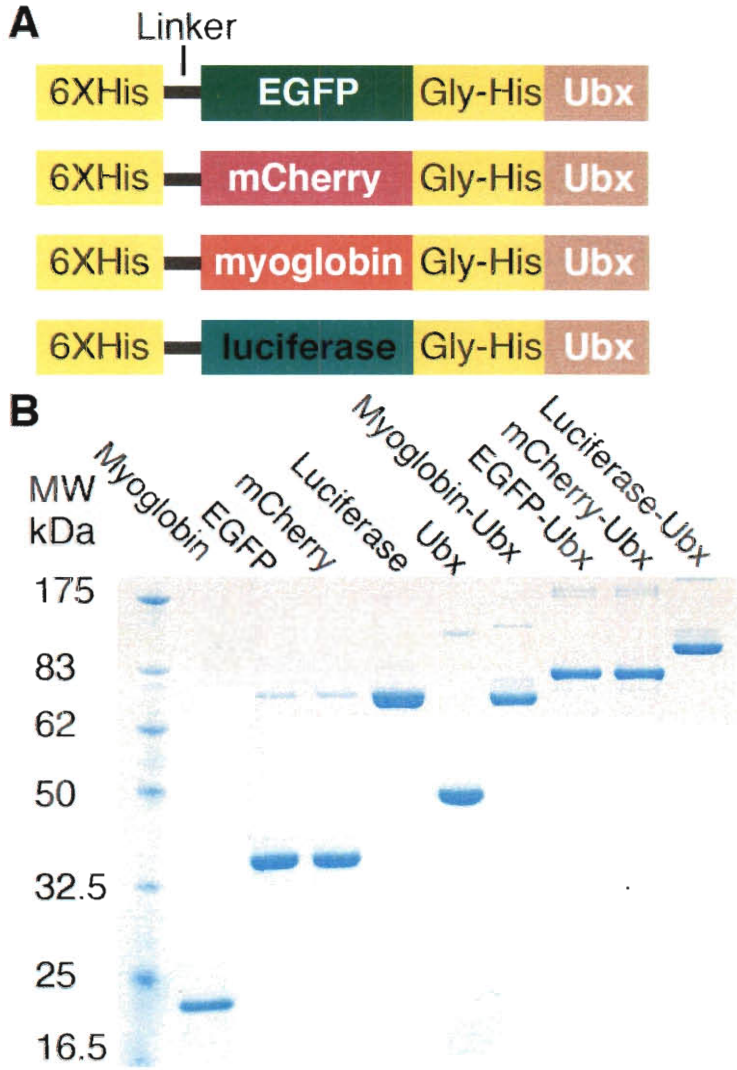

Figure 5.1 Generation of Ubx chimeras containing functional proteins. (A) Schematic of Ubx chimeras drawn with N-terminus to the left and C-terminus to the right. (B) SDS-PAGE gel of the isolated functional proteins, Ubx, as well as Ubx chimeras after purification. Figure is from Huang et al., 2011.

when using the sessile drop method. This arrangement also enables multiple harvests of materials over more extensive periods of incubation (at least 3 harvests from each trough with 4 hours between each harvest). Finally, the buffer reservoir method enables semi-automated harvesting of the materials using a needle that is connected to the axle of a motor via a string. This method can produce fibers that are at least 25 cm in combined length for each mg of protein added to the trough, compared to 15 cm per mg when using the sessile drop method. Unless otherwise specified, all materials described herein were produced using the buffer reservoir method.

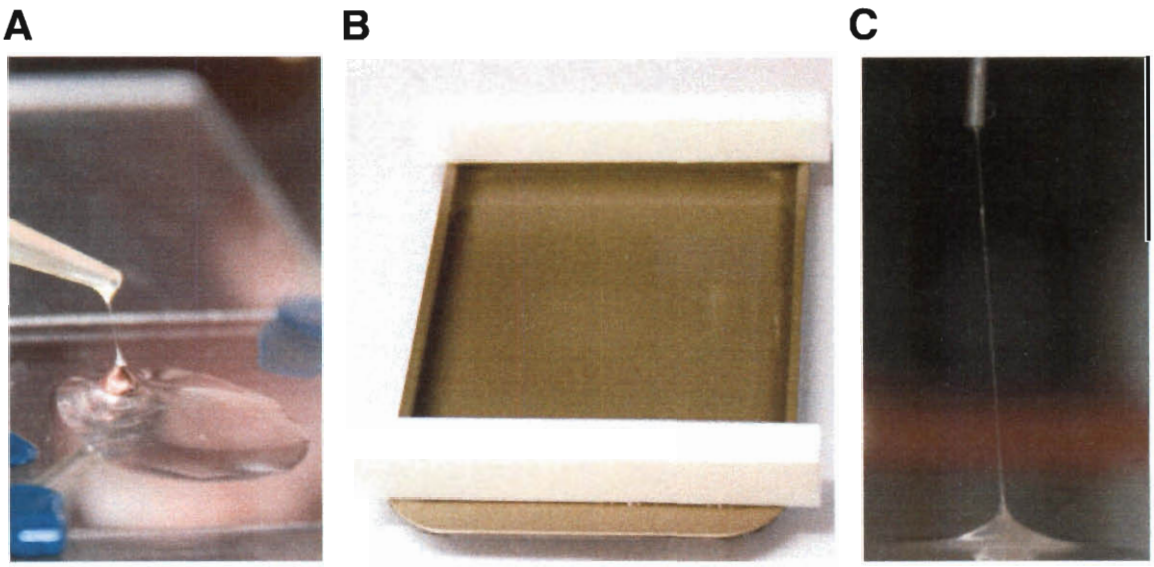

Figure 5.2 Generation of Ubx-based materials from sessile drop and buffer reservior. (A) Photograph showing the sessile drop method for fiber production. (B) Photograph of the tray system used for the production of chimeric materials using the buffer reservoir method (see Materials and Methods for a detailed description). (C) A fiber, suspended from a needle, was generated from the surface of the buffer reservoir. Figure is adapted from Huang et al., 2011.

5.2.3 Fusion chimeras exhibit anticipated secondary structures

X-Ray crystallographic structures demonstrate that myoglobin and EGFP/mCherry predominantly consist of α-helices and β-sheets respectively, whereas luciferase contains a mixture of α-helices and β-sheets (**Fig. 5.3A-C**) (Auld et al., 2010; Shu et al., 2006; Vojtechovsky et al., 1999).

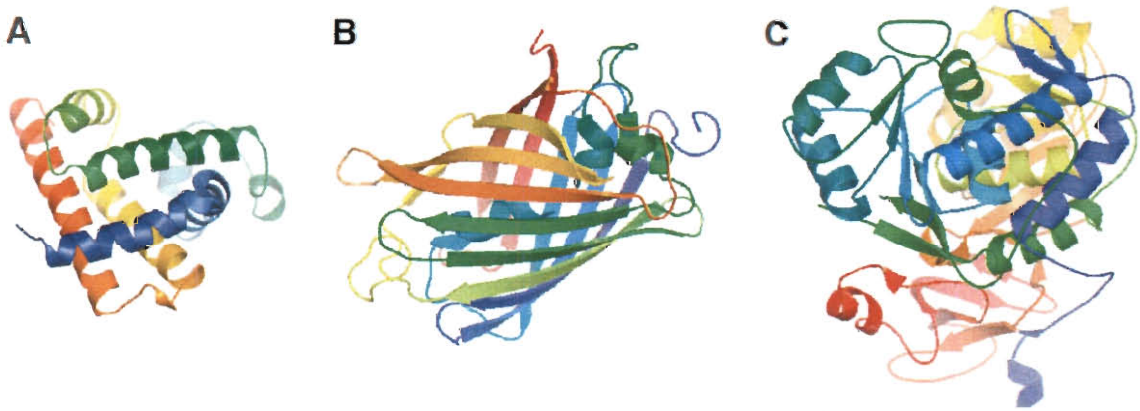

Figure 5.3 Appended proteins have different secondary structures. X-Ray crystallography structures demonstrate that (A) sperm whale myoglobin is predominantly α-helical, (B) mCherry is predominantly β-sheet, and (C) luciferase contains both α-helical and β–sheet components. Panels A-C were made with MacPyMOL (DeLano Scientific LLC) and protein data bank files 1A6M (Vojtechovsky et al., 1999), 2H5Q (Shu et al., 2006), and 3IEP (Auld et al., 2010), respectively. Figure is from Huang et al., 2011.

One challenge in creating fusion proteins is that the added sequences may sterically preclude the folding of one or more proteins, and the orientation of the two fused proteins may affect folding pathways. In our protein-Ubx chimeras, a Gly-His linker was included between Ubx and the fusion protein to ameliorate this problem. To confirm the retention of structure in both Ubx and the appended proteins, we examined the far-UV circular dichroism (CD) spectra of Ubx, the free functional proteins, and Ubx fusion chimeras. The secondary structure of Ubx is dominated by random coils with a small contribution from α-helices (Liu et al., 2008), traits revealed in the Ubx CD spectrum in **Fig. 5.4A-D**. Ubx chimeras incorporated the prominent secondary structural

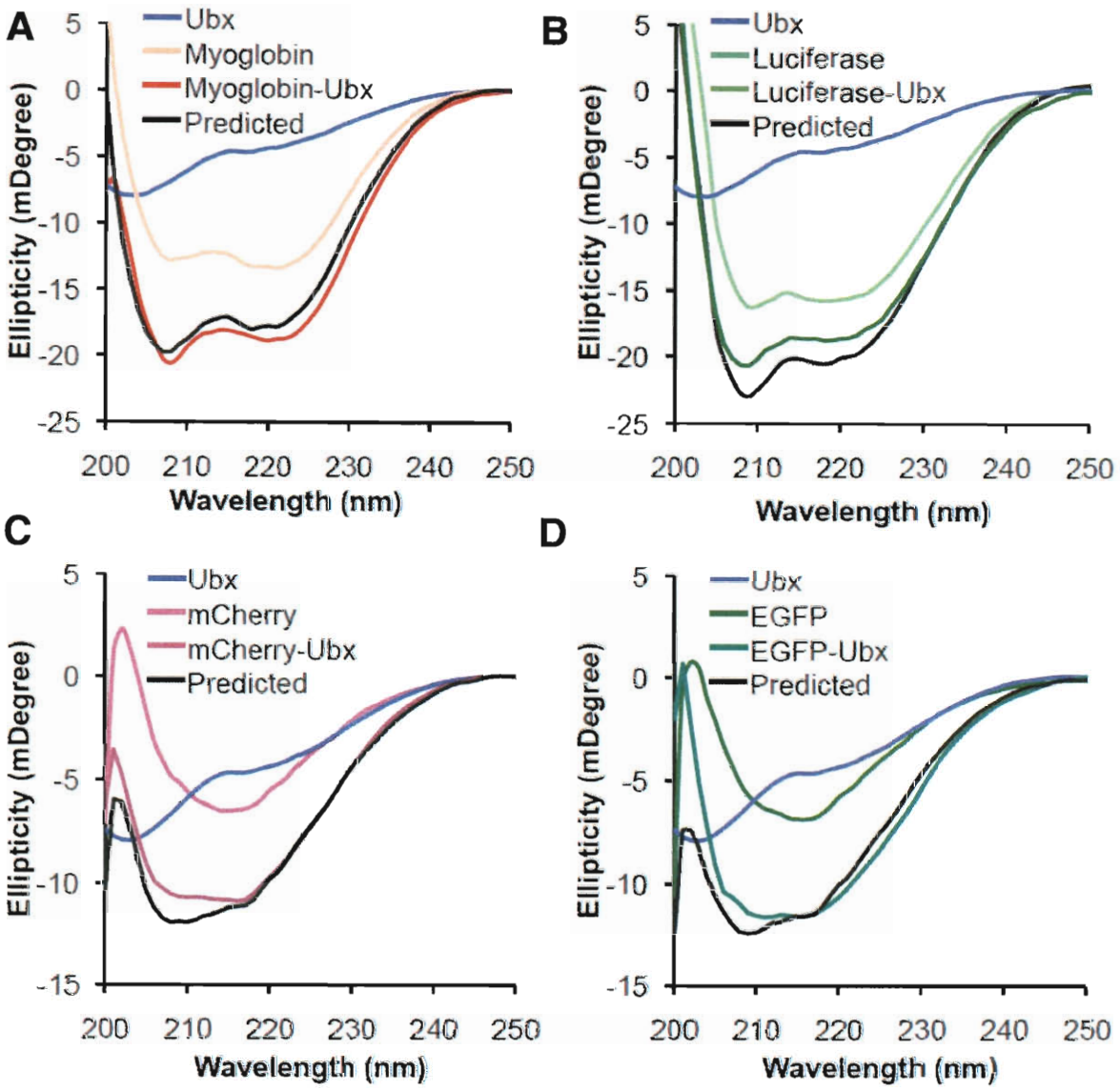

Figure 5.4 Secondary structures of fusion protein are incorporated into chimeras. CD measurements of parent proteins and fusion chimeras were performed using a protein concentration of 1 μM and a quartz cuvette with a 3 mm path length. Each predicted spectrum for the fusion proteins was the sum of the spectrum for the fused protein and that for Ubx. (A) Far-UV CD spectra of Ubx, Mb, and myoglobin-Ubx. (B) Far-UV CD spectra of Ubx, luciferase, and luciferase-Ubx. Myoglobin-Ubx and luciferase-Ubx both exhibit minima at 208 nm and 222 nm, indicating α-helical content. (C) Far-UV CD spectra of Ubx, mCherry and mCherry-Ubx. (D) Far-UV CD spectra of Ubx, EGFP and EGFP-Ubx. Luciferase, mCherry-Ubx and EGFP-Ubx show prominent minima at 217 nm, indicating β-sheet content. The measured and predicted spectra for fusion chimeras display high similarity, suggesting that that the secondary structures of fused proteins and Ubx are retained in the fusion chimeras. Figure is from Huang et al., 2011.

features of the fused proteins. The Mb-Ubx CD spectrum is dominated by minima at 208 and 222 nm, reflecting the α-helical character of the Mb portion of the chimera (**Fig. 5.4A**). Likewise, EGFP and mCherry are predominantly composed of β-sheet; consequently, the EGFP-Ubx and mCherry-Ubx spectra gain negative ellipticity at 217 nm and a more positive signal near 200 nm (**Fig. 5.4C,D**). Finally, the spectrum of Luciferase-Ubx incorporates signal from both the α–helical and β-sheet components of the luciferase protein (**Fig. 5.4B**). To determine whether any secondary structure was lost in the chimeric proteins, the spectra of Ubx and each functional protein, individually measured at molar equivalency, were added to predict the spectrum of the chimeric proteins (**Fig. 5.4A-D**). The remarkable similarity of the predicted spectra with the chimera spectra, measured at the same protein concentration, demonstrates that the secondary structures of fused proteins and Ubx are fully retained in the fusion-chimeras.

5.2.4 Protein functions are retained in fusion chimera monomers

Although CD spectroscopy confirms the overall structure of the materials is intact, small changes in structure or packing caused by chimera formation have the potential to alter or abrogate the function of the appended proteins. However, the purified chimera proteins retained the colorimetric features of the functional proteins: myoglobin-Ubx, mCherry-Ubx, and EGFP-Ubx exhibit the characteristic red/brown, green, or cherry color of the parent protein (**Fig. 5.5A,E,I**). Likewise, luciferase-Ubx produces luminescence in the presence of luciferin **(Fig. 5.5M)**. Therefore, the overall function of the proteins appears intact in the chimeras.

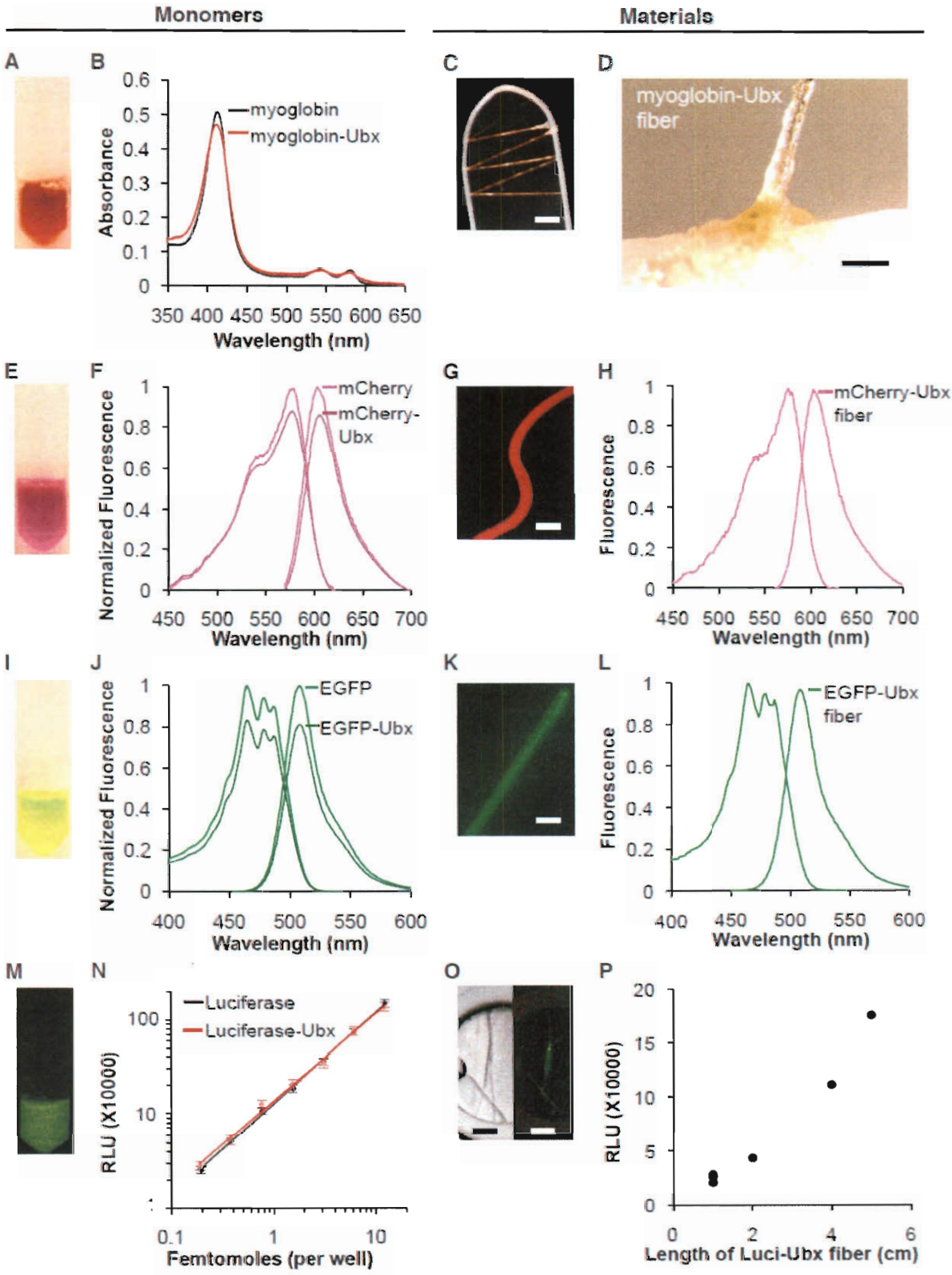
Monomers
Materials
A
B
C
D
myoglobin-Ubx fiber
myoglobin
myoglobin-Ubx
Absorbance
Wavelength (nm)
E
F
G
H
mCherry
mCherry-Ubx
mCherry-Ubx fiber
Normalized Fluorescence
Fluorescence
Wavelength (nm)
I
J
K
L
EGFP
EGFP-Ubx
EGFP-Ubx fiber
M
N
O
P
Luciferase
Luciferase-Ubx
RLU (X10000)
Femtomoles (per well)
Length of Luci-Ubx fiber (cm)

Figure 5.5 Functions of fused proteins are retained within monomeric chimeras and in materials. Myoglobin-Ubx monomers in solution are red/brown (A) and display the characteristic Soret peak in the absorption spectra (B). Photographs (C) and high-resolution light microscopy image (D) demonstrate that myoglobin-Ubx fibers, wrapped around a metal wire, are brownish in color. mCherry-Ubx solution is cherry in color (E), and its fluorescence excitation/emission spectra resemble those for mCherry (F). mCherry-Ubx fibers retained the cherry fluorescence (G) and exhibit near identical excitation/emission spectra to mCherry-Ubx monomers (H). EGFP-Ubx solution is green in color (I), and its fluorescence excitation/emission spectra resemble those for EGFP (J). EGFP-Ubx fibers retained the green fluorescence (K) and exhibit near identical excitation/emission spectra to EGFP-Ubx monomers (L). Luciferase-Ubx monomers produce luminescence in the presence of luciferin (M) and behave similarly to luciferase (N). Luciferase-Ubx fibers also produce luminescence (O) and the intensity depends on the length of the fiber (P). Scale bars, C: 5 mm; D, G, K: 50 μm, O: 2 mm. Figure is from Huang et al., 2011.

To determine whether chimera incorporation subtly alters the function of the appended proteins, we compared the spectroscopic, fluorescent, or catalytic properties of the individual proteins used in the fusion with those of monomeric chimeras and functionalized materials. These properties are extremely sensitive to the fine details of protein structure and amino acid packing. The absorption spectrum of Mb-Ubx shows the Soret peak at 417 nm and additional spectral features in the visible region, distinctive features of holo-myoglobin (**Fig. 5.5B**). EGFP-Ubx and mCherry-Ubx chimeras have fluorescence excitation/emission profiles similar to the parent proteins (**Fig. 5.5F,J**). Only a slight loss of absorbance is observed for Mb-Ubx and for fluorescence in mCherry-Ubx, and EGFP-Ubx (12%, 13%, and 19% respectively) relative to a molar equivalent of the free functional proteins. These small changes indicate that folding and hence spectroscopic properties may be affected in only a fraction of these chimeric proteins. Luciferase-Ubx generates luminescence from luciferin in a protein concentration-dependent manner, similar to that observed for recombinant luciferase under the same conditions (**Fig. 5.5N**). These data demonstrate that the functions of the

proteins fused with Ubx are significantly retained in the chimeric species. Furthermore, any conformational shifts required for function, for example in enzyme catalysis, are accommodated in the chimeras.

5.2.5 Ubx chimeric materials retain the functions of the appended proteins

Because Ubx materials are formed and stabilized by Ubx•Ubx interactions, inclusion of the functional proteins in Ubx chimeras has the potential to sterically preclude some or all of these interactions, ultimately compromising materials assembly. However, all of the Ubx chimeras created retained the ability to form materials (**Fig. 5.5C**,**G**,**K**,**O**). Furthermore, the ability of chimeras to self-assemble did not depend on the structure, charge, or size of the functional protein. Myoglobin is largely α-helical, EGFP and mCherry consist primarily of β-sheets, and luciferase contains mixed α/β structures. The charge at pH 8.0 of these proteins ranges from +2 to -9, and the size varies from 18 kDa to 61 kD. Using the buffer reservoir method, we are able to make chimeric Ubx fibers that are at least 25 cm in combined length from 1 mg of these chimeric proteins. These results demonstrate that Ubx self-assembly is compatible with protein chimeras encompassing a broad range of physical and functional properties.

For materials composed of protein chimeras to be useful, the appended proteins must retain their native functions after material assembly. Indeed, myoglobin fibers exhibit the characteristic brownish color of myoglobin (**Fig. 5.5D**). EGFP-Ubx and mCherry-Ubx fibers clearly exhibit the fluorescence properties of the parent proteins with similar excitation/emission spectra (**Fig. 5.5H**,**L**). Activity is retained both on the surface and in the interior of the fibers, as demonstrated in fibers that have been flayed open (**Fig. 5.6**). Luciferase-Ubx fibers display enzymatic activity by producing luminescence

dependent on the length of the fiber (**Fig. 5.5P**). Collectively these results demonstrate clearly that the functions of protein fused to Ubx are retained in the assembled materials to the extent we are able to detect the functional features within chimeric fibers.

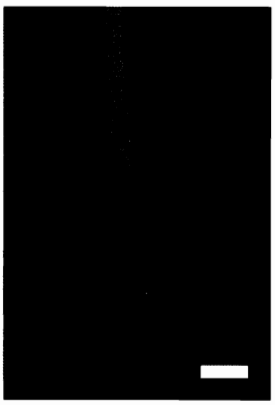

Figure 5.6 EGFP-Ubx fibers are fluorescent at the surface and in the interior. Fluorescence microscopy yields an image of an EGFP-Ubx fiber that shows the presence of fibrils in fibers that have uniform fluorescence. Scale bar: 50 μm. Figure is from Huang et al., 2011.

5.2.6 Manual patterning of Ubx chimeric materials via adhesion

The ability to functionalize materials using Ubx fusion chimeras opens the possibility of generating patterns of functional proteins. Ubx chimeric materials are self-adhesive and will form strong interactions via contact, features that allow formation of patterned materials post-assembly via fiber melding. To visually verify pattern formation, we exploited the contrasting colors of EGFP-Ubx and mCherry-Ubx. As shown in **Fig. 5.7A-C**, an EGFP-Ubx fiber and an mCherry-Ubx fiber can be fused via contact to produce a bundle with a green face and a cherry face. These adhesions are sufficiently strong to allow bundles to be twisted without fracturing the fibers **(Fig. 5.7D-F)**. The patterns of these twisted bundles can be varied by altering the motion of the individual

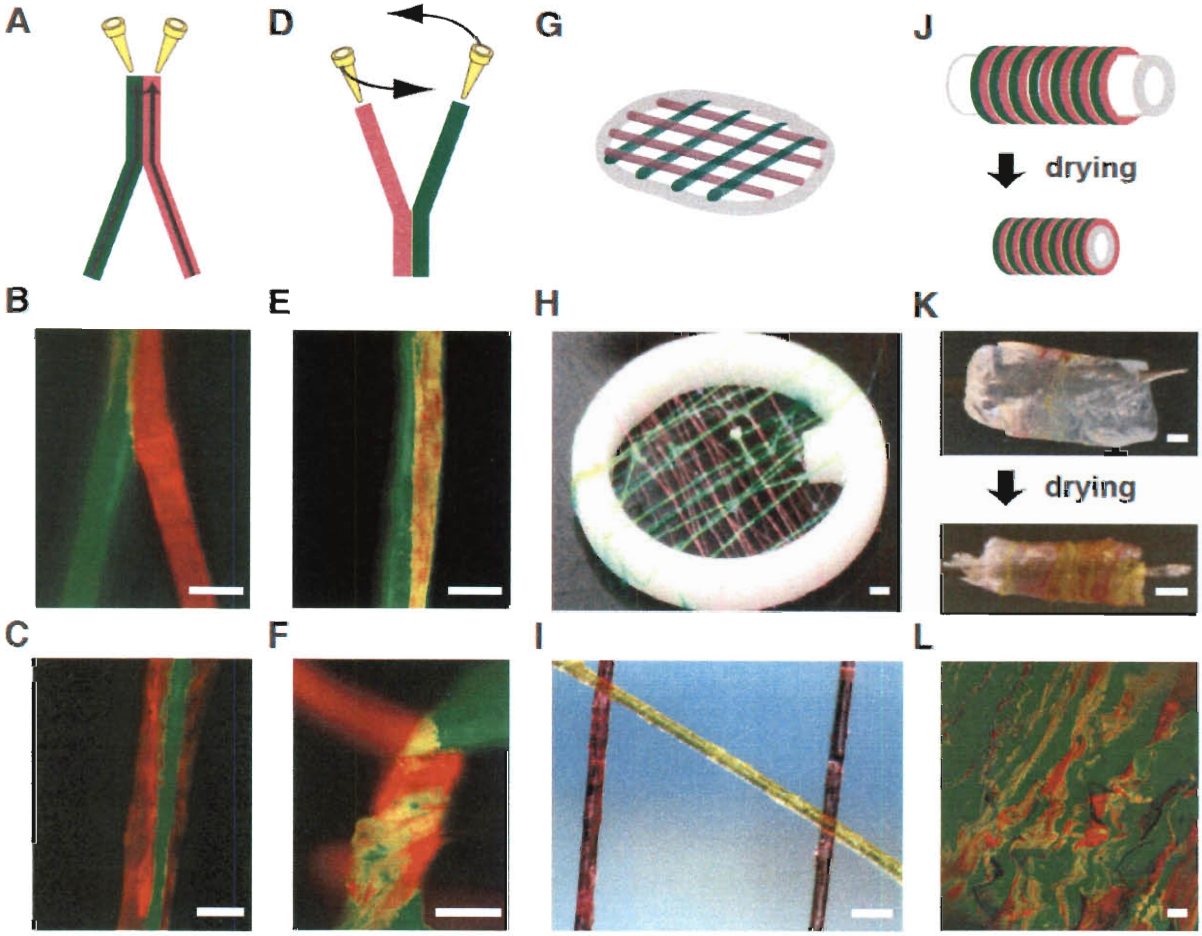

Figure 5.7 Manual patterning of Ubx chimeras in materials. (A) Schematic and (B, C) fluorescence microscopy images of bundles constructed from EGFP-Ubx and mCherry-Ubx fibers. (D) Schematic and (E, F) fluorescence images of a twist constructed using an EGFP-Ubx fiber and an mCherry-Ubx fiber. (G) Schematic and (H) photograph of a web made of EGFP-Ubx and mCherry-Ubx fibers on a Teflon ring. (I) Light microscopy image at high resolution of a lattice showing the color of the EGFP-Ubx and mCherry-Ubx fibers. (J) Schematic and (K) photograph showing Ubx fibers wound around a hollow agarose tube before and after drying. (L) Fluorescence microscopy image of the tube shown in (K) displaying the patterns of EGFP-Ubx and mCherry-Ubx. All scale bars are 50 μm except for H and K (1 mm). Figure is from Huang et al., 2011.

fibers. When two fibers are twisted around a central axis, alternate functionalities are exposed in the product. Conversely, when one fiber is twisted around a stationary fiber, then the stationary fiber forms a core encased by the mobile fiber. Due to the self-adhesive properties of Ubx-based materials, a series of fibers placed at 90° from one

another on a Teflon ring will meld to form a lattice (**Fig. 5.7G-I**), in which EGFP-Ubx fibers and mCherry-Ubx fibers are orthogonally stacked.

Ideally, EGFP-Ubx and mCherry-Ubx fibers could be alternately melded to create a striped sheet. However, the process of aligning many fibers in air is sufficiently slow that the fibers start to dry, at which point adherence is diminished. To circumvent this problem, EGFP-Ubx and mCherry-Ubx fibers were alternately wrapped around a tube composed of agarose gel (**Fig. 5.7J,K**). As the agarose tube dried and shrank, the hydrated fibers came into contact with one another and melded to form a striped sheet (**Fig. 5.7L**). By placing different chimera fibers at different positions on the tube, controlled spatial patterning of functional proteins on the surface can be achieved (**Fig. 5.7L**).

5.2.7 Surface self-assembly patterning of Ubx chimeric materials via solution arrangement

The resolution of manual patterning is limited by the diameter of the fibers, which is 5-30 μm (Huang et al., 2010), or the thickness of the film. In contrast, Ubx materials can also be patterned during assembly to produce finer patterns within single fibers or films. This single step functionalization/patterning method relies on materials assembly by sessile drops. In this approach, the two drops are placed near, but not in contact with, each other to allow EGFP-Ubx and mCherry-Ubx films to form separately. Then the drops are allowed to merge, and the two films meld with one another. By drawing a fiber from the boundary between these two drops, we can generate mixed chimera fibers in which one face is green and the other face is red (**Fig. 5.8A-C**), similar to the manually constructed fiber bundles. In contrast, drawing the fiber across the boundaries between

two adjacent drops produces striped fibers (**Fig. 5.8D-F**). For both faced fibers and striped fibers, the sharpness of the boundary is dependent on the length of time the two drops stay in contact. Short contact times yield very discrete boundaries, whereas long contact times produce gradients.

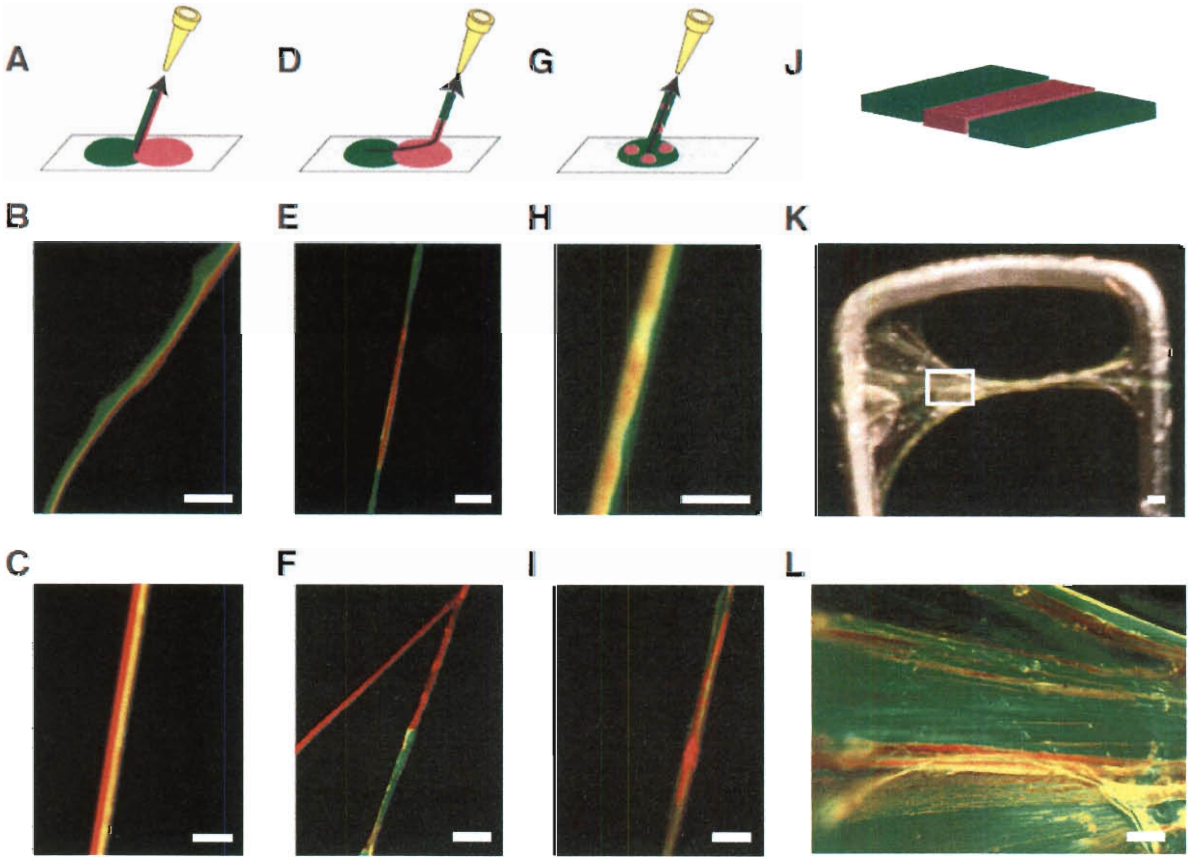

Figure 5.8 Patterning of Ubx chimeric materials during materials assembly. (A) Schematic and (B, C) fluorescence microscopy images of faced fibers produced along the boundary of side-by-side arranged solutions. (D) Schematic and (E, F) fluorescence microscopy images of striped fibers produced across the boundary of side-by-side solutions. (G) Schematic and (H, I) fluorescence images of spotted fibers produced from prearranged protein drops. (J) Schematic and (K) photograph of a film made from EGFP-Ubx and mCherry-Ubx chimeras. (L) Fluorescence microscopy image of a chimeric film containing EGFP-Ubx and mCherry-Ubx strands. All scale bars are 100 μm except for K (1 mm). Figure is from Huang et al., 2011.

In addition, spotted fibers can be created by careful placement of mCherry-Ubx solution onto a pre-polymerized EGFP-Ubx film (**Fig. 5.8G-I**). Finally, since Ubx films assemble at the solution surface, different patterns within the film can be produced by controlling placement of different chimera protein monomers within the "sessile drop" or "buffer resevoir" (**Fig. 5.8J-L**). Using these surface assembly methods enables the generation of finer patterns, producing stripes that are smaller than the diameter of the fibers within fibers and films (2 μm in width).

5.2.8 EGFP-Ubx chimera fibers have morphology similar to Ubx fibers

SEM analysis revealed that the morphology of Ubx-chimera fibers (made by buffer reservoir method) is comparable to that of Ubx fibers **(Fig. 5.9)**. Both have uniform diameters and display striations along the longitudinal axis of the fibers.

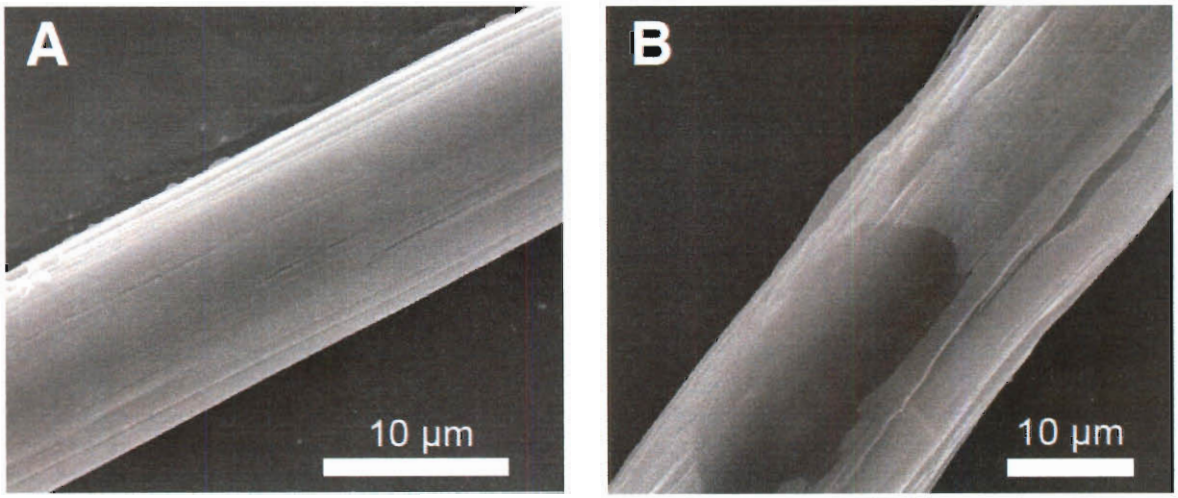

Figure 5.9. Ubx fibers and EGFP fibers have similar morphology. SEM image of (A) an Ubx fiber and (B) an EGFP-Ubx fiber.

5.2.9 EGFP-Ubx chimera fibers have diameter-dependent mechanical properties similar to Ubx fibers

To test whether incorporation of heterologous proteins via chimeras impacts the mechanical properties, tests of EGFP-Ubx fibers were performed (**Fig. 5.10**). Similar to Ubx fibers, EGFP-Ubx fibers demonstrated strong diameter-dependent mechanical properties (Huang et al., 2010). Compared to Ubx fibers of the same diameter, the EGFP-Ubx fusion chimera fibers have significantly smaller breaking strains. Indeed, a 20 μm Ubx fiber is ~120% extensible, whereas a 20 μm EGFP-Ubx fiber is 40% extensible. At the same diameters, the breaking stresses of the EGFP-Ubx chimera fibers are slightly higher than those of the Ubx fibers, suggesting that the presence of EGFP may contribute to the tensile stress of the fibers. In addition, EGFP-Ubx fibers wrinkle upon unloading, to an extent dependent on strain and fiber diameter, similar to Ubx fibers (**Fig. 5.11**).

From these data, we conclude that the nature of chimeric partner for Ubx is capable of influencing the mechanical properties of the fiber. Consequently, mechanical properties should always be measured when engineering a novel chimeric monomer for materials assembly.

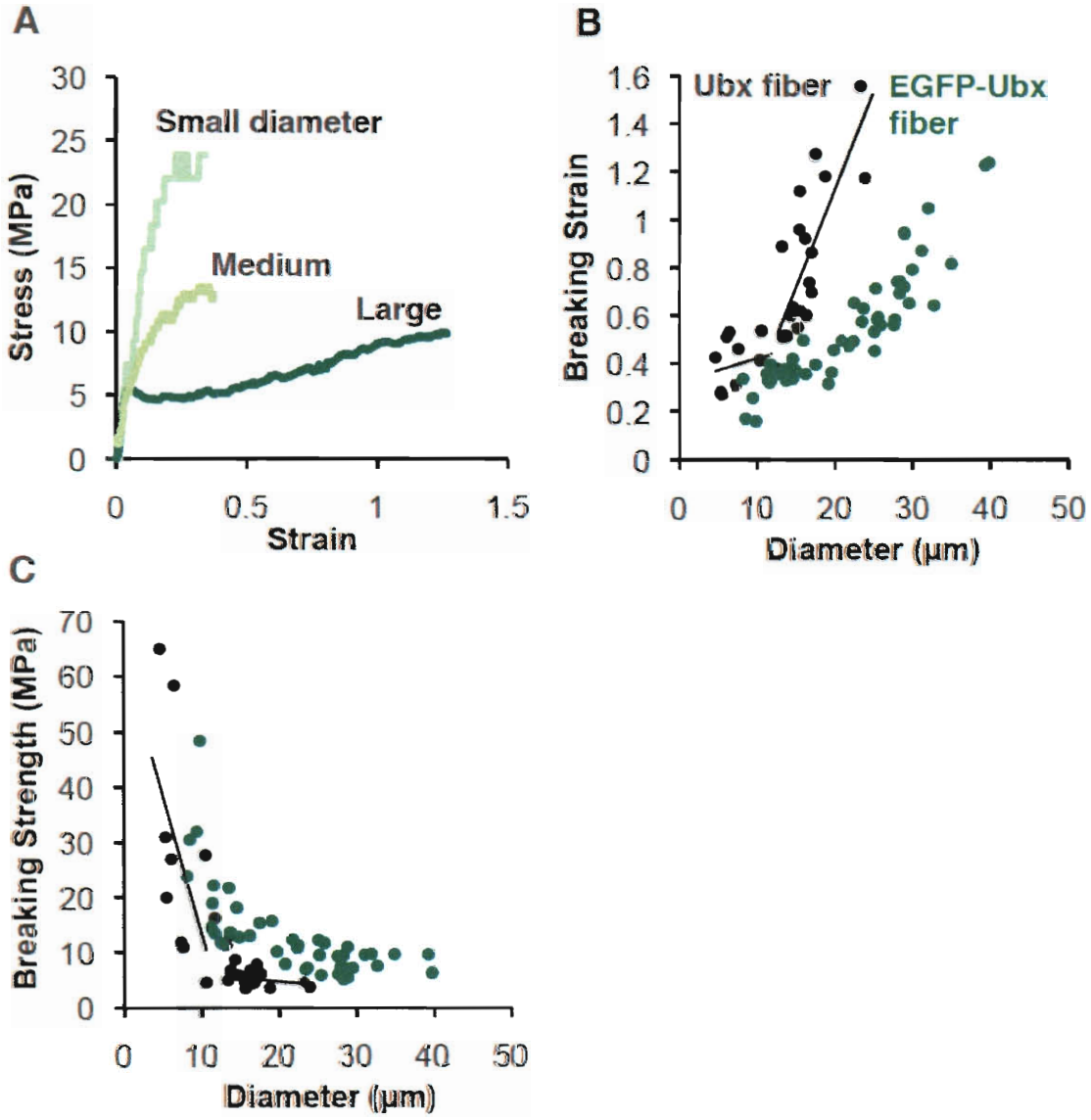

Figure 5.10 Mechanical properties of EGFP-Ubx chimera fibers. (A) EGFP-Ubx fibers display diameter-dependent mechanical properties. (B) Breaking strain vs diameter for fibers formed from Ubx and EGFP-Ubx. (C) Breaking stress vs. diameter for fibers formed from Ubx and EGFP-Ubx. In B and C, solid black circles represent Ubx fibers, whereas solid green circles represent EGFP-Ubx fibers.

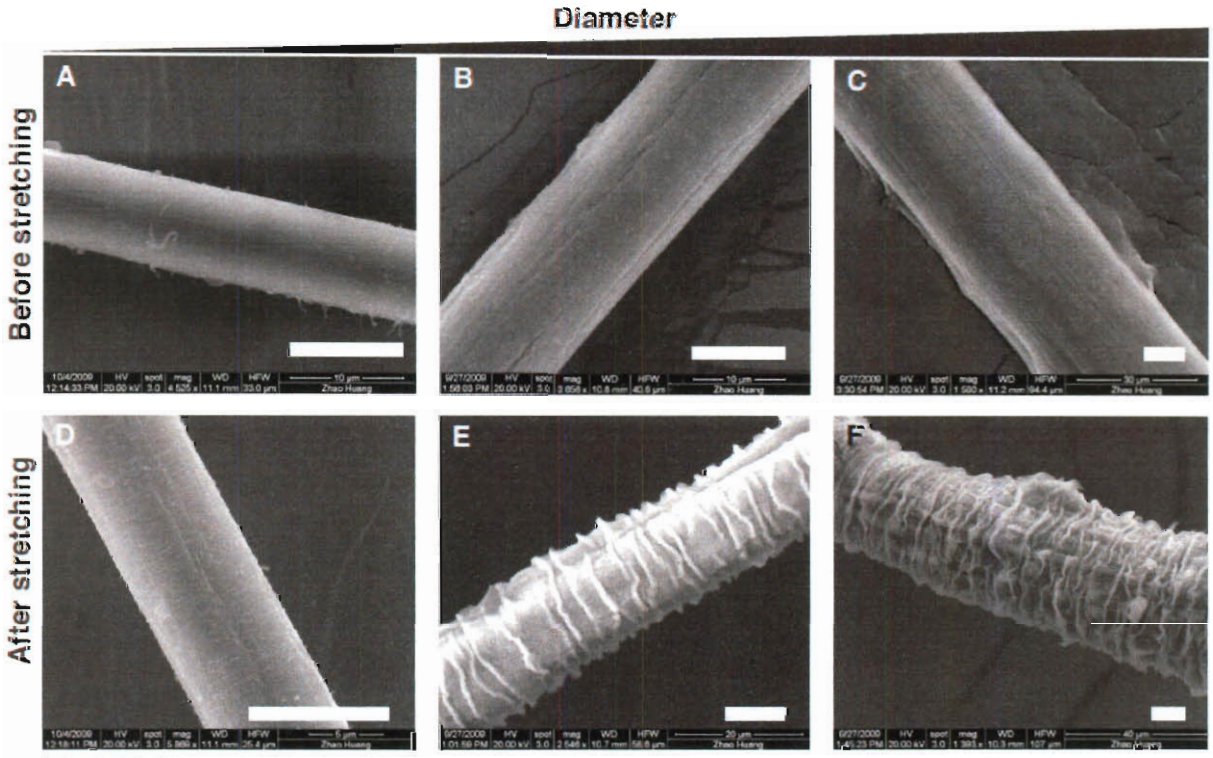

Figure 5.11 Deformation of EGFP-Ubx fibers is diameter-dependent. (A-F) SEM images of EGFP-Ubx fibers of different diameters before and after stretching. Plastic deformation is more pronounced as the diameters of EGFP-Ubx fibers increase, similar to Ubx fibers. (A,D) A 10 μm diameter EGFP-Ubx fiber before and after stretching. (B, E) A 15 μm diameter EGFP-Ubx fiber before and after stretching. (C,F) A 30 μm diameter EGFP-Ubx fiber before and after stretching. Scale bars: 10 μm

5.3 Conclusions

Proteins potentially provide highly efficient and selective functions that would be useful in many materials applications. Exploiting these functionalities requires methods to incorporate and pattern proteins into materials without sacrificing the structure or function of the added protein. The simplest way to add functionality is to create chimeras incorporating both a self-assembling protein and a functional protein. A challenge in creating functionalized materials from protein chimeras has been assembling the materials without damaging the structure or activity of the appended functional protein. Since elastin-like proteins (ELPs) coacervate at high temperatures, cycling between low

and high temperatures can both purify ELP chimeras and generate the materials. This approach has been very successful with peptides and stable folded proteins (Conley et al., 2009; Conrad et al., 2011; Floss et al., 2010; Kang et al., 2007). However, many proteins irreversibly denature at high temperatures, and thus are incompatible with the ELP assembly process. Likewise, self-assembly of recombinant silk proteins is often triggered by organic solvents, which also denature many proteins. To circumvent the harmful effects of silk assembly conditions on functional proteins, dragline silk sequences were fused to dentin, a protein that is unstructured in the absence of Ca^{2+}. Once assembled, exposure of the materials to Ca^{2+} triggered the refolding, and hence activity, of dentin (Huang et al., 2007).

In an exciting step forward, we have created several active, functionalized materials using Ubx as a platform to introduce new activities via formation of chimeric fusions. Since a large number of proteins cannot re-fold properly once unfolded, the mild conditions under which Ubx assembles permit facile incorporation of a wider range of full-length structured proteins. The structure and function of the appended proteins are retained during materials assembly. This method is compatible with proteins of various size, surface charge, and structure, and thus greatly extends the range of potential proteins and functions that can be utilized.

Finally, this report is the first to show the ability to pattern materials using functionalized protein chimeras. Patterning can produce complex three-dimensional structures in one or two steps without the need for additional equipment. The scale of the patterned features can be varied by patterning during assembly, manual patterning, or by using larger initial structures during manual patterning. Enabling incorporation of new

functions and patterning of functional chimeric proteins into complex three-dimensional structures significantly enhances the ability to engineer protein-based biomaterials and consequently broadens the range of potential applications.

CHAPTER 6

Ubx-based Materials as a Tissue Engineering Scaffold:[5]
In Vitro Biocompatibility of Ubx-based Materials

6.1 Introduction

In previous chapters, we demonstrated that Ubx-based materials have a number of desirable features required for tissue engineering scaffolds: Ubx assembles into diverse material morphologies under ambient conditions; Ubx fibers display mechanical properties that can be engineered by altering diameters; and Ubx materials can be functionalized by active proteins and arranged into various patterns. These properties provide unique advantages in applications where Ubx-based materials are used as tissue engineering scaffolds. Tissue engineering scaffolds must also have low toxicity and elicit limited inflammatory and immunogenic responses (Crawford and Hatton, 2008; Williams, 2008, 2009). Standard biocompatibility characterization of tissue engineering scaffolds includes testing using *in vitro* cell cultures, *in vivo* animal models, and clinical trials (Babensee et al., 1998; Ghanaati et al., 2010; Williams, 2008). *In vitro* cell culture is relatively inexpensive and is commonly used as the first step of biocompatibility screening.

In this chapter, in an attempt to assess the utility of Ubx-based materials as tissue engineering scaffolds, the *in vitro* biocompatibility of Ubx-based materials is examined

---

[5] P. M. Mountziaris contributed to electrospinning. P. Spicer contributed to the elution, direct contact, and attachment assays. Work was carried out in the laboratory of A. Mikos.

using (i) direct contact, (ii) elution, and (iii) attachment assays (Babensee et al., 1998; Sierpinski et al., 2006; Williams, 2008). In the direct contact assay, materials of interest are placed in contact with cells, and cell viability is examined to provide information on the toxicity of materials. In the elution assay, the material of interest is placed in cell culture media to allow leaching of potential toxic molecules. The media (without the material) is then transferred to cells, and cell viability is assessed to evaluate the toxicity of the leached molecules. In the attachment assay, the material of interest and cells are placed in a plate that prohibits cell attachment to the plate, which enables the examination of cell attachment to the materials.

6.2 Results

6.2.1 Producing Ubx-based fiber scaffolds

Fiber-based materials are good candidates for tissue engineering scaffolds because of their high surface to volume ratio and the large volume of space between fibers (Badami et al., 2006; Balguid et al., 2009; Beachley and Wen, 2010; Buttafoco et al., 2006). We chose to use mCherry-Ubx to produce scaffolds for *in vitro* biocompatibility tests because mCherry-Ubx materials have red fluorescence, which is easily visualized during material production, tissue culture, imaging procedures, and is distinct from green fluorescence used to visualize live cells. We produced mCherry-Ubx fiber lattices via manual assembly and mCherry-Ubx fiber meshes using electrospinning.

6.2.2 Electrospinning of mCherry-Ubx microfibers

Electrospinning enables the production of small-diameter fiber meshes as tissue engineering scaffolds (Boland et al., 2004; Buttafoco et al., 2006; Cao et al., 2009; Reneker and Chun, 1996; Reneker et al., 2000). During the electrospinning of mCherry-

Ubx fibers, mCherry-Ubx solution (12 mg/ml, in buffer G) was pressed through a needle opposite a collecting plate. A high voltage was applied between the needle and the plate, which results in the charging of mCherry-Ubx molecules, enabling them to overcome the surface tension and flow towards the collecting plate (**Fig. 1.7C**). A parallel array of electrospun mCherry-Ubx microfibers was deposited on the glass collection plate (**Fig. 6.1A**). Fluorescence microscopy imaging revealed red fluorescent fibers (**Fig. 6.1B**), indicating that at least some of the mCherry in the fibers remained functional in the electospun fibers. Compared to fibers generated using the sessile drop or buffer reservoir methods (5 μm – 30 μm), electrospinning enables the production of smaller diameter Ubx fibers (< 5 μm), which are hereafter referred as microfibers. However, only small patches of mCherry-Ubx electrospun microfibers (1 mm X 1 mm) could be produced, which was not enough for biocompatibility tests. Therefore, additional effort is required to achieve the formation of larger patches of mCherry-Ubx meshes, possibly by altering the solvent composition and protein concentrations.

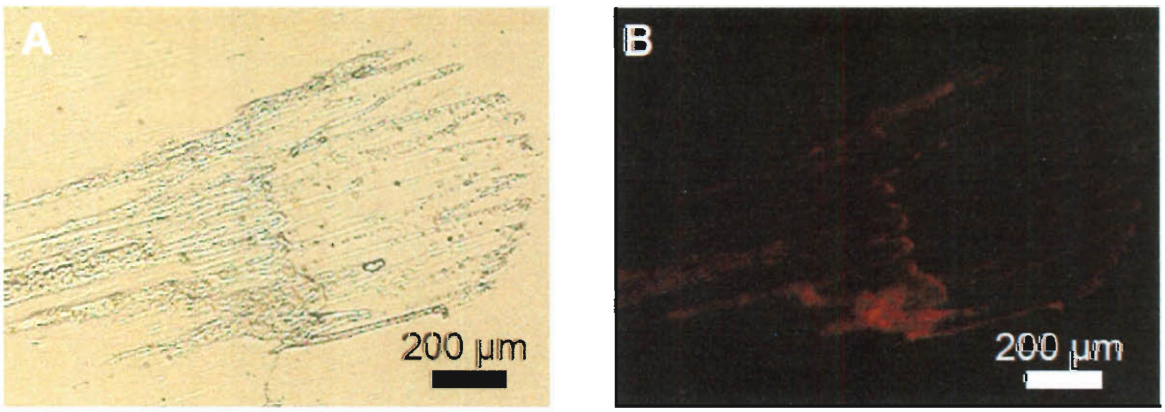

Figure 6.1 mCherry-Ubx-based micro-fibers generated by electrospinning. (A) Light microscopy and (B) Fluorescence microscopy image of mCherry-Ubx micro-fibers (< 5 μm in diameter) formed at the collection plate during electrospinning, using a voltage of 15 kV, mCherry-Ubx concentration of 12 mg/ml, target distance of 13 cm, flow rate of 2 ml/h, and a 22 gauge needle. In collaboration with Paschalia Mountiziaris and Antonios Mikos, Rice University.

6.2.3 Manual assembly of mCherry-Ubx lattices

Using the buffer reservoir method, mCherry fibers were generated and attached to custom-made Teflon rings (**Fig. 6.2A**). This system has a number of advantages: (i) the arrangement aids the transfer of the lattice into tissue culture plate wells, (ii) the ring anchors mCherry-Ubx fibers to the bottom of the wells, enabling contact with cells, (iii) the rings supports materials during autoclaving and UV sterilization procedures, and (iv) the fluorescent scaffold made from mCherry-Ubx enables visualization by confocal microscopy (**Fig. 6.2B**).

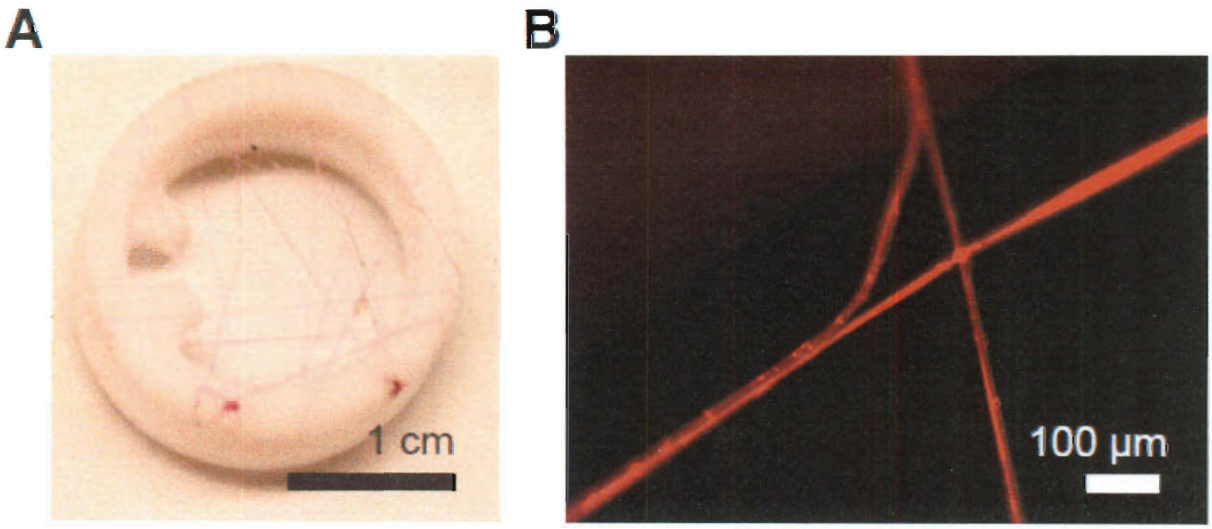

Figure 6.2 mCherry-Ubx fibers attached to Teflon rings, forming a lattice. (A) Photograph of mCherry-Ubx fibers on Teflon rings. (B) Fluorescence microscopy image of mCherry-Ubx fibers.

6.2.4 The effect of Ubx lattices on cell viability

Direct contact assay

To examine the toxicity of mCherry-Ubx lattices, mCherry-Ubx lattices attached to Teflon rings and empty Teflon rings were placed on top of rat fibroblasts in a 16 well tissue culture plate. Cell viability was assayed after 24 hours using calcein/ethidium staining, which stains live cells green and dead cells red. The controls are listed in **Fig.**

6.3. In wells containing mCherry-Ubx lattices placed above and in contact with the rat fibroblasts, the fraction of live cells is not significantly different from the live control ($p = 0.97$) and fraction of dead cells was near zero after 24 hours (**Fig. 6.3**). Both indicate that mCherry-Ubx lattices exert no significant toxic effect upon contacting rat fibroblasts.

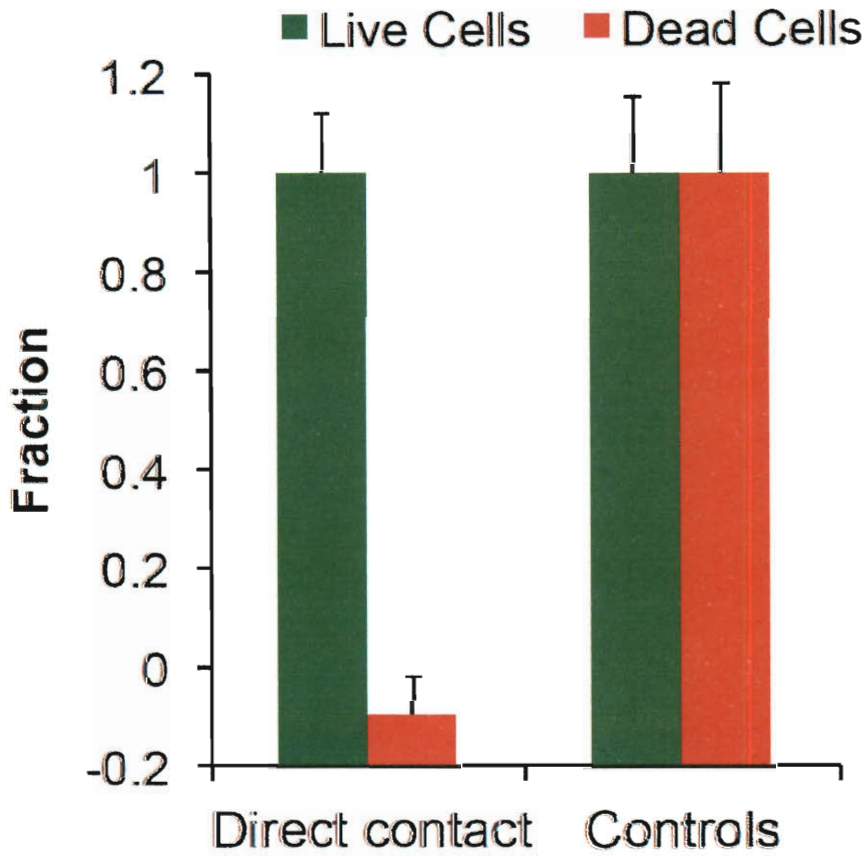

Figure 6.3 Direct contact assay demonstrates the low toxicity of mCherry-Ubx lattices upon contact. Teflon rings with mCherry-Ubx fibers were placed on top of confluent rat fibroblast cells. Cell viability was examined after 24 hr. For viability measurements, cells were stained by calcein/ethidium red. Live cells fluoresce green and dead cells fluoresce red, which was quantified using a plate reader mCherry-Ubx fibers were removed prior to quantification to prevent interference. Untreated cells that were cultured with media-only served as the positive (live) control, whereas cells exposed to 70% ethanol for 10 min served as the negative (dead) control. The fractions of both live and dead cells are calculated with reference to appropriate controls. Live fraction of cells in direct contact with mCherry Ubx fibers is not significantly different from the live control ($p = 0.97$), indicating low toxicity. In collaboration with Patrick Spicer and Antonios Mikos, Rice University.

Elution assay

The elution assay was carried out to investigate if potential toxic molecules are leached from Ubx lattices. In this assay, cell culture medium incubated with mCherry-Ubx lattices on Teflon rings for 24 hours was transferred to confluent rat fibroblasts for 24 hour incubation. Cell viability was examined using calcein/ethidium live/dead staining, using appropriate controls (**Fig. 6.4**).

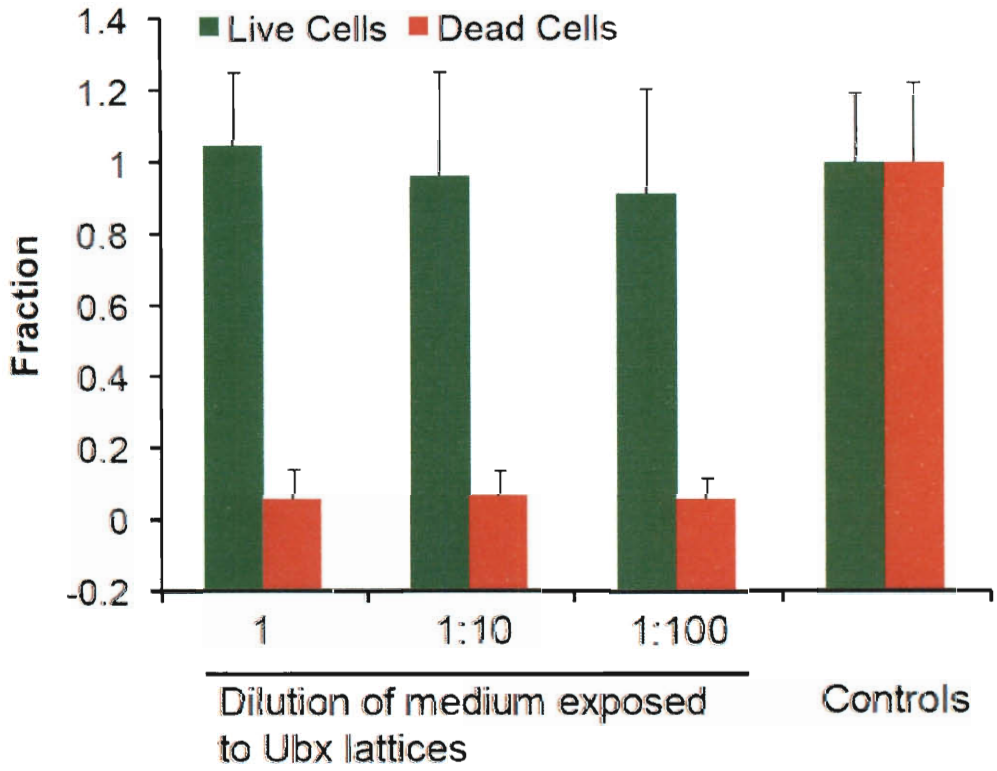

Figure 6.4 Elution assay demonstrates that mCherry-Ubx fibers generate low level of *in vitro* toxicity due to leaching. Media were incubated with mCherry-Ubx fibers for 24 hrs before transferring to confluent rat fibroblasts. Cell viability was examined after 24 hr incubation with 1X, 10X and 100X dilution of the transferred media. For viability measurements, cells were stained by calcein/ethidium red. Live cells have green fluorescence and dead cells have red fluorescence, which was quantified using a plate reader. Untreated cells that were cultured with media-only served as the positive (live) control, whereas cells exposed to 70% ethanol for 10 min served as the negative (dead) control. The fractions of both live and dead cells are calculated with reference to appropriate controls. Live fraction for cells exposed to medium directly and 1:10 and 1:100 fold dilutions is not significantly different from the live control ($p = 0.63$, 0.8, and 0.53 respectively), indicating low toxicity. In collaboration with Patrick Spicer and Antonios Mikos, Rice University.

If toxic molecules leached out of Ubx lattices, we would also expect to see a decrease in live cell fractions and an increase in dead cell fractions when medium incubated with mCherry-Ubx fibers was added to rat fibroblasts cultures (1X). Live and dead cell fractions should also increase and decrease as diluted media were used (10X, 100X). On the contrary, live fractions of cells exposed to undiluted and diluted media are not significantly different from the live control ($p = 0.63$, 0.80, and 0.53 respectively) (**Fig. 6.4, 10X, 100X**), suggesting that molecules leached from mCherry-Ubx fibers have low toxicity to rat fibroblasts.

6.2.5 The effect of Ubx lattices on cell attachment

The ability to enable cell attachment is another important feature for tissue engineering scaffolds, since cell attachment is a pre-requisite to proliferation and differentiation, which regenerates tissue function. To investigate the cell attachment capability of mCherry-Ubx lattices, trypsinized rat fibroblasts were added to mCherry-Ubx lattices on Teflon rings in low attachment plates, which prevent the competition of attachment between the plate and mCherry-Ubx fibers. Attachment of these cells is required for their survival, and unattached cells are washed away by media change after 24 hr incubation. Following ethidium/calcein live/dead staining, confocal and brightfield microscopy revealed that no cells were attached to either the low attachment plates or the Tefon rings (not shown). However, significant numbers of rat fibroblasts (green) attached to mCherry-Ubx fibers (red) as shown in **Fig. 6.5A**, demonstrating that mCherry-Ubx lattices enable the attachment of rat fibroblasts. In addition, cell protrusions form, demonstrating cells find mCherry-Ubx based materials suitable for migration and extension.

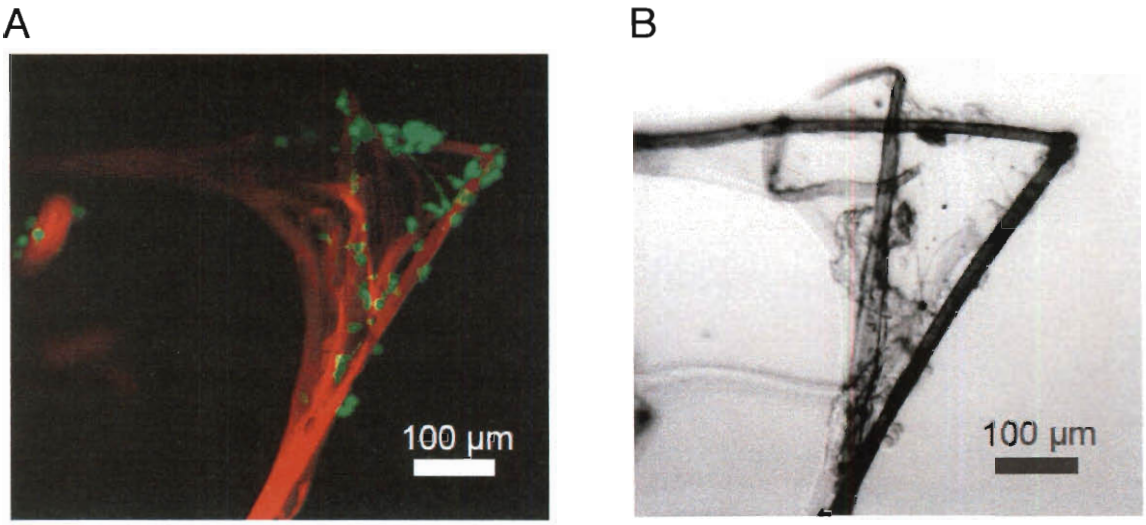

Figure 6.5 Rat fibroblasts attach to mCherry-Ubx lattices in attachment assay. Trypsinized rat fibroblasts were added to low attachment wells containing mCherry-Ubx fibers. Fluorescence (A) and bright field image (B) was taken after 24 hr incubation. Green: live cells stained by calcein. Red: mCherry-Ubx fibers. In collaboration with Patrick Spicer and Antonios Mikos, Rice University.

6.3 Conclusions

Tissue engineering scaffolds must be biocompatible, as defined by a low level of toxicity, inflammation, and immunogenic responses (Crawford and Hatton, 2008; Williams, 2008, 2009). *In vitro* testing is often used as the first step of biocompatibility screening because of its low cost. To characterize the *in vitro* biocompatibility of Ubx-based materials, we generated mCherry-Ubx lattices on Teflon rings and tested their effect on the survival and attachment of rat fibroblast cells. Direct contact assays demonstrated that mCherry-Ubx lattices have low contact toxicity. Elution assays showed that any molecules that may leach from mCherry-Ubx lattices have no significant toxicity. Finally, the attachment assay indicated that cultured rat fibroblast cells effectively attach to mCherry-Ubx lattices. Overall, these results suggest that mCherry-Ubx materials are biocompatible with rat fibroblasts *in vitro*. Ultimately, the

biocompatibility of Ubx and Ubx chimeric materials using *in vivo* animal models must be explored.

The next step is to investigate the biocompatibility of Ubx and other Ubx chimeric materials, which are also likely to be biocompatible given the conservation of Ubx sequence in all instances. Given the potential to create fusion Ubx chimeras containing growth factor and cell adhesion peptides, an attractive future goal is to produce chimeric scaffolds that incorporate the functions of these biomolecules.

CHAPTER 7

Developing Ubx-based Materials:
Ongoing Investigation and Future Work[6]

7.1 Investigating mechanisms driving surface assembly

Ubx-based materials have novel assembly conditions and sequence requirements. Understanding the prerequisite surface assembly of Ubx necessary to generate materials will therefore i) identify optimal conditions to improve the efficiency of Ubx materials production; ii) define sequences within Ubx that are important for assembly, enabling sequence engineering to alter assembly kinetics or mechanisms; and iii) provide new insight into the mechanisms driving protein-assembly at the air-water interface. Ubx assembly at the air-water interface disrupts hydrogen bonding of water molecules at the surface, which in turn reduces surface tension. The surface tension is therefore a good indicator of this surface assembly process, which can be monitored using Langmuir Trough and Pendant Drop techniques.

7.1.1 Monitoring surface tension using Pendant Drop

In Pendant Drop experiments, the shape of a hanging drop containing the molecule(s) of interest is monitored, which in turn enables the calculation of surface tension (**Fig. 7.1A**) (Arashiro and Demarquette, 1999). Preliminary experiments performed using a drop containing Ubx (600 μg/ml in equilibration buffer) revealed a biphasic decrease (phase I: 0-600 s; phase II 600-6000 s) in surface tension during Ubx

---

[6] K. Liu in the laboratory of L. Biswal contributed to the Pendant drop and Langmuir Trough experiments. R. Crouse contributed to X-ray fiber diffraction experiments conducted with equipment in the Rice Shared Equipment Authority.

surface assembly (**Fig. 7.1B**). This result leads to our hypothesis that Ubx materials form at the air-water interface via a two-phase process: During phase I, Ubx molecules move from bulk solution to the air-water interface, decreasing surface H- bonding and therefore

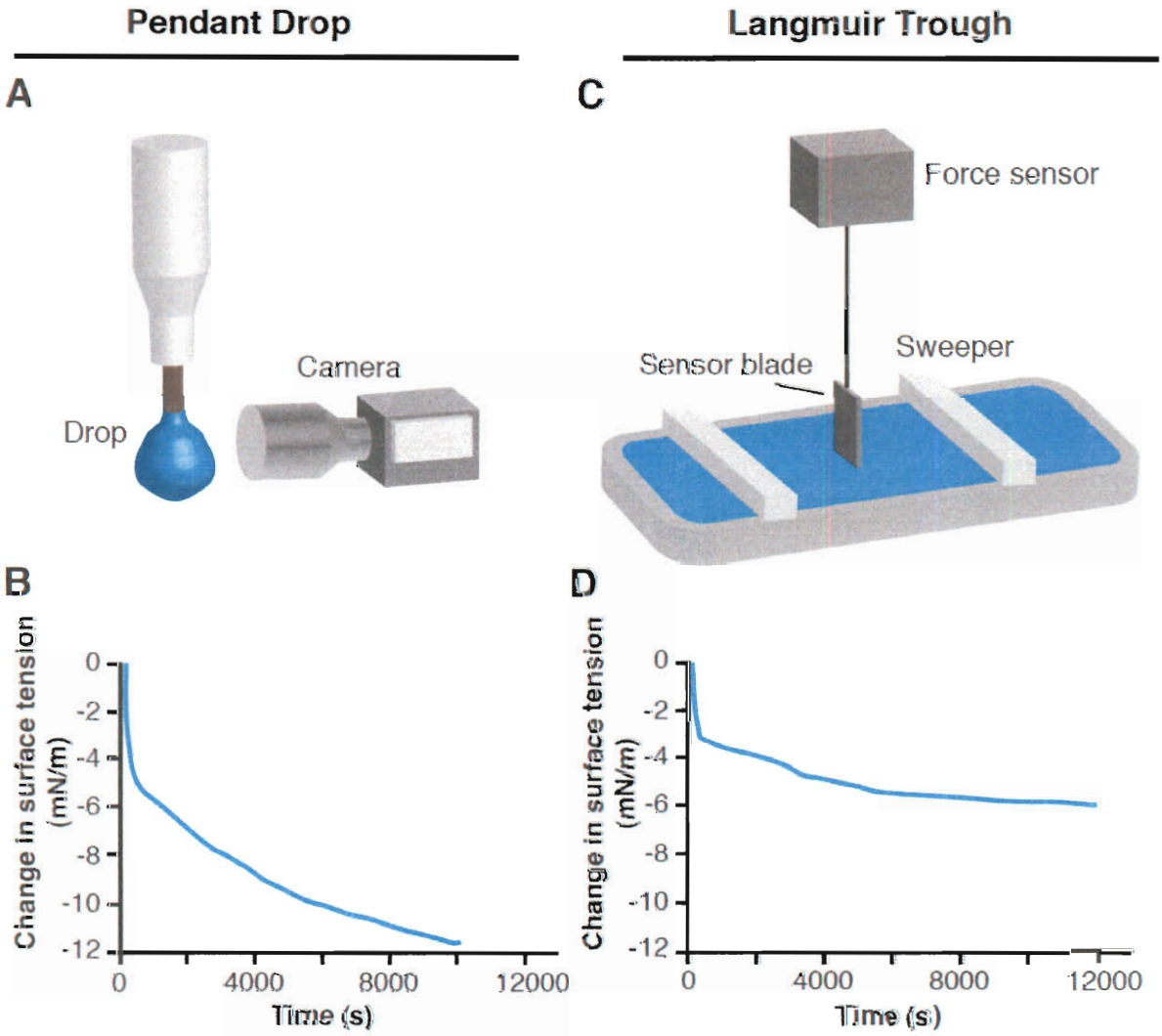

Figure 7.1 Methods used to monitor surface tension changes during assembly at the air-water interface. (A) In a Pendant Drop experiment, a drop containing the protein of interest was monitored by a camera. (B) The shape of the drop was analyzed to calculate surface tension over time, revealing a biphasic process. (C) In a Langmuir Trough experiment, molecules of interest are added to the surface of the solution, and the change in surface tension is measured over time by a blade attached to a force sensor. (D) Surface tension measured by Pendant Drop and Langmuir Trough decreases over time and shows a two-phase transition. In collaboration with Kaiwei Liu from Dr. Lisa Biswal's Lab, Rice University.

surface tension; during phase II, Ubx molecules at the air-water interface interact with each other to form fibrils, which further reduces surface tension. The time required for the completion of phase II is consistent with the sessile drop film assembly and fiber production process, which requires approximately 1.5 hours to 2 hours (5400 s-7200 s). These data support our hypothesis that Phase II must be completed to permit Ubx material formation.

7.1.2 Monitoring surface tension using Langmuir Trough

Langmuir Trough experiments are used to study monolayer assembly events at air-water interfaces. In a Langmuir Trough experiment, a force detector measures the change of surface tension generated by the molecules at the surface and a pair of movable barriers (sweepers) can be used to concentrate molecules at the air-water interface (**Fig. 7.1C**) (Adamson and Gast, 1997). Ubx protein dissolved in equilibration buffer (200 µl, 600 µg/ml) was added to the surface of the Langmuir Trough, and surface tension was monitored over time. Consistent with the Pendant Drop experiment, a biphasic transition in surface tension was observed (**Fig. 7.1D**), further supporting the hypothesis of two phases in the material formation process.

7.1.3 Future experiments to study kinetics of Ubx surface assembly

Overall, these preliminary results from Langmuir Trough and Pendant Drop experiments demonstrate that Ubx assembly can be monitored via changes in surface tension. The assembly of Ubx at the air-water interface appears to have two phases, and the change in surface tension is similar to what has been observed during the assembly of amyloid-β peptides (Jiang et al., 2009). To understand the kinetics of Ubx assembly in detail, additional repeats of Pendant Drop and Langmuir Trough need to be performed.

Considering that buffer composition (*e.g.*, pH, concentrations of solvents) and environmental conditions (*e.g.*, temperature, humidity) can affect the rate of amyloid assembly, investigating the effect of these parameters on Ubx assembly could be highly informative. Additionally, future Langmuir Trough and Pendant Drop experiments on Ubx deletion mutants can be performed to understand the role of Ubx sequence on the kinetics of Ubx assembly.

7.2 Improving the production of Ubx-based materials

Production of Ubx-based materials can be improved by (i) increasing protein expression, (ii) speeding up the materials assembly process, and/or (iii) simplifying and automating materials production procedures.

7.2.1 Increasing protein expression

A number of approaches can advance a higher level of protein expression, which in turn provides a larger amount of protein for subsequent processing. Currently *E. coli* cultures are grown in 1 L flasks and the largest expression capacity per incubator is limited to 12 L. The use of a fermenter could improve both the batch volume and the cell density, therefore improving Ubx expression. We have noted that the expression levels of Ubx chimeras are affected by the properties of appended proteins. For example, expression was enhanced for EGFP-Ubx but reduced for myoglobin-Ubx. Such variation in expression could be caused by the solubility, the stability, or the toxicity of the resulting chimera. Therefore, for future Ubx chimeras, it would be advantageous to choose proteins that demonstrate high solubility and stability, but low toxicity.

7.2.2 Increasing the rate of surface assembly

Manipulating the fast and/or the slow phase can potentially be exploited to accelerate Ubx surface assembly. The fast phase, during which Ubx molecules move to the air-water interface, can be accelerated by optimizing conditions such as protein concentration, buffer composition, pH, temperature, or humidity. Alternatively, reducing the depth of the trough would reduce the "travel distance" required for a Ubx molecule in bulk solution to the reach the surface and thereby reduce the time required for film formation. To accelerate the slow phase, during which Ubx molecules interact with each other, a narrowing buffer reservoir could be used (**Fig. 7.2**). This device would concentrate Ubx molecules at a small region of the surface to facilitate Ubx interactions.

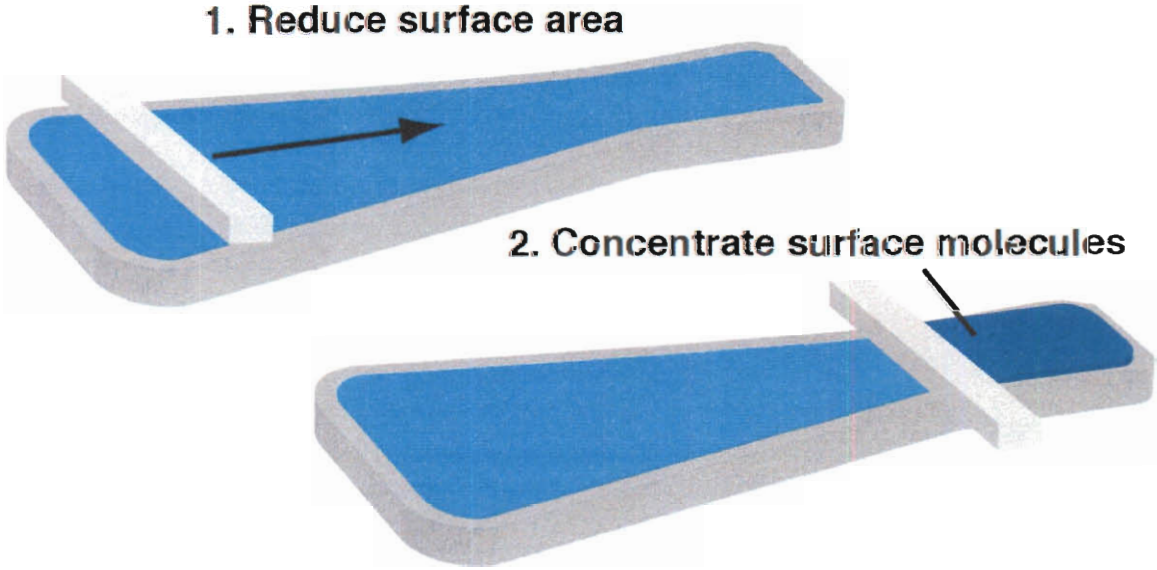

Figure 7.2 A buffer reservoir with a narrower end would aid the production of Ubx-based materials. Moving the sweeper along a buffer reservoir toward the narrower end would reduce surface area greatly, which in turn increases the concentration of Ubx molecules at the surface and facilitates their interactions.

7.2.3 Bypassing purification to produce Ubx-based materials

During the purification of Ubx from *E. coli*, we noticed that Ubx materials could be produced from the surface of the whole cell lysate without further purification. This feature is particularly interesting because bypassing the purification process would greatly accelerate the rate of Ubx materials production and reduce the cost. However, if Ubx materials are produced from the surface of the whole cell lysate, other bacterial proteins and lipids can be incorporated and may result in cellular toxicity or trigger immune responses. Therefore, this method may only be suitable for applications where Ubx-based materials do not make contact with cells.

7.3 Structural characterization of Ubx and Ubx chimeric materials

Protein-based materials have different secondary structures: spider dragline silks are made of β-crystalline regions joined by disordered regions; amyloid fibers consist of stacked β-sheets (Inouye and Kirschner, 2005; Johansson, 2003; Nilsson, 2004; Parkhe et al., 1997; Stromer and Serpell, 2005). Understanding the secondary structure of protein-based materials provides insight into their mechanism of assembly and may explain their mechanical properties.

X-Ray diffraction has been used to examine the structures of spider silk fibers, hair, and amyloid fibers (Riekel et al., 1999; Stromer and Serpell, 2005; Wille et al., 2009). Where a high-energy X-ray beam has been used (e.g., at a synchrotron), a single fiber can provide a satisfactory diffraction pattern for secondary structure interpretation (Wille et al., 2009). For weaker X-ray sources, (e.g., Rice's in-house X-ray diffraction instruments), bundles containing well-aligned fibers are frequently required to ensure sufficient signal (Parkhe et al., 1997). SHaPrP amyloid fibrils display a cross-β

meridional ring at approximately 4.8 Å resolution and broad equatorial diffraction near 10.5 Å, indicating the presence of cross-β sheets perpendicular to the fibril axis (Wille et al., 2009). Similar diffraction ring patterns were observed on spider silks, and the diffraction pattern changes depending on the hydration state of the fiber (Parkhe et al., 1997). In our preliminary X-ray diffraction experiments, mCherry-Ubx bundles containing 20 to 30 aligned fibers produce a diffraction pattern containing 3 major rings. The outer rings at 3.2 Å resolution may be due to residual salt and glucose that were incoporated into the fiber during material production and subsequently crystallized. There were also two other rings at approximately 5 Å and 10 Å resolution, similar to the rings present on the diffraction pattern of amyloid fibers (Wille et al., 2009). To fully understand the structure of Ubx fibers, additional fiber diffraction experiments will be performed on bundles made of Ubx and other Ubx chimeric fibers under different hydration states.

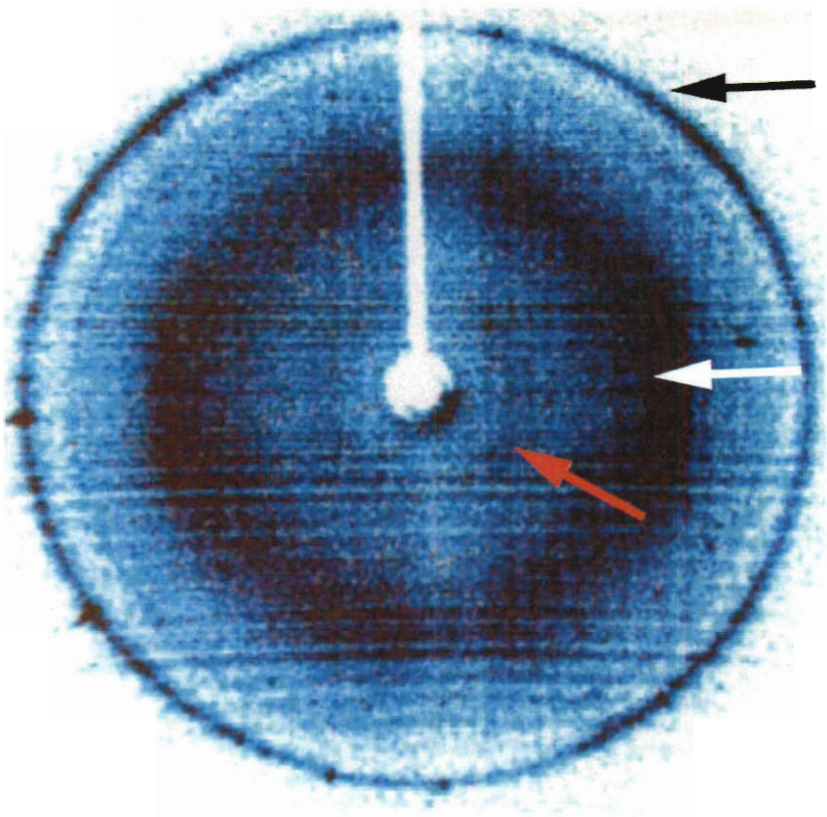

Figure 7.3 Fiber diffraction pattern from a mCherry-Ubx bundle. Black arrow, white arrow, and red arrow indicates 3.2 Å, 5 Å and 10 Å resolution respectively. In collaboration with Richard Crouse at Rice Shared Equipment Authority.

7.4 Engineering the mechanical properties of Ubx chimeric materials

Preliminary data demonstrate that mechanical properties of EGFP-Ubx fibers are different from Ubx fibers. At the same diameter, EGFP-Ubx fibers have a higher breaking stress but lower breaking strain. It is possible that the incorporation of the β-sheet barrel from EGFP into the fibers contributes to their strength, as β-sheet structures do for spider silk and silkworm fibers (Gosline et al., 1999; Jin and Kaplan, 2003; Lazaris et al., 2002; Romer and Scheibel, 2008; Shao and Vollrath, 2002). Appending proteins of different secondary structures to Ubx could potentially generate chimera fibers of different mechanical properties. Myoglobin and luciferase have α-helices and mixed α/β structures respectively. Future mechanical testing of myoglobin-Ubx and luciferase-Ubx

will help understand the effect of secondary structure on mechanical properties of Ubx-based materials.

7.5 Functionalization of Ubx chimeric materials using growth factors

Growth factors influence the attachment, proliferation, and differentiation of cells to accomplish complex events. For example, the binding of VEGFs to their cognate receptors promotes angiogenesis (Holmes et al., 2007), whereas laminin regulates the growth of neurons (Chernousov et al., 2008; Edgar, 1990; Martini, 1994). VEGF and laminin have been immobilized in hydrogels or electrospun fibers to induce angiogenesis (Hahn et al., 2005; Leslie-Barbick et al., 2009) and neuron growth (Biran et al., 2003; Koh et al., 2008).

Because of the ability to append functional proteins of various sizes and secondary structures to Ubx, growth factors or their functional domains can be introduced into functional chimeric materials. We expect VEGF-Ubx fibers to induce angiogenesis and laminin-Ubx chimeric fibers to promote neuron growth. By controlling the spatial arrangement of multiple growth factor/domains, complex event sequences that require cell attachment, proliferation, and differentiation can potentially be achieved in defined regions using Ubx-based substrates.

7.6 Research overview: *Now and future*

During my thesis research I have produced, characterized, and functionalized novel protein-based materials using *Drosophila* transcriptional factor Ultrabithorax. First, Ubx proteins produced recombinantly in *E. coli* self-assemble under protein-friendly conditions to form a variety of macroscale structures such as fibers, films, and sheets in a hierarchical manner. These structures can be manually combined to generate more

complex three-dimensional architectures such as thick fibers, bundles and twists. Second, mechanical tests revealed the diameter dependent mechanical properties of Ubx fibers. The tensile stress and the elasticity of large diameter Ubx fibers are comparable to or exceed that of elastin fibers. Third, Ubx chimeric materials can incorporate protein functions via gene fusions. Since Ubx materials assembly and processing do not require harsh chemical / physical conditions, functional proteins can be incorporated into Ubx chimeric materials, whose spatial pattern can be controlled using surface arrangement and the adhesion properties of Ubx chimeric materials. Finally, preliminary *in vitro* biocompatibility testing demonstrated that Ubx materials elicited low toxicity to rat fibroblasts, which suggests the potential for use as a tissue engineering scaffold in the future.

Future research on Ubx-based materials in following areas is key to the understanding of Ubx-based materials and development of their future applications. First, understanding the mechanism driving the surface assembly of Ubx could identify optimal conditions to improve the efficiency of Ubx materials production. This information would also provide new insight into the mechanisms driving protein-assembly at the air-water interface. Second, optimizing protein expression, materials assembly, and the automating of materials production will enable larger-scale materials production and reduce the production cost. Third, mechanical and structural characterization of Ubx chimeric materials will provide insight into the role of protein sequences and secondary structures in controlling mechanical properties. Finally, functionalization and patterning of growth factor-Ubx chimeric materials can be explored to create tissue engineering scaffolds that can trigger specific cellular responses at defined regions.

REFERENCES

Adamson, A.G., and Gast, A.W. (1997). Physical chemistry of surfaces. (New York, Wiley).

Agapov, I.I., Pustovalova, O.L., Moisenovich, M.M., Bogush, V.G., Sokolova, O.S., Sevastyanov, V.I., Debabov, V.G., and Kirpichnikov, M.P. (2009). Three-dimensional scaffold made from recombinant spider silk protein for tissue engineering. Doklady Biochemistry and Biophysics *426*, 127.

Altman, G.H., Diaz, F., Jakuba, C., Calabro, T., Horan, R.L., Chen, J.S., Lu, H., Richmond, J., and Kaplan, D.L. (2003). Silk-based biomaterials. Biomaterials *24*, 401.

Amsden, J.J., Perry, H., Boriskina, S.V., Gopinath, A., Kaplan, D.L., Dal Negro, L., and Omenetto, F.G. (2009). Spectral analysis of induced color change on periodically nanopatterned silk films. Optics Express *17*, 21271.

Arashiro, E.Y., and Demarquette, N.R. (1999). Use of the pendant drop method to measure interfacial tension between molten polymers. Materials Research *2*, 23.

Astbury, W.T., and Woods, H.J. (1934). X-ray studies of the structure of hair, wool, and related fibres II - The molecular structure and elastic properties of hair keratin. Proceedings of the Royal Society of London Series B-Containing Papers of a Biological Character *114*, 314.

Auger, F.A., Rouabhia, M., Goulet, F., Berthod, F., Moulin, V., and Germain, L. (1998). Tissue-engineered human skin substitutes developed from collagen-populated hydrated gels: Clinical and fundamental applications. Medical & Biological Engineering & Computing *36*, 801.

Auld, D.S., Lovell, S., Thorne, N., Lea, W.A., Maloney, D.J., Shen, M., Rai, G., Battaile, K.P., Thomas, C.J., Simeonov, A., *et al.* (2010). Molecular basis for the high-affinity binding and stabilization of firefly luciferase by PTC124. Proceedings of the National Academy of Sciences of the United States of America *107*, 4878.

Ayub, Z.H., Arai, M., and Hirabayashi, K. (1993). Mechanism of the gelation of fibroin solution. Bioscience Biotechnology and Biochemistry *57*, 1910.

Babensee, J.E., Anderson, J.M., McIntire, L.V., and Mikos, A.G. (1998). Host response to tissue engineered devices. Advanced Drug Delivery Reviews *33*, 111.

Badami, A.S., Kreke, M.R., Thompson, M.S., Riffle, J.S., and Goldstein, A.S. (2006). Effect of fiber diameter on spreading, proliferation, and differentiation of osteoblastic cells on electrospun poly(lactic acid) substrates. Biomaterials *27*, 596.

Badrossamay, M.R., McIlwee, H.A., Goss, J.A., and Parker, K.K. (2010). Nanofiber assembly by rotary jet-spinning. Nano Letters *10*, 2257.

Balguid, A., Mol, A., van Marion, M.H., Bank, R.A., Bouten, C.V.C., and Baaijens, F.P.T. (2009). Tailoring fiber diameter in electrospun poly(epsilon-caprolactone) scaffolds for optimal cellular infiltration in cardiovascular tissue engineering. Tissue Engineering Part A *15*, 437.

Baneyx, F., and Schwartz, D.T. (2007). Selection and analysis of solid-binding peptides. Current Opinion in Biotechnology *18*, 312.

Beachley, V., and Wen, X.J. (2009). Fabrication of nanofiber reinforced protein structures for tissue engineering. Materials Science & Engineering C-Materials for Biological Applications *29*, 2448.

Beachley, V., and Wen, X.J. (2010). Polymer nanofibrous structures: Fabrication, biofunctionalization, and cell interactions. Progress in Polymer Science *35*, 868.

Beachy, P.A., Varkey, J., Young, K.E., Vonkessler, D.P., Sun, B.I., and Ekker, S.C. (1993). Cooperative binding of an Ultrabithorax homeodomain protein to nearby and distant DNA sites. Molecular and Cellular Biology *13*, 6941.

Beniash, E., Hartgerink, J.D., Storrie, H., Stendahl, J.C., and Stupp, S.I. (2005). Self-assembling peptide amphiphile nanofiber matrices for cell entrapment. Acta Biomaterialia *1*, 387.

Betre, H., Setton, L.A., Meyer, D.E., and Chilkoti, A. (2002). Characterization of a genetically engineered elastin-like polypeptide for cartilaginous tissue repair. Biomacromolecules *3*, 910.

Bettinger, C.J., Cyr, K.M., Matsumoto, A., Langer, R., Borenstein, J.T., and Kaplan, D.L. (2007). Silk fibroin microfluidic devices. Advanced Materials *19*, 2847.

Bini, E., Foo, C.W.P., Huang, J., Karageorgiou, V., Kitchel, B., and Kaplan, D.L. (2006). RGD-functionalized bioengineered spider dragline silk biomaterial. Biomacromolecules *7*, 3139.

Biran, R., Noble, M.D., and Tresco, P.A. (2003). Directed nerve outgrowth is enhanced by engineered glial substrates. Experimental Neurology *184*, 141.

Boland, E.D., Matthews, J.A., Pawlowski, K.J., Simpson, D.G., Wnek, G.E., and Bowlin, G.L. (2004). Electrospinning collagen and elastin: Preliminary vascular tissue engineering. Frontiers in Bioscience *9*, 1422.

Bondos, S.E. (2006). Methods for measuring protein aggregation. Current Analytical Chemistry *2*, 157.

Bondos, S.E., and Bicknell, A. (2003). Detection and prevention of protein aggregation before, during, and after purification. Analytical Biochemistry *316*, 223.

Bondos, S.E., Mudali, S., Hanson, M., and Matthews, K.S. (2002). Redox regulation of DNA binding by Drosophila Ultrabithorax Ib. Developmental Biology *247*, 489.

Bradford, M.M. (1976). Rapid and sensitive method for quantitation of microgram quantities of protein utilizing principle of protein-dye binding. Analytical Biochemistry *72*, 248.

Brooks, A.E., Stricker, S.M., Joshi, S.B., Kamerzell, T.J., Middaugh, C.R., and Lewis, R.V. (2008). Properties of synthetic spider silk fibers based on Argiope aurantia MASP2. Biomacromolecules *9*, 1506.

Buttafoco, L., Kolkman, N.G., Engbers-Buijtenhuijs, P., Poot, A.A., Dijkstra, P.J., Vermes, I., and Feijen, J. (2006). Electrospinning of collagen and elastin for tissue engineering applications. Biomaterials *27*, 724.

Cao, H., Chen, X., Huang, L., and Shao, Z.Z. (2009). Electrospinning of reconstituted silk fiber from aqueous silk fibroin solution. Materials Science & Engineering C-Materials for Biological Applications *29*, 2270.

Cen, L., Liu, W., Cui, L., Zhang, W.J., and Cao, Y.L. (2008). Collagen tissue engineering: Development of novel biomaterials and applications. Pediatric Research *63*, 492.

Chernousov, M.A., Yu, W.M., Chen, Z.L., Carey, D.J., and Strickland, S. (2008). Regulation of Schwann cell function by the extracellular matrix. Glia *56*, 1498.

Chew, S.Y., Wen, J., Yim, E.K.F., and Leong, K.W. (2005). Sustained release of proteins from electrospun biodegradable fibers. Biomacromolecules *6*, 2017.

Chilkoti, A., Christensen, T., and MacKay, J.A. (2006). Stimulus responsive elastin biopolymers: Applications in medicine and biotechnology. Current Opinion in Chemical Biology *10*, 652.

Choi, J.Y., Jung, K.Y., Lee, J.S., Cho, S.K., Jheon, S.H., and Lim, J.O. (2010). Fabrication and in vivo evaluation of the electrospun small diameter vascular grafts composed of Elastin/PLGA/PCL and Heparin-VEGF. Tissue Engineering and Regenerative Medicine *7*, 149.

Cigada, A. (2008). Biomaterials, tissue engineering, gene therapy. Journal of Applied Biomaterials & Biomechanics *6*, 127.

Conley, A.J., Joensuu, J.J., Jevnikar, A.M., Menassa, R., and Brandle, J.E. (2009). Optimization of elastin-like polypeptide fusions for expression and purification of recombinant proteins in plants. Biotechnology and Bioengineering *103*, 562.

Conrad, U., Plagmann, I., Malchow, S., Sack, M., Floss, D.M., Kruglov, A.A., Nedospasov, S.A., Rose-John, S., and Scheller, J. (2011). Elpylated anti-human TNF therapeutic single-domain antibodies for prevention of lethal septic shock. Plant Biotechnology Journal *9*, 22.

Corsini, P., Perez-Rigueiro, J., Guinea, G.V., Plaza, G.R., Elices, M., Marsano, E., Carnasciali, M.M., and Freddi, G. (2007). Influence of the draw ratio on the tensile and fracture behavior of NMMO regenerated silk fibers. Journal of Polymer Science Part B-Polymer Physics *45*, 2568.

Coulombe, P.A., and Omary, M.B. (2002). 'Hard' and 'Soft' principles defining the structure, function and regulation of keratin intermediate filaments. Current Opinion in Cell Biology *14*, 110.

Cox, B.A., Starcher, B.C., and Urry, D.W. (1974). Coacervation of tropoelastin results in fiber formation. Journal of Biological Chemistry *249*, 997.

Craig, C.L., and Riekel, C. (2002). Comparative architecture of silks, fibrous proteins and their encoding genes in insects and spiders. Comparative Biochemistry and Physiology B-Biochemistry & Molecular Biology *133*, 493.

Crawford, A., and Hatton, P.V. (2008). Cell-biomaterial interactions in skeletal tissue engineering. Biomedicine & Pharmacotherapy *62*, 493.

Daamen, W.F., Veerkamp, J.H., van Hest, J.C., and van Kuppevelt, T.H. (2007). Elastin as a biomaterial for tissue engineering. Biomaterials *28*, 4378.

Deming, T.J. (2007). Synthetic polypeptides for biomedical applications. Progress in Polymer Science *32*, 858.

Demura, M., Takekawa, T., Asakura, T., and Nishikawa, A. (1992). Characterization of low-temperature-plasma treated silk fibroin fabrics by ESCA and the use of the fabrics as an enzyme-immobilization support. Biomaterials *13*, 276.

Domachuk, P., Tsioris, K., Omenetto, F.G., and Kaplan, D.L. (2010). Bio-microfluidics: Biomaterials and biomimetic designs. Advanced Materials *22*, 249.

Dror, Y., Ziv, T., Makarov, V., Wolf, H., Admon, A., and Zussman, E. (2008). Nanofibers made of globular proteins. Biomacromolecules *9*, 2749.

Du, C.L., Wang, M.Q., Liu, J.Y., Pan, M.L., Cai, Y.R., and Yao, J.M. (2008). Improvement of thermostability of recombinant collagen-like protein by incorporating a foldon sequence. Applied Microbiology and Biotechnology *79*, 195.

Dutta, R.C., and Dutta, A.K. (2009). Cell-interactive 3D-scaffold: Advances and applications. Biotechnology Advances *27*, 334.

Edgar, D. (1990). The expression and interactions of laminin in the developing nervous-system. Cell Differentiation and Development *32*, 377.

Eisenbarth, E. (2007). Biomaterials for tissue engineering. Advanced Engineering Materials *9*, 1051.

Elvin, C.M., Carr, A.G., Huson, M.G., Maxwell, J.M., Pearson, R.D., Vuocolo, T., Liyou, N.E., Wong, D.C.C., Merritt, D.J., and Dixon, N.E. (2005). Synthesis and properties of crosslinked recombinant pro-resilin. Nature *437*, 999.

Engler, A.J., Sen, S., Sweeney, H.L., and Discher, D.E. (2006). Matrix elasticity directs stem cell lineage specification. Cell *126*, 677.

Falconnet, D., Csucs, G., Grandin, H.M., and Textor, M. (2006). Surface engineering approaches to micropattern surfaces for cell-based assays. Biomaterials *27*, 3044.

Fan, H.B., Liu, H.F., Toh, S.L., and Goh, J.C.H. (2009). Anterior cruciate ligament regeneration using mesenchymal stem cells and silk scaffold in large animal model. Biomaterials *30*, 4967.

Faury, G. (2001). Function-structure relationship of elastic arteries in evolution: From microfibrils to elastin and elastic fibres. Pathologie Biologie *49*, 310.

Floss, D.M., Schallau, K., Rose-John, S., Conrad, U., and Scheller, J. (2010). Elastin-like polypeptides revolutionize recombinant protein expression and their biomedical application. Trends in Biotechnology *28*, 37.

Folch, A., and Toner, M. (2000). Microengineering of cellular interactions. Annual Review of Biomedical Engineering *2*, 227.

Fratzl, P., Misof, K., Zizak, I., Rapp, G., Amenitsch, H., and Bernstorff, S. (1998). Fibrillar structure and mechanical properties of collagen. Journal of Structural Biology *122*, 119.

Fratzl, P., and Weinkamer, R. (2007). Nature's hierarchical materials. Progress in Materials Science *52*, 1263.

Fuchs, E., and Weber, K. (1994). Intermediate filaments - structure, dynamics, function, and disease. Annual Review of Biochemistry *63*, 345.

Galant, R., and Carroll, S.B. (2002). Evolution of a transcriptional repression domain in an insect Hox protein. Nature *415*, 910.

Galler, K.M., Cavender, A., Yuwono, V., Dong, H., Shi, S.T., Schmalz, G., Hartgerink, J.D., and D'Souza, R.N. (2008). Self-assembling peptide amphiphile nanofibers as a scaffold for dental stem cells. Tissue Engineering Part A *14*, 2051.

Gelain, F., Bottai, D., Vescovi, A., and Zhang, S.G. (2006). Designer self-assembling peptide nanofiber scaffolds for adult mouse neural stem cell 3-dimensional cultures. PLOS One *1*.

Georges, P.C., Hui, J.J., Gombos, Z., McCormick, M.E., Wang, A.Y., Uemura, M., Mick, R., Janmey, P.A., Furth, E.E., and Wells, R.G. (2007). Increased stiffness of the rat liver precedes matrix deposition: Implications for fibrosis. American Journal of Physiology-Gastrointestinal and Liver Physiology *293*, G1147.

Ghanaati, S., Orth, C., Unger, R.E., Barbeck, M., Webber, M.J., Motta, A., Migliaresi, C., and Kirkpatrick, C.J. (2010). Fine-tuning scaffolds for tissue regeneration: Effects of formic acid processing on tissue reaction to silk fibroin. Journal of Tissue Engineering and Regenerative Medicine *4*, 464.

Gobin, A.S., and West, J.L. (2002). Cell migration through defined, synthetic extracellular matrix analogues. FASEB Journal *16*, 751.

Gosline, J., Lillie, M., Carrington, E., Guerette, P., Ortlepp, C., and Savage, K. (2002). Elastic proteins: Biological roles and mechanical properties. Philosophical Transactions of the Royal Society B Biological Science *357*, 121.

Gosline, J.M., Guerette, P.A., Ortlepp, C.S., and Savage, K.N. (1999). The mechanical design of spider silks: From fibroin sequence to mechanical function. Journal of Experimental Biology *202*, 3295.

Greer, A.M., Huang, Z., Oriakhi, A., Lu, Y., Lou, J., Matthews, K.S., and Bondos, S.E. (2009). The Drosophila transcription factor Ultrabithorax self-assembles into protein-based biomaterials with multiple morphologies. Biomacromolecules *10*, 829.

Grevellec, J., Marquie, C., Ferry, L., Crespy, A., and Vialettes, V. (2001). Processability of cottonseed proteins into biodegradable materials. Biomacromolecules *2*, 1104.

Grip, S., Johansson, J., and Hedhammar, M. (2009). Engineered disulfides improve mechanical properties of recombinant spider silk. Protein Science *18*, 1012.

Guess, K.B., and Viney, C. (1998). Thermal analysis of major ampullate (drag line) spider silk: The effect of spinning rate on tensile modulus. Thermochimica Acta *315*, 61.

Guler, M.O., Hsu, L., Soukasene, S., Harrington, D.A., Hulvat, J.F., and Stupp, S.I. (2006). Presentation of RGDs epitopes on self-assembled nanofibers of branched peptide amphiphiles. Biomacromolecules *7*, 1855.

Gupta, M.K., Khokhar, S.K., Phillips, D.M., Sowards, L.A., Drummy, L.F., Kadakia, M.P., and Naik, R.R. (2007). Patterned silk films cast from ionic liquid solubilized fibroin as scaffolds for cell growth. Langmuir *23*, 1315.

Ha, S.W., Tonelli, A.E., and Hudson, S.M. (2005). Structural studies of Bombyx mori silk fibroin during regeneration from solutions and wet fiber spinning. Biomacromolecules *6*, 1722.

Hahn, M.S., Miller, J.S., and West, J.L. (2005). Laser scanning lithography for surface micropatterning on hydrogels. Advanced Materials *17*, 2939.

Halstenberg, S., Panitch, A., Rizzi, S., Hall, H., and Hubbell, J.A. (2002). Biologically engineered protein-graft-poly(ethylene glycol) hydrogels: A cell adhesive and plasma in-degradable biosynthetic material for tissue repair. Biomacromolecules *3*, 710.

Han, T.H., Lee, W.J., Lee, D.H., Kim, J.E., Choi, E.Y., and Kim, S.O. (2010). Peptide/graphene hybrid assembly into core/shell nanowires. Advanced Materials *22*, 2060.

Hansen, J.C., Lu, X., Ross, E.D., and Woody, R.W. (2006). Intrinsic protein disorder, amino acid composition, and histone terminal domains. Journal of Biological Chemistry *281*, 1853.

Hardy, J.G., and Scheibel, T.R. (2009). Silk-inspired polymers and proteins. Biochemical Society Transactions *37*, 677.

Hartgerink, J.D., Beniash, E., and Stupp, S.I. (2001). Self-assembly and mineralization of peptide-amphiphile nanofibers. Science *294*, 1684.

Hayashi, C.Y., Blackledge, T.A., and Lewis, R.V. (2004). Molecular and mechanical characterization of Aciniform silk: Uniformity of iterated sequence modules in a novel member of the spider silk fibroin gene family. Molecular Biology and Evolution *21*, 1950.

Healy, K.E., Thomas, C.H., Rezania, A., Kim, J.E., McKeown, P.J., Lom, B., and Hockberger, P.E. (1996). Kinetics of bone cell organization and mineralization on materials with patterned surface chemistry. Biomaterials *17*, 195.

Heim, M., Keerl, D., and Scheibel, T. (2009). Spider silk: From soluble protein to extraordinary fiber. Angewandte Chemie-International Edition *48*, 3584.

Heim, M., Romer, L., and Scheibel, T. (2010). Hierarchical structures made of proteins. The complex architecture of spider webs and their constituent silk proteins. Chemical Society Reviews *39*, 156.

Helenius, J., Heisenberg, C.P., Gaub, H.E., and Muller, D.J. (2008). Single-cell force spectroscopy. Journal of Cell Science *121*, 1785.

Hermanson, K.D., Harasim, M.B., Scheibel, T., and Bausch, A.R. (2007a). Permeability of silk microcapsules made by the interfacial adsorption of protein. Physical Chemistry Chemical Physics *9*, 6442.

Hermanson, K.D., Huemmerich, D., Scheibel, T., and Bausch, A.R. (2007b). Engineered microcapsules fabricated from reconstituted spider silk. Advanced Materials *19*, 1810.

Herrero-Vanrell, R., Rincon, A.C., Alonso, M., Reboto, V., Molina-Martinez, I.T., and Rodriguez-Cabello, J.C. (2005). Self-assembled particles of an elastin-like polymer as vehicles for controlled drug release. Journal of Controlled Release *102*, 113.

Hinman, M.B., Jones, J.A., and Lewis, R.V. (2000). Synthetic spider silk: A modular fiber. Trends in Biotechnology *18*, 374.

Hofmann, S., Foo, C.T.W.P., Rossetti, F., Textor, M., Vunjak-Novakovic, G., Kaplan, D.L., Merkle, H.P., and Meinel, L. (2006). Silk fibroin as an organic polymer for controlled drug delivery. Journal of Controlled Release *111*, 219.

Holmes, K., Roberts, O.L., Thomas, A.M., and Cross, M.J. (2007). Vascular endothelial growth factor receptor-2: Structure, function, intracellular signalling and therapeutic inhibition. Cellular Signalling *19*, 2003.

Holmquist, B., and Vallee, B.L. (1973). Tryptophan quantitation by magnetic circular-dichroism in native and modified proteins. Biochemistry *12*, 4409.

Hu, X., Vasanthavada, K., Kohler, K., McNary, S., Moore, A.M.F., and Vierra, C.A. (2006). Molecular mechanisms of spider silk. Cellular and Molecular Life Sciences *63*, 1986.

Huang, J., Wong, C., George, A., and Kaplan, D.L. (2007). The effect of genetically engineered spider silk-dentin matrix protein 1 chimeric protein on hydroxyapatite nucleation. Biomaterials *28*, 2358.

Huang, L., McMillan, R.A., Apkarian, R.P., Pourdeyhimi, B., Conticello, V.P., and Chaikof, E.L. (2000). Generation of synthetic elastin-mimetic small diameter fibers and fiber networks. Macromolecules *33*, 2989.

Huang, S.L., Wu, L.C., Liang, H.K., Pan, K.T., Horng, J.T., and Ko, M.T. (2004). PGTDB: A database providing growth temperatures of prokaryotes. Bioinformatics *20*, 276.

Huang, Z., Lu, Y., Majithia, R., Shah, J., Meissner, K., Matthews, K.S., Bondos, S.E., and Lou, J. (2010). Size dictates mechanical properties for protein fibers self-assembled by the Drosophila Hox transcription factor Ultrabithorax. Biomacromolecules *11*, 3644.

Huang, Z., Salim, T., Brawley, A., Patterson, J., Matthews, K.S. and Bondos, S.E. (2011). Functionalization and patterning of protein-based materials using active Ultrabithorax chimeras. Advanced Functional Materials *In Press*

Hubbell, J.A. (1999). Bioactive biomaterials. Current Opinion in Biotechnology *10*, 123.

Huemmerich, D., Scheibel, T., Vollrath, F., Cohen, S., Gat, U., and Ittah, S. (2004). Novel assembly properties of recombinant spider dragline silk proteins. Current Biology *14*, 2070.

Huemmerich, D., Slotta, U., and Scheibel, T. (2006). Processing and modification of films made from recombinant spider silk proteins. Applied Physics A-Materials Science & Processing *82*, 219.

Hughes, C.L., and Kaufman, T.C. (2002). Hox genes and the evolution of the arthropod body plan. Evolution & Development *4*, 459.

Hwang, D.S., Sim, S.B., and Cha, H.J. (2007). Cell adhesion biomaterial based on mussel adhesive protein fused with RGD peptide. Biomaterials *28*, 4039.

Hwang, D.S., Waite, J.H., and Tirrell, M. (2010). Promotion of osteoblast proliferation on complex coacervation-based hyaluronic acid - recombinant mussel adhesive protein coatings on titanium. Biomaterials *31*, 1080.

Hynd, M.R., Frampton, J.P., Burnham, M.R., Martin, D.L., Dowell-Mesfin, N.M., Turner, J.N., and Shain, W. (2007). Functionalized hydrogel surfaces for the patterning of multiple biomolecules. Journal of Biomedical Materials Research Part A *81A*, 347.

Imen, E.H., Nakamura, M., Mie, M., and Kobatake, E. (2009). Construction of multifunctional proteins for tissue engineering: Epidermal growth factor with collagen binding and cell adhesive activities. Journal of Biotechnology *139*, 19.

Inouye, H., and Kirschner, D.A. (2005). Alzheimer's beta-amyloid: Insights into fibril formation and structure from congo red binding. Subcell Biochem *38*, 203.

Jang, E., and Koh, W.G. (2010). Multiplexed enzyme-based bioassay within microfluidic devices using shape-coded hydrogel microparticles. Sensors and Actuators B-Chemical *143*, 681.

Jhon, M.S., and Andrade, J.D. (1973). Water and hydrogels. Journal of Biomedical Materials Research *7*, 509.

Jiang, D.L., Dinh, K.L., Ruthenburg, T.C., Zhang, Y., Su, L., Land, D.P., and Zhou, F.M. (2009). A kinetic model for beta-amyloid adsorption at the air/solution interface and its implication to the beta-amyloid aggregation process. Journal of Physical Chemistry B *113*, 3160.

Jimenez, J.L., Nettleton, E.J., Bouchard, M., Robinson, C.V., Dobson, C.M., and Saibil, H.R. (2002). The protofilament structure of insulin amyloid fibrils. Proceedings of the National Academy of Sciences of the United States of America *99*, 9196.

Jin, H.J., Fridrikh, S.V., Rutledge, G.C., and Kaplan, D.L. (2002). Electrospinning Bombyx mori silk with poly(ethylene oxide). Biomacromolecules *3*, 1233.

Jin, H.J., and Kaplan, D.L. (2003). Mechanism of silk processing in insects and spiders. Nature *424*, 1057.

Johansson, J. (2003). Molecular determinants for amyloid fibril formation: Lessons from lung surfactant protein C. Swiss Medical Weekly *133*, 275.

Ju, Y.M., Choi, J.S., Atala, A., Yoo, J.J., and Lee, S.J. (2010). Bilayered scaffold for engineering cellularized blood vessels. Biomaterials *31*, 4313.

Junghans, F., Morawietz, M., Conrad, U., Scheibel, T., Heilmann, A., and Spohn, U. (2006). Preparation and mechanical properties of layers made of recombinant spider silk proteins and silk from silk worm. Applied Physics A-Materials Science & Processing *82*, 253.

Kang, H.J., Kim, J.H., Chang, W.J., Kim, E.S., and Koo, Y.M. (2007). Heterologous expression and optimized one-step separation of levansucrase via elastin-like polypeptides tagging system. Journal of Microbiology and Biotechnology *17*, 1751.

Kaplan, D. L., Adams, W.W., Farmer, B., and Viney, C. (1994). Silk - Biology, structure, properties, and genetics. Silk Polymers *544*, 2.

Kaplan, D.L. (1998). Fibrous proteins - Silk as a model system. Polymer Degradation and Stability *59*, 25.

Karthikeyan, R., Balaji, S., and Sehgal, P.K. (2007). Industrial applications of keratins - A review. Journal of Scientific & Industrial Research *66*, 710.

Kaufmann, P.M., Heimrath, S., Kim, B.S., and Mooney, D.J. (1997). Highly porous polymer matrices as a three-dimensional culture system for hepatocytes. Cell Transplantation *6*, 463.

Kharlampieva, E., Kozlovskaya, V., Gunawidjaja, R., Shevchenko, V.V., Vaia, R., Naik, R.R., Kaplan, D.L., and Tsukruk, V.V. (2010). Flexible silk-inorganic nanocomposites: From transparent to highly reflective. Advanced Functional Materials *20*, 840.

Khoshnoodi, J., Sigmundsson, K., Cartailler, J.P., Bondar, O., Sundaramoorthy, M., and Hudson, B.G. (2006). Mechanism of chain selection in the assembly of collagen IV - A prominent role for the alpha 2 chain. Journal of Biological Chemistry *281*, 6058.

Kim, D.H., Kim, Y.S., Amsden, J., Panilaitis, B., Kaplan, D.L., Omenetto, F.G., Zakin, M.R., and Rogers, J.A. (2009). Silicon electronics on silk as a path to bioresorbable, implantable devices. Applied Physics Letters *95*, 133701

Kim, D.H., Viventi, J., Amsden, J.J., Xiao, J.L., Vigeland, L., Kim, Y.S., Blanco, J.A., Panilaitis, B., Frechette, E.S., Contreras, D., *et al.* (2010). Dissolvable films of silk fibroin for ultrathin conformal bio-integrated electronics. Nature Materials *9*, 511.

Kim, E.J., Kang, I.K., Jang, M.K., and Park, Y.B. (1998). Preparation of insulin-immobilized polyurethanes and their interaction with human fibroblasts. Biomaterials *19*, 239.

Kim, U.J., Park, J.Y., Li, C.M., Jin, H.J., Valluzzi, R., and Kaplan, D.L. (2004). Structure and properties of silk hydrogels. Biomacromolecules *5*, 786.

Kim, W., and Conticello, V.P. (2007). Protein engineering methods for investigation of structure-function relationships in protein-based elastomeric materials. Polymer Reviews *47*, 93.

Kjeang, E., Sinton, D., and Harrington, D.A. (2006). Strategic enzyme patterning for microfluidic biofuel cells. Journal of Power Sources *158*, 1.

Kluge, J.A., Rabotyagova, U., Leisk, G.G., and Kaplan, D.L. (2008). Spider silks and their applications. Trends in Biotechnology *26*, 244.

Koh, H.S., Yong, T., Chan, C.K., and Ramakrishna, S. (2008). Enhancement of neurite outgrowth using nano-structured scaffolds coupled with laminin. Biomaterials *29*, 3574.

Kuhl, P.R., and Griffith-Cima, L.G. (1996). Tethered epidermal growth factor as a paradigm for growth factor-induced stimulation from the solid phase. Nature Medicine *2*, 1022.

Kusuhara, H., Isogai, N., Enjo, M., Otani, H., Ikada, Y., Jacquet, R., Lowder, E., and Landis, W.J. (2009). Tissue engineering a model for the human ear: Assessment of size, shape, morphology, and gene expression following seeding of different chondrocytes. Wound Repair and Regeneration *17*, 136.

Kyle, S., Aggeli, A., Ingham, E., and McPherson, M.J. (2009). Production of self-assembling biomaterials for tissue engineering. Trends in Biotechnology *27*, 423.

Lagziel-Simis, S., Cohen-Hadar, N., Moscovich-Dagan, H., Wine, Y., and Freeman, A. (2006). Protein-mediated nanoscale biotemplating. Current Opinion in Biotechnology *17*, 569.

Lammel, A., Schwab, M., Slotta, U., Winter, G., and Scheibel, T. (2008). Processing conditions for the formation of spider silk microspheres. Chemsuschem *1*, 413.

Lawrence, B.D., Cronin-Golomb, M., Georgakoudi, I., Kaplan, D.L., and Omenetto, F.G. (2008). Bioactive silk protein biomaterial systems for optical devices. Biomacromolecules *9*, 1214.

Lawrence, B.D., Marchant, J.K., Pindrus, M.A., Omenetto, F.G., and Kaplan, D.L. (2009). Silk film biomaterials for cornea tissue engineering. Biomaterials *30*, 1299.

Lazaris, A., Arcidiacono, S., Huang, Y., Zhou, J.F., Duguay, F., Chretien, N., Welsh, E.A., Soares, J.W., and Karatzas, C.N. (2002). Spider silk fibers spun from soluble recombinant silk produced in mammalian cells. Science *295*, 472.

Leal-Egana, A., and Scheibel, T. (2010). Silk-based materials for biomedical applications. Biotechnology and Applied Biochemistry *55*, 155.

Lee, K.Y., and Mooney, D.J. (2001). Hydrogels for tissue engineering. Chemical Reviews *101*, 1869.

Lee, S.M., Pippel, E., Gosele, U., Dresbach, C., Qin, Y., Chandran, C.V., Brauniger, T., Hause, G., and Knez, M. (2009). Greatly increased toughness of infiltrated spider silk. Science *324*, 488.

Leslie-Barbick, J.E., Moon, J.J., and West, J.L. (2009). Covalently-immobilized vascular endothelial growth factor promotes endothelial cell tubulogenesis in poly(ethylene glycol) diacrylate hydrogels. Journal of Biomaterials Science-Polymer Edition *20*, 1763.

Lewis, E.B. (1978). Gene complex controlling segmentation in Drosophila. Nature *276*, 565.

Li, B., and Daggett, V. (2003). The molecular basis of the temperature- and pH-induced conformational transitions in elastin-based peptides. Biopolymers *68*, 121.

Li, D., and Xia, Y.N. (2004). Electrospinning of nanofibers: Reinventing the wheel? Advanced Materials *16*, 1151.

Li, M.Y., Mondrinos, M.J., Gandhi, M.R., Ko, F.K., Weiss, A.S., and Lelkes, P.I. (2005). Electrospun protein fibers as matrices for tissue engineering. Biomaterials *26*, 5999.

Li, W.J., Laurencin, C.T., Caterson, E.J., Tuan, R.S., and Ko, F.K. (2002). Electrospun nanofibrous structure: A novel scaffold for tissue engineering. Journal of Biomedical Materials Research *60*, 613.

Liebmann, B., Huemmerich, D., Scheibel, T., and Fehr, M. (2008). Formulation of poorly water-soluble substances using self-assembling spider silk protein. Colloids and Surfaces A-Physicochemical and Engineering Aspects *331*, 126.

Liivak, O., Blye, A., Shah, N., and Jelinski, L.W. (1998). A microfabricated wet-spinning apparatus to spin fibers of silk proteins. Structure-property correlations. Macromolecules *31*, 2947.

Liu, Y., Matthews, K.S., and Bondos, S.E. (2008). Multiple intrinsically disordered sequences alter DNA binding by the homeodomain of the Drosophila Hox protein Ultrabithorax. Journal of Biological Chemistry *283*, 20874.

Lutolf, M.P., and Hubbell, J.A. (2003). Synthesis and physicochemical characterization of end-linked poly(ethylene glycol)-co-peptide hydrogels formed by michael-type addition. Biomacromolecules *4*, 713.

Lutolf, M.P., and Hubbell, J.A. (2005). Synthetic biomaterials as instructive extracellular microenvironments for morphogenesis in tissue engineering. Nature Biotechnology *23*, 47.

Lutolf, M.P., Raeber, G.P., Zisch, A.H., Tirelli, N., and Hubbell, J.A. (2003). Cell-responsive synthetic hydrogels. Advanced Materials *15*, 888.

Madsen, B., Shao, Z.Z., and Vollrath, F. (1999). Variability in the mechanical properties of spider silks on three levels: Interspecific, intraspecific and intraindividual. International Journal of Biological Macromolecules *24*, 301.

Maheshwari, G., Brown, G., Lauffenburger, D.A., Wells, A., and Griffith, L.G. (2000). Cell adhesion and motility depend on nanoscale RGD clustering. Journal of Cell Science *113*, 1677.

Makarava, N., Bocharova, O.V., Salnikov, V.V., Breydo, L., Anderson, M., and Baskakov, I.V. (2006). Dichotomous versus palm-type mechanisms of lateral assembly of amyloid fibrils. Protein Science *15*, 1334.

Marelli, B., Alessandrino, A., Fare, S., Freddi, G., Mantovani, D., and Tanzi, M.C. (2010). Compliant electrospun silk fibroin tubes for small vessel bypass grafting. Acta Biomaterialia *6*, 4019.

Marshall, R.C., Orwin, D.F.G., and Gillespie, J.M. (1991). Structure and biochemistry of mammalian hard keratin. Electron Microscopy Reviews *4*, 47.

Martini, R. (1994). Expression and functional roles of neural cell-surface molecules and extracellular-matrix components during development and regeneration of peripheral-nerves. Journal of Neurocytology *23*, 1.

Martyn, C.N., and Greenwald, S.E. (2001). A hypothesis about a mechanism for the programming of blood pressure and vascular disease in early life. Clinical and Experimental Pharmacology and Physiology *28*, 948.

Maskarinec, S.A., and Tirrell, D.A. (2005). Protein engineering approaches to biomaterials design. Current Opinion in Biotechnology *16*, 422.

Matsumoto, K., Uejima, H., Iwasaki, T., Sano, Y., and Sumino, H. (1996). Studies on regenerated protein fibers. III. Production of regenerated silk fibroin fiber by the self-dialyzing wet spinning method. Journal of Applied Polymer Science *60*, 503.

McClure, M.J., Sell, S.A., Simpson, D.G., Walpoth, B.H., and Bowlin, G.L. (2010). A three-layered electrospun matrix to mimic native arterial architecture using polycaprolactone, elastin, and collagen: A preliminary study. Acta Biomaterialia *6*, 2422.

McGrath, E.J., and Kersey, P. (2009). Quantification of wound oedema after dermatological surgery. British Journal of Dermatology *161*, 1376.

McGrath, K., and Kaplan, D (1997). Protein-based materials (Boston, Birkhauser).

Merabet, S., Saadaoui, M., Sambrani, N., Hudry, B., Pradel, J., Affolter, M., and Graba, Y. (2007). A unique Extradenticle recruitment mode in the Drosophila Hox protein Ultrabithorax. Proceedings of the National Academy of Sciences of the United States of America *104*, 16946.

Merle, C., Perret, S., Lacour, T., Jonval, V., Hudaverdian, S., Garrone, R., Ruggiero, F., and Theisen, M. (2002). Hydroxylated human homotrimeric collagen I in Agrobacterium tumefaciens-mediated transient expression and in transgenic tobacco plant. FEBS Letters *515*, 114.

Metwalli, E., Slotta, U., Darko, C., Roth, S.V., Scheibel, T., and Papadakis, C.M. (2007). Structural changes of thin films from recombinant spider silk proteins upon post-treatment. Applied Physics A-Materials Science & Processing *89*, 655.

Mohammed, J.S., DeCoster, M.A., and McShane, M.J. (2004). Micropatterning of nanoengineered surfaces to study neuronal cell attachment in vitro. Biomacromolecules *5*, 1745.

Moroy, G., Alix, A.J.P., and Hery-Huynh, S. (2005). Structural characterization of human elastin derived peptides containing the GXXP sequence. Biopolymers *78*, 206.

Moy, R.L., Lee, A., and Zalka, A. (1991). Commonly used suture materials in skin surgery. American Family Physician *44*, 2123.

Murphy, A.R., and Kaplan, D.L. (2009). Biomedical applications of chemically-modified silk fibroin. Journal of Materials Chemistry *19*, 6443.

Nagaoka, M., Jiang, H.L., Hoshiba, T., Akaike, T., and Cho, C.S. (2010). Application of recombinant fusion proteins for tissue engineering. Annals of Biomedical Engineering *38*, 683.

Nagarkar, S., Nicolai, T., Chassenieux, C., and Lele, A. (2010). Structure and gelation mechanism of silk hydrogels. Physical Chemistry Chemical Physics *12*, 3834.

Nagarkar, S., Patil, A., Lele, A., Bhat, S., Bellare, J., and Mashelkar, R.A. (2009). Some mechanistic insights into the gelation of regenerated silk fibroin SOL. Industrial & Engineering Chemistry Research *48*, 8014.

Narmoneva, D.A., Oni, O., Sieminski, A.L., Zhang, S.G., Gertler, J.P., Kamm, R.D., and Lee, R.T. (2005). Self-assembling short oligopeptides and the promotion of angiogenesis. Biomaterials *26*, 4837.

Nazarov, R., Jin, H.J., and Kaplan, D.L. (2004). Porous 3-D scaffolds from regenerated silk fibroin. Biomacromolecules *5*, 718.

Neal, R.A., McClugage, S.G., Link, M.C., Sefcik, L.S., Ogle, R.C., and Botchwey, E.A. (2009). Laminin nanofiber meshes that mimic morphological properties and bioactivity of basement membranes. Tissue Engineering Part C-Methods *15*, 11.

Neuenschwander, S., and Hoerstrup, S.P. (2004). Heart valve tissue engineering. Transplant Immunology *12*, 359.

Nicol, A., Gowda, D.C., and Urry, D.W. (1992). Cell-adhesion and growth on synthetic elastomeric matrices containing arg-gly-asp-ser-3. Journal of Biomedical Materials Research *26*, 393.

Nilsson, M.R. (2004). Techniques to study amyloid fibril formation in vitro. Methods *34*, 151.

Omenetto, F.G., and Kaplan, D.L. (2010). New opportunities for an ancient material. Science *329*, 528

Ong, S.R., Trabbic-Carlson, K.A., Nettles, D.L., Lim, D.W., Chilkoti, A., and Setton, L.A. (2006). Epitope tagging for tracking elastin-like polypeptides. Biomaterials *27*, 1930.

Pakkanen, O., Hamalainen, E.R., Kivirikko, K.I., and Myllyharju, J. (2003). Assembly of stable human type I and III collagen molecules from hydroxylated recombinant chains in the yeast Pichia pastoris - effect of an engineered c-terminal oligomerization domain foldon. Journal of Biological Chemistry *278*, 32478.

Papapostolou, D., Smith, A.M., Atkins, E.D.T., Oliver, S.J., Ryadnov, M.G., Serpell, L.C., and Woolfson, D.N. (2007). Engineering nanoscale order into a designed protein fiber. Proceedings of the National Academy of Sciences of the United States of America *104*, 10853.

Parker, S.T., Domachuk, P., Amsden, J., Bressner, J., Lewis, J.A., Kaplan, D.L., and Omenetto, F.G. (2009). Biocompatible silk printed optical waveguides. Advanced Materials *21*, 2411.

Parkhe, A.D., Seeley, S.K., Gardner, K., Thompson, L., and Lewis, R.V. (1997). Structural studies of spider silk proteins in the fiber. Journal of Molecular Recognition *10*, 1.

Pasquali-Ronchetti, I., and Baccarani-Contri, M. (1997). Elastic fiber during development and aging. Microscopy Research and Technique *38*, 428.

Place, E.S., Evans, N.D., and Stevens, M.M. (2009). Complexity in biomaterials for tissue engineering. Nature Materials *8*, 457.

Powell, J.T., Vine, N., and Crossman, M. (1992). On the accumulation of d-aspartate in elastin and other proteins of the aging aorta. Atherosclerosis *97*, 201.

Qiu, W.G., Teng, W.B., Cappello, J.Y., and Wu, X. (2009). Wet-spinning of recombinant silk-elastin-like protein polymer fibers with high tensile strength and high deformability. Biomacromolecules *10*, 602.

Rabotyagova, O.S., Cebe, P., and Kaplan, D.L. (2009). Self-assembly of genetically engineered spider silk block copolymers. Biomacromolecules *10*, 229.

Rajagopalan, P., Marganski, W.A., Brown, X.Q., and Wong, J.Y. (2004). Direct comparison of the spread area, contractility, and migration of BALB/C 3T3 fibroblasts adhered to fibronectin- and RGD-modified substrata. Biophysical Journal *87*, 2818.

Rammensee, S., Huemmerich, D., Hermanson, K.D., Scheibel, T., and Bausch, A.R. (2006). Rheological characterization of hydrogels formed by recombinantly produced spider silk. Applied Physics A-Materials Science & Processing *82*, 261.

Rammensee, S., Slotta, U., Scheibel, T., and Bausch, A.R. (2008). Assembly mechanism of recombinant spider silk proteins. Proceedings of the National Academy of Sciences of the United States of America *105*, 6590.

Rauscher, S., Baud, S., Miao, M., Keeley, F.W., and Pomes, R. (2006). Proline and glycine control protein self-organization into elastomeric or amyloid fibrils. Structure *14*, 1667.

Reiersen, H., Clarke, A.R., and Rees, A.R. (1998). Short elastin-like peptides exhibit the same temperature-induced structural transitions as elastin polymers: Implications for protein engineering. Journal of Molecular Biology *283*, 255.

Remes, A., and Williams, D.F. (1992). Immune-response in biocompatibility. Biomaterials *13*, 731.

Reneker, D.H., and Chun, I. (1996). Nanometre diameter fibres of polymer, produced by electrospinning. Nanotechnology *7*, 216.

Reneker, D.H., Yarin, A.L., Fong, H., and Koombhongse, S. (2000). Bending instability of electrically charged liquid jets of polymer solutions in electrospinning. Journal of Applied Physics *87*, 4531.

Ricchelli, F., Buggio, R., Drago, D., Salmona, M., Forloni, G., Negro, A., Tognon, G., and Zatta, P. (2006). Aggregation/fibrillogenesis of recombinant human prion protein and Gerstmann-Straussler-Scheinker disease peptides in the presence of metal ions. Biochemistry *45*, 6724.

Riekel, C., Branden, C., Craig, C., Ferrero, C., Heidelbach, F., and Muller, M. (1999). Aspects of X-ray diffraction on single spider fibers. International Journal of Biological Macromolecules *24*, 179.

Rodriguez-Cabello, J.C., Prieto, S., Reguera, J., Arias, F.J., and Ribeiro, A. (2007). Biofunctional design of elastin-like polymers for advanced applications in nanobiotechnology. Journal of Biomaterials Science-Polymer Edition *18*, 269.

Rodriguez-Cabello, J.C., Prieto, S., Arias, F.J., Reguera, J., and Ribeiro, A. (2006). Nanobiotechnological approach to engineered biomaterial design: The example of elastin-like polymers. Nanomedicine *1*, 267.

Romer, L., and Scheibel, T. (2007). Basis for new material - Spider silk protein. Chemie in Unserer Zeit *41*, 306.

Romer, L., and Scheibel, T. (2008). The elaborate structure of spider silk structure and function of a natural high performance fiber. Prion *2*, 154.

Romero, P., Obradovic, Z., Li, X.H., Garner, E.C., Brown, C.J., and Dunker, A.K. (2001). Sequence complexity of disordered protein. Proteins-Structure Function and Genetics *42*, 38.

Ronshaugen, M., McGinnis, N., and McGinnis, W. (2002). Hox protein mutation and macroevolution of the insect body plan. Nature *415*, 914.

Sahoo, S., Ang, L.T., Goh, J.C.H., and Toh, S.L. (2010). Growth factor delivery through electrospun nanofibers in scaffolds for tissue engineering applications. Journal of Biomedical Materials Research Part A *93A*, 1539.

Sakiyama-Elbert, S.E., and Hubbell, J.A. (2001). Functional biomaterials: Design of novel biomaterials. Annual Review of Materials Research *31*, 183.

Saravanan, D. (2006). Spider silk - Structure, properties and spinning. Journal of Texile and Apparel, Technology and Management *5*, 1.

Sargeant, T.D., Guler, M.O., Oppenheimer, S.M., Mata, A., Satcher, R.L., Dunand, D.C., and Stupp, S.I. (2008). Hybrid bone implants: Self-assembly of peptide amphiphile nanofibers within porous titanium. Biomaterials *29*, 161.

Scheibel, T. (2004). Spider silks: Recombinant synthesis, assembly, spinning, and engineering of synthetic proteins. Microbial Cell Factories *3*, 14.

Schmidt, D., Mol, A., Breymann, C., Achermann, J., Odermatt, B., Gossi, M., Neuenschwander, S., Pretre, R., Genoni, M., Zund, G., *et al.* (2006a). Living autologous heart valves engineered from human prenatally harvested progenitors. Circulation *114*, I125.

Schmidt, D., Mol, A., Odermatt, B., Neuenschwander, S., Breymann, C., Gossi, M., Genoni, M., Zund, G., and Hoerstrup, S.P. (2006b). Engineering of biologically active living heart valve leaflets using human umbilical cord-derived progenitor cells. Tissue Engineering *12*, 3223.

Schneider, A., Wang, X.Y., Kaplan, D.L., Garlick, J.A., and Egles, C. (2009). Biofunctionalized electrospun silk mats as a topical bioactive dressing for accelerated wound heating. Acta Biomaterialia *5*, 2570.

Seliktar, D., Black, R.A., Vito, R.P., and Nerem, R.M. (2000). Dynamic mechanical conditioning of collagen-gel blood vessel constructs induces remodeling in vitro. Annals of Biomedical Engineering *28*, 351.

Sell, S.A., McClure, M.J., Garg, K., Wolfe, P.S., and Bowlin, G.L. (2009). Electrospinning of collagen/biopolymers for regenerative medicine and cardiovascular tissue engineering. Advanced Drug Delivery Reviews *61*, 1007.

Shao, Z., and Vollrath, F. (2002). Surprising strength of silkworm silk. Nature *418*, 741.

Shen, Y.X., Qian, Y.Q., Zhang, H.X., Zuo, B.Q., Lu, Z.F., Fan, Z.H., Zhang, P., Zhang, F., and Zhou, C.L. (2010). Guidance of olfactory ensheathing cell growth and migration on electrospun silk fibroin scaffolds. Cell Transplantation *19*, 147.

Shin, H. (2007). Fabrication methods of an engineered microenvironment for analysis of cell-biomaterial interactions. Biomaterials *28*, 126.

Shu, X.K., Shaner, N.C., Yarbrough, C.A., Tsien, R.Y., and Remington, S.J. (2006). Novel chromophores and buried charges control color in mFruits. Biochemistry *45*, 9639.

Sierpinski, P., Crider, C., and Van Dyke, M. (2006). Biocompatibility of tissue engineering scaffolds made from keratin biomaterials. FASEB Journal *20*, A413.

Silva, G.A., Czeisler, C., Niece, K.L., Beniash, E., Harrington, D.A., Kessler, J.A., and Stupp, S.I. (2004). Selective differentiation of neural progenitor cells by high-epitope density nanofibers. Science *303*, 1352.

Slotta, U.K., Rammensee, S., Gorb, S., and Scheibel, T. (2008). An engineered spider silk protein forms microspheres. Angewandte Chemie-International Edition *47*, 4592.

Srokowski, E.M., and Woodhouse, K.A. (2008). Development and characterisation of novel cross-linked bio-elastomeric materials. Journal of Biomaterials Science-Polymer Edition *19*, 785.

Stark, M., Grip, S., Rising, A., Hedhammar, M., Engstrom, W., Hjalm, G., and Johansson, J. (2007). Macroscopic fibers self-assembled from recombinant miniature spider silk proteins. Biomacromolecules *8*, 1695.

Stegemann, J.P., Kaszuba, S.N., and Rowe, S.L. (2007). Review: Advances in vascular tissue engineering using protein-based biomaterials. Tissue Engineering *13*, 2601.

Stromer, T., and Serpell, L.C. (2005). Structure and morphology of the Alzheimer's amyloid fibril. Microscopy Research and Technique *67*, 210.

Su, Y., and Chang, P.T. (2001). Acidic pH promotes the formation of toxic fibrils from beta-amyloid peptide. Brain Research *893*, 287.

Sugihara, A., Sugiura, K., Morita, H., Ninagawa, T., Tubouchi, K., Tobe, R., Izumiya, M., Horio, T., Abraham, N.G., and Ikehara, S. (2000). Promotive effects of a silk film on epidermal recovery from full-thickness skin wounds. Proceedings of the Society for Experimental Biology and Medicine *225*, 58.

Tan, X.X., Bondos, S., Li, L.K., and Matthews, K.S. (2002). Transcription activation by Ultrabithorax Ib protein requires a predicted alpha-helical region. Biochemistry *41*, 2774.

Temenoff, J.S., Shin, H., Conway, D.E., Engel, P.S., and Mikos, A.G. (2003). In vitro cytotoxicity of redox radical initiators for cross-linking of oligo(poly(ethylene glycol) fumarate) macromers. Biomacromolecules *4*, 1605.

Teng, W.B., Cappello, J., and Wu, X.Y. (2009). Recombinant silk-elastinlike protein polymer displays elasticity comparable to elastin. Biomacromolecules *10*, 3028.

Teule, F., Furin, W.A., Cooper, A.R., Duncan, J.R., and Lewis, R.V. (2007). Modifications of spider silk sequences in an attempt to control the mechanical properties of the synthetic fibers. Journal of Materials Science *42*, 8974.

Tour, E., Hittinger, C.T., and McGinnis, W. (2005). Evolutionarily conserved domains required for activation and repression functions of the Drosophila Hox protein Ultrabithorax. Development *132*, 5271.

Trabbic, K.A., and Yager, P. (1998). Comparative structural characterization of naturally- and synthetically-spun fibers of Bombyx Mori fibroin. Macromolecules *31*, 462.

Um, I.C., Ki, C.S., Kweon, H.Y., Lee, K.G., Ihm, D.W., and Park, Y.H. (2004). Wet spinning of silk polymer - II. Effect of drawing on the structural characteristics and properties of filament. International Journal of Biological Macromolecules *34*, 107.

Um, I.C., Kweon, H.Y., Park, Y.H., and Hudson, S. (2001). Structural characteristics and properties of the regenerated silk fibroin prepared from formic acid. International Journal of Biological Macromolecules *29*, 91.

Urry, D.W. (1993). Molecular machines - How motion and other functions of living organisms can result from reversible chemical-changes. Angewandte Chemie-International Edition in English *32*, 819.

Urry, D.W., Pattanaik, A., Xu, J., Woods, T.C., McPherson, D.T., and Parker, T.M. (1998). Elastic protein-based polymers in soft tissue augmentation and generation. Journal of Biomaterials Science-Polymer Edition *9*, 1015.

Uversky, V.N., and Fink, A.L. (2004). Conformational constraints for amyloid fibrillation: The importance of being unfolded. Biochimica et Biophysica Acta-Proteins and Proteomics *1698*, 131.

van Beek, J.D., Kummerlen, J., Vollrath, F., and Meier, B.H. (1999). Supercontracted spider dragline silk: A solid-state nmr study of the local structure. International Journal of Biological Macromolecules *24*, 173.

van Hest, J.C.M., and Tirrell, D.A. (2001). Protein-based materials, toward a new level of structural control. Chemical Communications, 1897.

Vaz, C.M., van Tuijl, S., Bouten, C.V.C., and Baaijens, F.P.T. (2005). Design of scaffolds for blood vessel tissue engineering using a multi-layering electrospinning technique. Acta Biomaterialia *1*, 575.

Velema, J., and Kaplan, D. (2006). Biopolymer-based biomaterials as scaffolds for tissue engineering. Tissue Engineering I: Scaffold Systems for Tissue Engineering *102*, 187.

Vendrely, C., and Scheibel, T. (2007). Biotechnological production of spider-silk proteins enables new applications. Macromolecular Bioscience *7*, 401.

Vepari, C., and Kaplan, D.L. (2007). Silk as a biomaterial. Progress in Polymer Science *32*, 991.

Vepari, C.P., and Kaplan, D.L. (2006). Covalently immobilized enzyme gradients within three-dimensional porous scaffolds. Biotechnology and Bioengineering *93*, 1130.

Vogel, V. (2006). Mechanotransduction involving multimodular proteins: Converting force into biochemical signals. Annual Review of Biophysics and Biomolecular Structure *35*, 459.

Vogel, V., and Sheetz, M.P. (2009). Cell fate regulation by coupling mechanical cycles to biochemical signaling pathways. Current Opinion in Cell Biology *21*, 38.

Vojtechovsky, J., Chu, K., Berendzen, J., Sweet, R.M., and Schlichting, I. (1999). Crystal structures of myoglobin-ligand complexes at near-atomic resolution. Biophysical Journal *77*, 2153.

Vollrath, F., and Knight, D.P. (1999). Structure and function of the silk production pathway in the spider nephila edulis. International Journal of Biological Macromolecules *24*, 243.

Vollrath, F., and Knight, D.P. (2001). Liquid crystalline spinning of spider silk. Nature *410*, 541.

Vollrath, F., Madsen, B., and Shao, Z. (2001). The effect of spinning conditions on the mechanics of a spider's dragline silk. Proceedings of Biological Sciences *268*, 2339.

Vollrath, F., and Porter, D. (2009). Silks as ancient models for modern polymers. Polymer *50*, 5623.

Voytik-Harbin, S.L., Brightman, A.O., Waisner, B.Z., Robinson, J.P., and Lamar, C.H. (1998). Small intestinal submucosa: A tissue-derived extracellular matrix that promotes tissue-specific growth and differentiation of cells in vitro. Tissue Engineering *4*, 157.

Weatherbee, S.D., Nijhout, H.F., Grunert, L.W., Halder, G., Galant, R., Selegue, J., and Carroll, S. (1999). Ultrabithorax function in butterfly wings and the evolution of insect wing patterns. Current Biology *9*, 109.

Welsh, E.R., and Tirrell, D.A. (2000). Engineering the extracellular matrix: A novel approach to polymeric biomaterials. I. Control of the physical properties of artificial protein matrices designed to support adhesion of vascular endothelial cells. Biomacromolecules *1*, 23.

Wen, H.X., Lan, X.Q., Zhang, Y.S., Zhao, T.F., Wang, Y.J., Kajiura, Z., and Nakagaki, M. (2010). Transgenic silkworms (Bombyx mori) produce recombinant spider dragline silk in cocoons. Molecular Biology Reports *37*, 1815.

West, J.L., and Hubbell, J.A. (1999). Polymeric biomaterials with degradation sites for proteases involved in cell migration. Macromolecules *32*, 241.

White, R.A.H., and Wilcox, M. (1984). Protein products of the bithorax complex in Drosophila. Cell *39*, 163.

Wille, H., Bian, W., McDonald, M., Kendall, A., Colby, D.W., Bloch, L., Ollesch, J., Borovinskiy, A.L., Cohen, F.E., Prusiner, S.B., *et al.* (2009). Natural and synthetic prion structure from x-ray fiber diffraction. Proceedings of the National Academy of Sciences of the United States of America *106*, 16990.

Williams, D.F. (2008). On the mechanisms of biocompatibility. Biomaterials *29*, 2941.

Williams, D.F. (2009). On the nature of biomaterials. Biomaterials *30*, 5897.

Wong, J.Y., Leach, J.B., and Brown, X.Q. (2004). Balance of chemistry, topography, and mechanics at the cell-biomaterial interface: Issues and challenges for assessing the role of substrate mechanics on cell response. Surface Science *570*, 119.

Woolfson, D.N., and Mahmoud, Z.N. (2010). More than just bare scaffolds: Towards multi-component and decorated fibrous biomaterials. Chemical Society Reviews *39*, 3464.

Wright, C.F., Teichmann, S.A., Clarke, J., and Dobson, C.M. (2005). The importance of sequence diversity in the aggregation and evolution of proteins. Nature *438*, 878.

Wu, W.J., Vrhovski, B., and Weiss, A.S. (1999). Glycosaminoglycans mediate the coacervation of human tropoelastin through dominant charge interactions involving lysine side chains. Journal of Biological Chemistry *274*, 21719.

Wu, Y.H., Shen, Q.C., and Hu, S.S. (2006). Direct electrochemistry and electrocatalysis of heme-proteins in regenerated silk fibroin film. Analytica Chimica Acta *558*, 179.

Xia, X.X., Qian, Z.G., Ki, C.S., Park, Y.H., Kaplan, D.L., and Lee, S.Y. (2010). Native-sized recombinant spider silk protein produced in metabolically engineered Escherichia coli results in a strong fiber. Proceedings of the National Academy of Sciences of the United States of America *107*, 14059.

Xie, F., Zhang, H.H., Shao, H.L., and Hu, X.C. (2006). Effect of shearing on formation of silk fibers from regenerated Bombyx mori silk fibroin aqueous solution. International Journal of Biological Macromolecules *38*, 284.

Xu, C.Y., Inai, R., Kotaki, M., and Ramakrishna, S. (2004). Aligned biodegradable nanotibrous structure: A potential scaffold for blood vessel engineering. Biomaterials *25*, 877.

Xu, J.W., Johnson, T.S., Motarjem, P.M., Peretti, G.M., Randolph, M.A., and Yaremchuk, M.J. (2005). Tissue-engineered flexible ear-shaped cartilage. Plastic and Reconstructive Surgery *115*, 1633.

Xu, M., and Lewis, R.V. (1990). Structure of a protein superfiber - spider dragline silk. Proceedings of the National Academy of Sciences of the United States of America *87*, 7120.

Yamamoto, M., Tabata, Y., and Ikada, Y. (1999). Growth factor release from gelatin hydrogel for tissue engineering. Journal of Bioactive and Compatible Polymers *14*, 474.

Yanagisawa, S., Zhu, Z.H., Kobayashi, I., Uchino, K., Tamada, Y., Tamura, T., and Asakura, T. (2007). Improving cell-adhesive properties of recombinant Bombyx mori silk by incorporation of collagen or fibronectin derived peptides produced by transgenic silkworms. Biomacromolecules *8*, 3487.

Yang, X., Ogbolu, K.R., and Wang, H. (2008). Multifunctional nanofibrous scaffold for tissue engineering. Journal of Experimental Nanoscience *3*, 329.

Yao, J.M., and Asakura, T. (2003). Synthesis and structural characterization of silk-like materials incorporated with an elastic motif. Journal of Biochemistry *133*, 147.

Yao, J.M., Masuda, H., Zhao, C.H., and Asakura, T. (2002). Artificial spinning and characterization of silk fiber from Bombyx mori silk fibroin in hexafluoroacetone hydrate. Macromolecules *35*, 6.

Zeugolis, D.I., Paul, R.G., and Attenburrow, G. (2008). Post-self-assembly experimentation on extruded collagen fibres for tissue engineering applications. Acta Biomaterialia *4*, 1646.

Zhang, F., Zuo, B.Q., Zhang, H.X., and Bai, L. (2009). Studies of electrospun regenerated SF/TSF nanofibers. Polymer *50*, 279.

Zhang, S.G., and Zhao, X.J. (2004). Design of molecular biological materials using peptide motifs. Journal of Materials Chemistry *14*, 2082.

Zhang, S.M., Greenfield, M.A., Mata, A., Palmer, L.C., Bitton, R., Mantei, J.R., Aparicio, C., de la Cruz, M.O., and Stupp, S.I. (2010). A self-assembly pathway to aligned monodomain gels. Nature Materials *9*, 594.

Zhang, Y.Q. (1998). Natural silk fibroin as a support for enzyme immobilization. Biotechnology Advances *16*, 961.

Zhang, Y.Q., Ma, Y., Xia, Y.Y., Shen, W.D., Mao, J.P., Zha, X.M., Shirai, K., and Kiguchi, K. (2006). Synthesis of silk fibroin-insulin bioconjugates and their characterization and activities in vivo. Journal of Biomedical Materials Research Part B-Applied Biomaterials *79B*, 275.

Zhao, C.H., Yao, J.M., Masuda, H., Kishore, R., and Asakura, T. (2003). Structural characterization and artificial fiber formation of Bombyx mori silk fibroin in hexafluoro-iso-propanol solvent system. Biopolymers *69*, 253.

Zhu, Y.B., Cao, Y., Pan, J., and Liu, Y.X. (2010). Macro-alignment of electrospun fibers for vascular tissue engineering. Journal of Biomedical Materials Research Part B-Applied Biomaterials *92B*, 508.